EXPERIMENTAL AND ANALYTICAL INVESTIGATION OF OSCILLATIONS IN FLOWS OVER CAVITIES

Thesis by

Virendra Sarohia

In Partial Fulfillment of the Requirements

for the Degree of

Doctor of Philosophy

California Institute of Technology

Pasadena, California

1975

(Submitted March 1975)

ACKNOWLEDGEMENTS

I wish to extend my deep appreciation to Professors Anatol Roshko and Toshi Kubota for their invaluable guidance in this research. My sincere thanks to Dr. Wilhelm Behrens for his assistance during the early part of the experiments.

I am grateful to Messrs. Samuel L. Roman, Vince K. Sodha and Paul E. Baloga of Aeronautics Laboratories for their kind assistance and cooperation.

It is a pleasure to thank Mrs. Virginia M. Conner for typing the manuscript.

I am indebted to the California Institute of Technology, Pickering/Link Foundation, and the Government of India for their financial assistance. I acknowledge gratefully the financial support provided by the U. S. Army Research Office through Contract No. DAHC-04-72-C-0028, which made this experimental study possible.

Last, but not the least, I thank my wife Venita and daughter Radhika for their encouragement and forbearance throughout these difficult years.

ABSTRACT

In this study, an analytical and experimental approach has been used to investigate the phenomenon of flow induced oscillations in cavities. Laminar axisymmetric flows over shallow cavities at low subsonic speeds were experimentally investigated using constant-temperature hot-wire anemometry. This study comprised the following: study of the effect of the freestream and cavity configuration on onset of cavity oscillations; measurements of cavity shear layer under a wide range of cavity and flow configurations, and the distribution of the phase of the propagating disturbances during both first and second mode of cavity oscillation for a fixed Reynolds number at the upstream corner. Both motion and instant pictures of cavity shear flow, visualized by smoke injection, were obtained. Experiments were also done to investigate the effect of artificial excitation and of mass injection on the onset of cavity oscillations.

The present study indicates that the cavity depth has little effect on oscillations in shallow cavities, except when the depth is of the order of the thickness of the cavity shear flow. For such cavity configurations, measurements indicate a strong stabilizing effect of depth on laminar cavity shear layer. Results of motion pictures and hot-wire surveys of the cavity shear layer show that, close to the downstream cavity corner, large lateral motion of the shear layer occurs, which results in a periodic shedding of vortices at a frequency of cavity oscillations. Mean velocity measurements show growth rates as high as $\frac{d\theta}{dx} \simeq 0.022$ where θ is the shear layer momentum

thickness and x is the streamwise coordinate. These are attributed to strong imposed velocity fluctuations on the flow, by the oscillating cavity system.

Phase measurements indicate that the disturbances propagate at a constant phase speed through the cavity shear layer. The wave length of the propagating disturbance bears an approximate integral relation to cavity width, in each mode of cavity oscillation given by $b \simeq \lambda(N+\frac{1}{2})$ where b is the cavity width, λ the wave length of the propagating disturbance and N is an integer, which takes values 0, 1, 2, ••• etc. depending upon the mode of oscillation.

Stability calculations of the measured mean velocity profile were made by numerically integrating the governing equation of motion. These numerical results were used to compute the phase and the integrated amplification of the growing disturbances, through the cavity shear layer. Finally, the mode of cavity oscillation can be predicted for a given cavity flow by studying simultaneously the phase and integrated amplification of various disturbance frequencies through the shear layer and applying the mode relation.

TABLE OF CONTENTS

Table of Contents (Continued)

Table of Contents (Continued)

NOMENCLATURE

a	freestream acoustic speed
b, b' and b''	cavity widths (cavity lengths)
c	phase speed = ω/α
d	cavity depth
d'	inner diameter of the axi-symmetric model
D	outer diameter of the axi-symmetric model
f	frequency in Hz
F(S)	amplification rate of the spatially growing disturbances of non-dimensional frequency S
h	distance from slit to edge in edgetone system
k	non-dimensional propagation speed of disturbance = U_c/U_e
K(f)	integrated amplification of a disturbance of frequency f through the cavity flow
ℓ	nose length of the model
m	an integer
M	freestream Mach number
n	an integer
N	an integer depicting mode of cavity oscillation
p	pressure
P	mean pressure
S	non-dimensional frequency $\frac{f\theta}{U_e}$
t	time
u	velocity in direction x
U	mean velocity in direction x

Nomenclature (Continued)

U_c	convective speed of the disturbances in the cavity shear layer
U_∞	freestream velocity in front of the model
v	velocity in direction y
V	mean velocity in direction y
x	streamwise coordinate
y	transverse coordinate
α	wave number
ω	circular frequency
$\delta(x)$	shear layer thickness at x
δ_o	shear layer thickness at separation where x = 0
$\theta(x)$	shear layer momentum thickness at x
θ_o	shear layer momentum thickness at separation where x = 0
λ	disturbance wave length
ν	kinematic viscosity
ρ	density
ψ	phase angle by which the phase at a given location lags behind x = 0
ψ'	stream function
$\frac{fb}{U_e}, \frac{f\theta}{U_e}, \frac{f\delta}{U_e}$	non-dimensional frequencies
$Re_{\delta_o} = \frac{U_e \delta_o}{\nu}$ and $Re_{\theta_o} = \frac{U_e \delta_o}{\nu}$	Reynolds numbers

Nomenclature (Continued)

$\sqrt{\overline{u'^2}}$	root mean square velocity fluctuations in direction x
$\overline{u'^2}$	mean square velocity fluctuations in direction x
$(\ )_{min}$	corresponds to the conditions for onset of cavity oscillations

LIST OF FIGURES

List of Figures (Continued)

List of Figures (Continued)

List of Figures (Continued)

I. INTRODUCTION

The problem of fluid flow (gases or liquids) over cavities on solid surfaces has gained renewed significance. For example, uncovered cavities on flight vehicles are necessary to house optical instruments. Other applications occur in the transonic wind tunnel where slotted walls are used, in continuous laser cavities, and even cavities of ship hulls. Flow over cavities is of interest because the presence of cavities changes the drag and heat transfer and may cause intense periodic oscillations, which in turn may lead to severe buffeting of the aerodynamic structure and production of sound.

Periodic oscillations in cavities have been observed over a large range of Mach numbers and Reynolds numbers, with both laminar and turbulent boundary layers and over a wide range of length to depth ratios. In general, cavities are divided into open and closed cavities as defined by Charwat et al.[10] Open cavities refer to flow over cavities where the boundary layer separates at the upstream corner and reattaches near the downstream corner. Cavities are closed when the separated layer reattaches at the cavity bottom and again separates ahead of the downstream wall. At supersonic speeds and for a turbulent layer, the dividing line between open and closed cavities was found to be $\frac{b}{d} \simeq 11$ by Charwat et al. Present experiments at low subsonic speeds with laminar separation show a demarcation line between an open and a closed cavity to be around $\frac{b}{d} \simeq 7\text{-}8$.

Open cavities may further be divided into shallow and deep cavities. On the basis of previous experiments,[15, 39] the

oscillations in deep cavities are in fundamental acoustic depth modes. Deep cavities act as resonators and the shear layer above the cavity provides a forcing mechanism. Resonant oscillations are established under certain flow conditions, corresponding to natural acoustic depth modes of the cavities.

In contrast to deep cavities, present experiments of flow over shallow cavities at low subsonic speed show that the phenomenon of cavity oscillations is not one of standing longitudinal acoustic waves, but is one of propagating disturbances which get amplified through the shear layer. The important length scale, therefore, in shallow cavity flows, is the width b of the cavity. On the basis of past experiments,[15, 39, 53] a very rough division between shallow and deep cavities is $\frac{b}{d} \simeq 1$. For $\frac{b}{d} > 1$ the cavities may be considered shallow and for $\frac{b}{d} < 1$ the cavities may be considered deep.

Tani et al.[53] classify cavities into shallow and deep cavities on the basis of smoothness of flow over cavities. They argue that deep cavities are characterized by smooth separated flow which results in a low pressure drag. On the contrary, shallow cavities result in less smooth flow giving a higher pressure drag coefficient. Their pressure measurements indicate the demarcation line to be at $\frac{b}{d} \simeq 1.4$.

Previous work on cavity oscillations has been mainly experimental. Because of the practical importance of oscillations in bomb bays, experiments were performed at Boeing,[6] Douglas[5] and at the Royal Aircraft Establishment.[46] The first experiments covering

a wide range of geometrical and flow parameters were performed by Karamcheti.[20] Further extensive work was performed by East,[15] Heller et al.,[19] McGregor and White,[37] Plumblee et al.,[39] Rossiter[45, 46] and others.

Karamcheti studied the acoustic field of two-dimensional shallow cavities in the range of Mach numbers from 0.25 to 1.5 by schlieren and interferometric observations. Karamcheti noticed that for a fixed freestream Mach number and depth, there exists a minimum width below which no sound emission is noticed. For a fixed depth, this minimum width decreases as the Mach number increases. It was further noticed that for a fixed Mach number and depth, minimum width with laminar separation is smaller compared to the turbulent one, i.e., $b_{min_{lamin}} < b_{min_{turb}}$. For a fixed cavity, Karamcheti further noted a minimum Mach number below which no sound emission was noticed. Under a non-oscillating cavity configuration, schlieren and spark shadowgraph pictures showed that the shear layer bridges the cavities without strong interaction with the downstream corner. No detailed study of the aerodynamic and geometric conditions for the onset of cavity oscillations was undertaken.

The effects of Mach number on non-dimensional frequency $\frac{fb}{U_e}$ have been studied by many investigators for both laminar and turbulent boundary layers. On the basis of high speed shadowgraphs of cavity oscillations, Rossiter[45] speculated that periodic vortices are shed at the upstream corner in sympathy with the pressure oscillation produced by interaction of the vortices with the downstream corner. Based on this idea Rossiter derived a formula for the

oscillation frequency. Heller[19] and Covert studied shallow cavities over a wide range of Mach numbers and correlated a great many experimental results with Rossiter's formula. In Rossiter's formulations of cavity oscillation frequency, the vortices shed from the upstream cavity corner are assumed to convect at a constant phase velocity through the shear layer, resulting in a linear phase distribution. It is further assumed that the phase velocity of these vortices is independent of the cavity geometry and flow configuration. Rossiter's formula does not shed any light on the possible mode or modes in which the cavity is most likely to oscillate. Unfortunately, no detailed and systematic measurements of cavity shear layer have been made in the past to verify Rossiter's assumptions.

Another approach used by Plumblee et al.[39] to explain the mechanism of flow induced oscillations in cavities is that the phenomenon of sound generation in a cavity is basically that of an enclosure responding to its normal acoustic modes. Plumblee calculates the acoustic modes of a rectangular cavity with five cavity walls having infinite impedance and an opening whose radiation impedance has to be determined. Results obtained from this theory compared quite well with their experiments. This approach cannot predict which natural acoustic modes are actually being excited. The stability of the shear layer plays an important role in shallow cavity oscillations. This has been neglected in their formulations. Furthermore, the present study indicates that the mechanism of cavity oscillations in shallow cavities is not one of standing longitudinal acoustic waves, as has been assumed by Plumblee et al.

For a given flow, the prerequisite of a minimum width for the onset of cavity oscillations strongly suggests that the mechanism of cavity oscillations depends upon the stability characteristics of the shear layer. Woolley[54,55] and Karamcheti extended their stability analysis of non-parallel jets for edge-tone generation to explain the main features of cavity oscillations qualitatively. Their measurements[21, 50, 51] of edge-tone flow field indicated that the phase and propagation speed of the disturbances in the jet, does not agree with the linearized stability theory of the incompressible two-dimensional parallel jet. According to the stability theory of non-parallel shear flows, the stability characteristic of the flow is a function of local quantities, viz., thickness of the shear layer, mean velocity profile, etc., which result in different amplification rates, as a disturbance of fixed frequency propagates downstream through the flow. This explains their measurements of edge-tone flow field in which, according to them, a non-linear distribution of the phase and convective speed of the disturbances occurs. They speculated that a similar behavior would occur in cavity flows and extended their results accordingly. On the basis of stability of almost parallel shear flow, they concluded that the frequency of cavity oscillations is the one which received the maximum total integrated amplification through the shear layer. Their theory does not take into consideration the presence of the downstream corner which this study indicates to be the key factor in inducing self-sustained oscillations in the cavity shear layer. Present experiments further show that the presence of a back face, in fact, results in an integral

relation between wave length of the propagating disturbances and the cavity width, in each mode of cavity operation.

It was therefore felt that a detailed measurement of the cavity shear layer was necessary for better understanding of the mechanism. Flow visualization and measurements of the cavity shear layer, from which phase distribution, phase velocity of the propagating disturbance, etc. can be determined, would be of great help in understanding the phenomenon of cavity oscillations. A stability analysis of the measured mean velocity profile would help further to study the amplification rates of various frequencies through the shear layer. This information will assist in the study of integrated amplification of various frequencies through the cavity shear flow. Because of sustained velocity fluctuations, study of the phase of the disturbances at the downstream corner in relation to the upstream corner will shed further light on the underlying mechanism of flow induced cavity oscillations.

II. BASIC FEATURES OF FLOW INDUCED OSCILLATIONS

In this section the main features of cavity oscillations will be outlined. Dimensional grouping of various parameters of importance will be undertaken. This will be followed by a brief review of the theoretical work on prediction of the frequency of cavity oscillations.

II. a. Main Features of Cavity Oscillations

Periodic cavity oscillations such as those shown below have been observed by many investigators over a wide range of Mach and Reynolds numbers. The main features for shallow cavities are summarized below. These features of cavity oscillations prevail in both laminar and turbulent boundary layer separation.

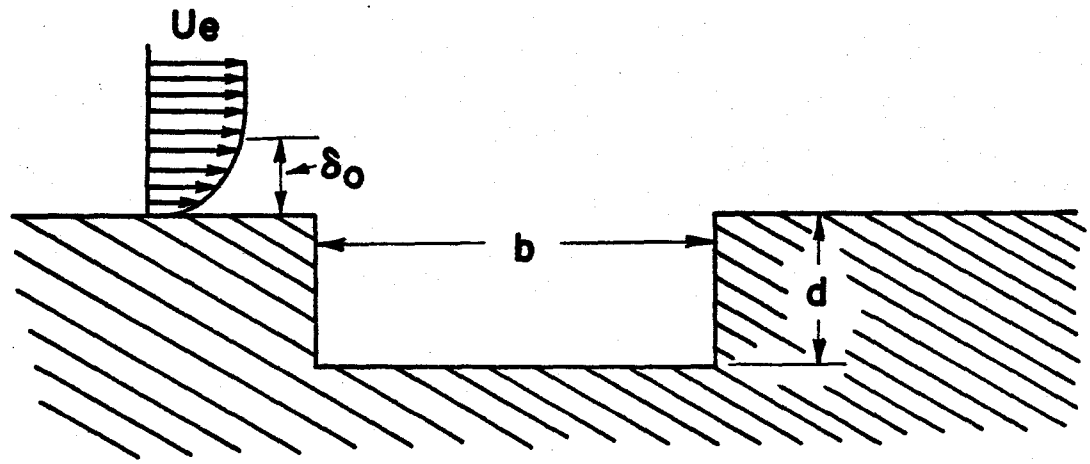

(i) For a fixed value of edge velocity U_e, shear layer thickness δ_0 at the upstream corner and depth d of the cavity, there exists a minimum width b below which no oscillations occur (see sketch for cavity parameters).

(ii) For fixed U_e, δ_0 and d, when cavity oscillations begin ($b > b_{min}$), frequency decreases linearly as b increases. This process continues until a critical value of width b is reached, when the

oscillation jumps to a higher mode. At this critical value, the cavity oscillations randomly switch from one mode to the other. At a given time, a cavity oscillates in one mode only. As the width is further increased, the oscillation may shift to a still higher mode and the process continues until the signal becomes irregular. Conversely, as the width b decreases, the oscillations switch to a lower mode, until a minimum width is reached when oscillations disappear suddenly. No significant region of hysteresis is noticed when oscillation frequency steps up or down, when width b increases or decreases, respectively.

(iii) For a fixed value of shear layer thickness δ_0, width b and depth d, there exists a minimum edge velocity $U_{e_{min}}$ below which no oscillations occur.

(iv) For fixed δ_0, b and d, for edge velocity $U_e > U_{e_{min}}$, the frequency of oscillations increases linearly with U_e. The frequency keeps increasing up to a certain critical value U_e when the oscillation jumps to a higher mode. At this critical velocity, two modes occur randomly. As stated before, the cavity oscillates only in one mode at a time. The process of jumping to higher modes with increasing U_e is terminated by appearance of an irregular signal. When the edge velocity is decreased, the frequency decreases and the oscillations jump to lower modes. No significant region of hysteresis is noticed between modes as edge velocity is changed.

(v) For a fixed value of the edge velocity U_e, depth d and width b, there exists a maximum value of shear layer thickness $\delta_{0_{max}}$ above which the cavity does not oscillate. As the shear layer

thickness δ_0 is decreased ($\delta_0 < \delta_{0_{max}}$), the frequency of cavity oscillations increases.

(vi) The frequency of cavity oscillations is independent of depth d for fixed value of U_e, δ_0 and b except when $\frac{d}{\delta_0} \sim 0(1)$. When depth d is of the order of shear layer thickness, frequency decreases as d is increased. But for $b \gg d$, i.e., deep cavities, the oscillations are in acoustic depth mode (Cf Ref. 15).

The main features of cavity oscillations will be stated in non-dimensional form in the following section when a parametric study of cavity oscillations will be undertaken.

II. b. Parametric Study

The main parameters determining the minimum width b_{min} are:

$$b_{min} = F\left[U_e, \delta_0, \nu, d, a, \text{ mean velocity profile at separation, boundary layer laminar or turbulent at separation, etc.}\right]$$

Grouping these variables into dimensionless quantities, we have

$$\left(\frac{b}{\delta_0}\right)_{min} = F'\left[Re_{\delta_0}, \frac{d}{\delta_0}, M, \text{ mean velocity profile at separation, etc.}\right]$$

On similar grounds, the non-dimensional frequency $\frac{fb}{U_e}$ can be written as a function

$$\frac{fb}{U_e} = F''\left[Re_{\delta_0}, \frac{d}{\delta_0}, \frac{b}{\delta_0}, M, \text{ mean velocity profile at separation, etc.}\right]$$

In light of the main features of cavity oscillations, discussed above in section II.a., we can state for low subsonic speeds that,

(i) For fixed value of Reynolds number Re_{δ_0} and depth $\frac{d}{\delta_0}$ there exists a minimum width $(\frac{b}{\delta_0})_{min}$ below which no cavity oscillations occur.

(ii) For a fixed cavity width $\frac{b}{\delta_0}$ and cavity depth $\frac{d}{\delta_0}$, there exists a minimum Reynolds number $(Re_{\delta_0})_{min}$ below which no cavity oscillations occur.

(iii) For a fixed cavity width $\frac{b}{\delta_0}$ and Reynolds number Re_{δ_0}, there exists a minimum depth $(\frac{d}{\delta_0})$ below which cavity does not oscillate.

The effect of non-dimensional quantities on width $(\frac{b}{\delta_0})_{min}$ and frequency $(\frac{fb}{U_e})$ will be studied systematically.

II. c. Theoretical Investigation of Cavity Oscillations

Recently, cavity oscillations have been studied theoretically by Bilanin et al,[7] McGregor et al,[37] Plumblee et al,[39] Rossiter[45] etc. Their work will be briefly described in this section.

(i) Plumblee's hypothesis is that the phenomenon of sound generation in a cavity is basically that of an enclosure responding to its natural acoustic modes. Plumblee et al. calculated the acoustic modes of a rectangular cavity with five walls having an infinite impedance and an opening whose radiation impedance has to be determined. Their results lead to a set of discrete frequencies of cavity oscillations depending on length to depth ratio. They conclude that resonant response is in the depth mode, for cavities of length to depth ratio of one or less, and in the lengthwise mode for cavities wherein

length is twice or thrice the depth. They further speculate that boundary layer noise may be taken as the forcing function in excitation of cavity oscillations. The results obtained experimentally are in reasonable agreement with those obtained by the above theory. This theory does not take into account the stability characteristics of the shear layer. The approach therefore fails to predict which natural modes are actually excited and why the frequency jumps occur.

(ii) Shear Layer Deflection Model

This model of cavity oscillations is based on the exchange of mass as the mean dividing streamline deflects in and out of the cavity with the frequency of cavity oscillations. As the mean dividing streamline deflects in, the pressure inside the cavity increases causing the mean streamline to deflect out. This causes a drop in pressure inside the cavity below the freestream pressure resulting in deflection of the mean streamline away from the external flow.

A theoretical model for mean dividing streamline motion was constructed using the Nyborg's[38] theory for edge-tone generation. In this model, the dividing streamline is assumed to form a line of fluid particles emanating from the upstream corner and propagating towards the downstream corner. An integral equation is derived for self-maintained cavity oscillations whose solution permits a set of frequencies at which a cavity can oscillate. Since cavity oscillations occur in a single mode at a given time, it is argued that the instability of the shear layer, which is not taken into account in the theory, prevents activation of the other modes which are not observed experimentally. Nyborg's theory is now described briefly (see sketch for nomenclature).

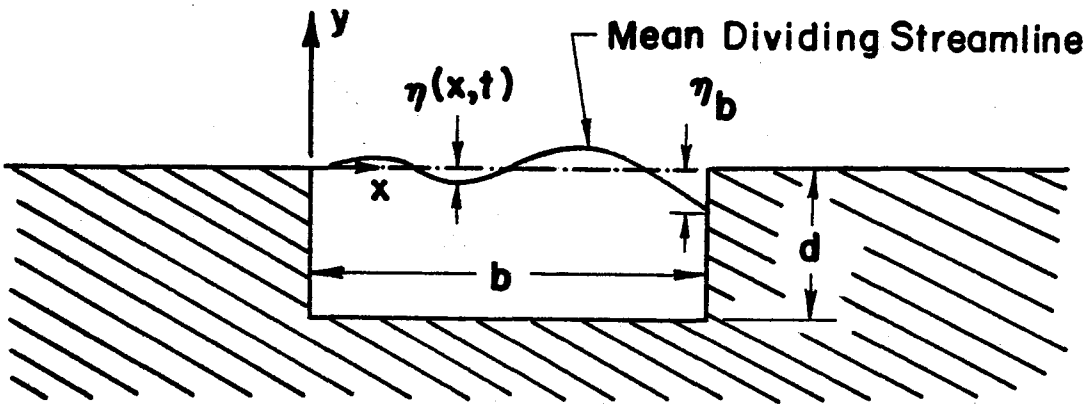

Let $\eta(x, t)$ describe the mean dividing streamline position. It is assumed that the horizontal component of velocity u of the fluid particls is independent of y and time, i.e., $u = u(x)$. If ϵ is the time required for the fluid particle to travel from $x = 0$ to x, then

$$\epsilon = \int_0^x \frac{d\zeta}{u(\zeta)}$$

If v defines the vertical component of the particle, then vertical displacement at any point x and time t is given by

$$\eta(x, t) = \int_{t-\epsilon}^{t} v(\tau)d\tau$$

Assuming that v at the upstream corner of the cavity is zero, i.e., $v(0, t) = 0$, then the vertical displacement can be written as

$$\eta(x, t) = \int_{t-\epsilon}^{t} (t-\tau)(\frac{dv}{d\tau})d\tau$$

The displacement at the downstream corner, i.e., $x = b$ is given by

$$\eta(b, t) = \int_{t=\epsilon_o}^{t} (t-\tau)(\frac{dv}{d\tau})d\tau$$

where ϵ_o is the time required for the disturbance to travel from $x = 0$ to $x = b$. With the assumption that the vertical displacement

$(\frac{dv}{d\tau})$ depends only upon instant horizontal position $[b-x(\tau)]$, and the instant value of vertical displacement $y(\tau)$ at the downstream corner, Nyborg got the following integral equation for the vertical displacement of the shear layer

$$\eta(x,t) = \int_{t-\epsilon}^{t} (t-\tau)g[b-x(\tau)]\phi[\eta(b,t)]d\tau$$

where $$g[b-x]\phi[\eta(b,t)] = \frac{dv}{d\tau}$$

At the downstream corner, where $x = b$,

$$\eta(b,t) = \int_{t-\epsilon_0}^{t} (t-\tau)g[b-x(\tau)]\phi[\eta(b,t)]d\tau \qquad (A)$$

where $$\epsilon_0 = \int_0^b \frac{d\zeta}{u(\zeta)}$$

Nyborg assumed some trial functions for ϕ and g which lead in integral equation (A) to a set of discrete frequencies of cavity oscillations. This theory does not take into account the stability of the shear layer, which plays an important role in the phenomenon of flow induced cavity oscillations. Thus the theory is inadequate to explain in which mode the cavity is most likely to oscillate and why a jump among various cavity modes occurs.

(iii) Rossiter proposed a model for possible modes of oscillation of shallow cavities. Shadowgraphs obtained by Rossiter show that pressure fluctuations at the downstream corner of the cavity are accompanied by periodic shedding of vortices from the upstream corner. Passage of the vortex over the downstream corner produces pressure fluctuations which in turn cause a vortex to be shed from the upstream corner. The basic reasoning behind Rossiter's formulation is that used by Powell[40] in describing the mechanism of

edgetone generation. Since the flow over cavities is an edgetone phenomenon, Powell's results are summarized below:

Powell argued that the presence of the edge in the jet induced a velocity perturbation at the jet slit, of a frequency which received maximum amplification through the jet. With the hypothesis that the underlying mechanism is one of a feedback, Powell arrived at a phase and frequency formula given by*

$$\frac{\psi(h)}{2\pi} = \frac{h}{\lambda} = (n + \frac{1}{4})$$

and

$$\frac{fh}{U_c} = (n + \frac{1}{4})$$

where n is the integer describing the mode of edgetone oscillations and h is the distance from jet slit to the edge.

Based on the feedback theory of edgetones, Rossiter arrived at his vortex wave interaction model. Bilanin and Covert[7] studied theoretically the possible modes of oscillation of shallow cavities and after detailed mathematical reasoning, arrived at a formula similar to one proposed by Rossiter. Heller et al.[19] correlated a great many experimental results which agreed with Rossiter's formulation. Rossiter's vortex wave interaction model is described briefly (see sketch).

---

* Similar formula of phase distribution was arrived at by Curle[12]

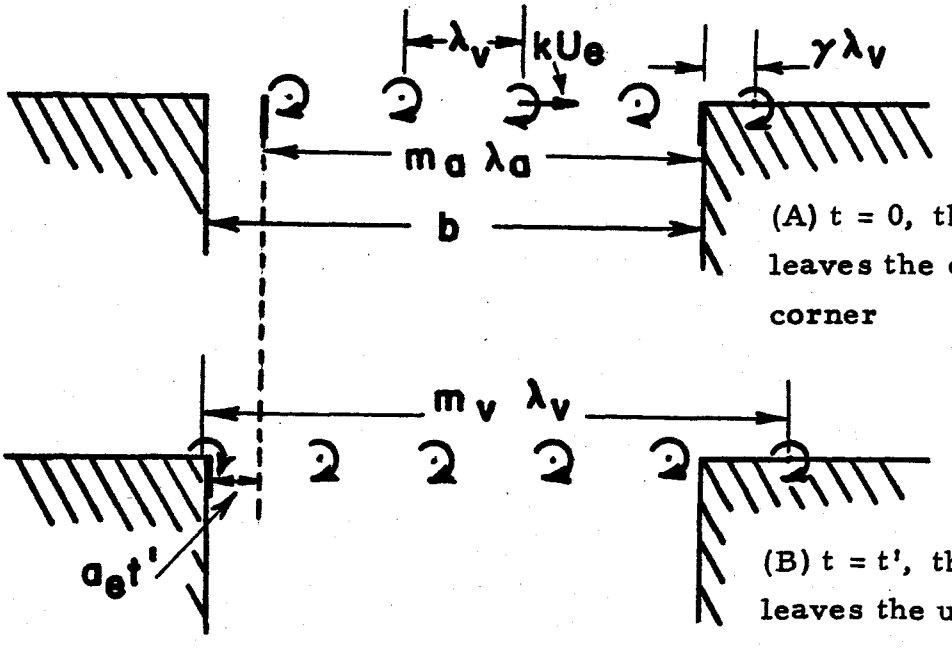

(A) t = 0, the sound wave leaves the downstream corner

(B) t = t', the vortex leaves the upstream corner

It is assumed that vortices shed from the upstream cavity corner are caused by pressure perturbations which in turn are postulated to be caused by the interaction of vortices with the downstream cavity corner. Assuming that these vortices convect at an average speed kU_e, then, since vortices and pressure perturbation are produced at the same frequency, one has

$$f = \frac{kU_e}{\lambda_v} = \frac{a_e}{\lambda_a} \qquad (1)$$

a_e is the average acoustic speed inside the cavity, λ_a the wave length of sound waves in the cavity, and λ_v is the spacing of the vortices in the shear layer.

It is further assumed that there is a phase lag between the time the vortex passes over the downstream corner and when the pressure perturbations are produced. To take into account this lag, one assumes that at the time pressure pulse is produced at the

downstream corner, the vortex is $\gamma \lambda_v$ behind this corner.

Fig. (A) gives the situation when the sound wave just leaves the downstream corner. The vortex which produced this sound wave is $\gamma \lambda_v$ behind the downstream corner. At a later time $t = t'$, a vortex is shed from the upstream corner and the flow pattern is shown in Fig. (B). Then one has

$$m_v \lambda_v = b + \gamma \lambda_v + k U_e t' \tag{2}$$

$$b = m_a \lambda_v + a t' \tag{3}$$

By solving (1), (2) and (3), we get

$$\frac{fb}{U_e} = \frac{(m_a + m_v - \gamma)}{(M_e \frac{a_e}{a} + \frac{1}{k})}$$

where $M_e = \frac{U_e}{a_e}$ is the edge Mach number. It is further assumed that $m_a + m_v = m$ an integer, and if $a_e = a$, we have

$$\frac{fb}{U_e} = \frac{(m-\gamma)}{(M_e + \frac{1}{k})}$$

For low subsonic speeds $M_e \simeq 0$, Rossiter's formula reduces to

$$\frac{fb}{U_e} = k(m-\gamma) \text{ where } m = 1, 2, 3 \text{ ------}$$

depending upon mode of cavity oscillations.

It should be noticed that, for low speeds, Rossiter's vortex wave interaction formula for cavity oscillation yields Powell's formula for edgetone if $\gamma = -0.25$. In other words, a vortex is

$\frac{1}{4}\lambda_v$ in front of the downstream corner when the acoustic wave leaves the corner.

Detailed experimental measurements of the flow field about the cavity are needed for the verification of various models of cavity oscillations.

III. EXPERIMENTAL ARRANGEMENT

III. a. Model and Wind Tunnel

In the present study, axisymmetric cavity flows were analyzed. The disturbances induced by the end walls of finite span two-dimensional cavities were thus avoided. These axisymmetric models were employed with outer diameter D of 1", 2", and 6". These models had an arrangement for variation of depth d in steps and continuously varying width b. The one-inch diameter model with a hemispherical nose was used mostly for preliminary experimental work. The main quantitative work was done on the two-inch and six-inch models. The two-inch diameter model had ojive-shape noses while an elliptic nose was used for the six-inch model. For all these models, the boundary layer at separation was laminar. The details of these models are given in Fig. 1.

The two-inch model was made of aluminum with step depths d of 0.875", 0.5", 0.25", 0.125" and 0.05". The width b could be varied continuously from 0." to 2.5". The accuracy of measuring width b was ± 0.002". This model had a family of three ojive nose shapes with $\frac{\ell}{D}$ of 0.6", 1.12 and 2.12. To check the effect of any pressure gradient before separation on cavity oscillations, the length ℓ of the ojive nose was varied by means of extensions of diameter equal to 2" and lengths equal to 1.5" and 3.0". To analyze cavity flow, a hot-wire probe was inserted from outside into the shear layer. The probe could be moved with ± 0.001" accuracy across and along the shear layer. This model had a provision for injecting smoke from inside the cavity.

This two-inch cavity model was studied in a six-inch open jet tunnel. Most of the experiments were done with the nose of the cavity at approximately one jet diameter downstream. The model was carefully centered along the axis of the jet. The longitudinal velocity fluctuations $\sqrt{\overline{u'^2}}/U_\infty$ were approximately 0.3% at U_∞ = 50 ft/sec. The intensity of longitudinal velocity fluctuations increases as one goes downstream along the jet. Mean velocity was constant throughout the potential jet core in which all the experiments were done. The model was moved as far as 15" downstream along the jet where $\sqrt{\overline{u'^2}}/U_\infty$ was 1.3%.

The second model tested, shown in Fig. 2, was of six-inch diameter D. It had a semi-ellipsoidal head with a major to minor axis ratio of 3. This model was made out of aluminum and brass. Cavity depths d could be set at 0.5", 1", 1.5" and 2". The width could be varied remotely through a gear box, as shown in the schematic layout of the model in Fig. 2. The model had provision for insertion of a hot-wire from inside the cavity. This probe could be moved along and across the axis of the model. Another hot wire probe was brought from the top of the wind tunnel and could be moved very precisely up and down and along the axis of the model. The two hot-wire probes could be moved circumferentially relative to each other to check the axisymmetry of the cavity flow. A microphone could be inserted at both the upstream and the downstream cavity corners. A Brüel and Kjaer 1/8" condenser microphone was employed to measure the pressure fluctuations inside the cavity. The ellipsoidal nose of the model had two static pressure orifices

diagonally opposite to each other. These pressure taps, which could be moved circumferentially, were used initially to align the model with the freestream velocity.

This six-inch model was tested in a 2' x 2' rectangular test section, open circuit wind tunnel. The velocity in the test section could be as high as 90 ft/sec. The longitudinal velocity fluctuations in the test section $\sqrt{\overline{u'^2}}/U_\infty$ were 0.35% at $U_\infty \simeq 50$ ft/sec. Before inserting the model into the tunnel, the mean velocity throughout the test section was checked. Below $U_\infty = 10$ ft/sec, the mean flow inside the test section was not sufficiently uniform. Above $U_\infty = 10$ ft/sec, the flow throughout the test section was within 1% of the mean. Most of the experiments, therefore, were done with U_∞ more than 10 ft/sec.

III. b. Instrumentation

Constant temperature hot-wire anemometry was extensively used in measuring both mean and fluctuating quantities. Thermo-Systems Inc.'s constant temperature anemometer model 1050 was used. Throughout this study the probe wire of 0.0002" diameter and 0.08" length was held in the fine tips of the hot-wire probe. The output of the hot-wire was fed to a Hewlett-Packard Model 3590A wave analyzer, to analyze the frequency contents of the cavity flow. The wave analyzer had variable band-widths of 10, 100, 1000 and 3100 HZ to locate closely separated signals. Electronic sweeping was used and the output of the wave-analyzer was fed to a Thermo-System-R.M.S. voltmeter. The mean square output from the R.M.S. meter (available as D.C.) was fed to an x-y plotter to measure the relative amplitude of the frequency content in the hot-wire signal.

Hot-wire output was also displayed on the oscilloscope simultaneously.

For phase angle and phase velocity measurements, the output of the two hot wires was analyzed on an SAI Correlation and Probability Analyzer. The SAI-43A Correlation and Probability Analyzer is an all-digital high speed processing instrument which provides real time computation for auto and cross correlations. The output of the correlation measurement was displayed on an oscilloscope or plotted on an x-y plotter.

To measure the pressure fluctuations inside the cavity, a $\frac{1}{8}$" Brüel and Kjaer condenser microphone was employed. To study the non-oscillating cavity shear layer, ($b < b_{min}$) the flow in the wind tunnel was excited artificially by means of a 30-watt L. B. J. speaker which was installed flush with the bottom wall of the wind tunnel, far ahead of the model.

III.c. Flow Visualization and Mass Injection

Flow around the cavity was visualized by heating the one-inch diameter model. Density gradient, caused by heating of the air adjacent to the model, was employed for taking spark shadowgraphs. To get good details of the cavity flow, considerable heating was required which could change the flow characteristics of the cavity flow. To avoid this difficulty, smoke pictures were taken by injecting smoke from inside the cavity. The latter was done at various locations, viz., close to the upstream and downstream corner, just after the downstream corner, etc., to study the details of flow around the cavity. The model was lighted from above. Both still and motion

pictures of the cavity flow were taken.

To study the effect of mass injection on cavity oscillations, air was injected circumferentially all along the base of the cavity. Provision was also made to inject the smoke just below the upstream corner to visualize the flow with and without mass injection. Since only a qualitative study was undertaken, no effort was made to measure the rate of mass injected.

IV. EXPERIMENTAL RESULTS

This section describes the experimental results of cavity-flow measurements. All measurements were made for shear flows which were laminar at separation.

IV.a. Minimum Width for Oscillations to Occur

It has been observed experimentally for flow over cavities that, for given flow conditions, there exists a minimum width b_{min} below which no oscillations occur. Also, no cavity oscillations occur below a minimum velocity $U_{e_{min}}$ for a given cavity geometry and boundary layer thickness δ_o at separation.

Fig. 3 shows the energy in the various modes of cavity oscillation as a function of width $\frac{1}{b}$. The energy in a particular mode was determined by passing the signal through the wave analyzer. The figure also indicates the frequency of oscillations f as a function of width $\frac{1}{b}$. Throughout this experiment, depth $\frac{d}{\delta_o} = 12.5$ and Reynolds number $Re_{\delta_o} = 1.04 \times 10^3$ were kept constant. The measurement of the fluctuating periodic signal was made at a fixed point from the downstream corner of the cavity. At width b_{min} approximately equal to 0.38", a strong periodic signal appeared, resulting in a sharp increase in the mode energy. For width $b > b_{min}$, the cavity began to oscillate in the second mode of oscillation with the absence of the first mode. As b was increased, the frequency of cavity oscillations decreased and the energy in the mode kept increasing until a critical value of $b \simeq 0.55$" was reached. The energy in the second mode fell suddenly and the cavity switched to the third mode of oscillation. At this width, the oscillations randomly switched among the two modes

and the energy in the two modes increased and decreased respectively. At a given moment, the cavity was oscillating in one of the two modes. As the width b was increased further, the frequency of the third mode fell again until the energy in the third mode was not measurable, due to the increased turbulence in the shear layer. A similar distribution of energy occurred when the width $\frac{b}{\delta_o}$ and the depth $\frac{d}{\delta_o}$ were kept constant and U_e was changed. At $U_{e_{min}}$, a sudden jump in the mode energy occurred, similar to the one at minimum width.

A thorough study of the cavity shear flow showed that the separated laminar shear layer remained so until maximum width b_{max} was reached. A maximum width $\frac{b_{max}}{\theta_o} \geq 100$ was observed. This width is nearly twice as large as the distance of transition from separation of the laminar free shear layer.[47, 48]

For cavity widths $b > b_{max}$, an altogether different cavity flow was observed, with transition of the separated laminar shear layer occurring around $\frac{x}{\theta_o} \simeq 40\text{-}50$. For these widths, the cavity shear flows were basically irregular and turbulent in nature. No periodic signals were noticed for these turbulent cavity flows, i.e., for $b > b_{max}$.

Fig. 4 shows the sequence of oscilloscope traces for a fixed free-stream velocity $U_\infty = 50$ ft/sec and depth $d = 0.5''$, when b was varied for $b \leq b_{min}$. For this cavity flow, the minimum width was $0.275''$. It should be noted that for width $b < b_{min}$, periodic velocity fluctuations existed in the shear layer which scaled with width b (cf Fig. 3). As the minimum width was reached, i.e., $b = 0.275''$, a sudden jump in the mode energy occurred, and the cavity shear

flow began to oscillate violently. The last two oscilloscope traces were taken at $b_{min} = 0.275''$ but at different times. They clearly show how periodic signals appear and disappear randomly.

Flow visualization by smoke injection (which will be discussed later) indicated that for $b < b_{min}$, the separated flow stayed laminar as it passed over the cutout and attached just below the downstream corner. The flow behaved in a similar fashion as width b was increased, until the minimum gap for the given flow was reached. At $b = b_{min}$, the shear layer close to the downstream corner began to oscillate vigorously and this resulted in a large increase in the mode energy.

On the basis of the above experiments, the minimum width for a given flow and cavity depth is defined as the shortest gap for which a sudden increase in the cavity's mode energy occurs (cf Fig. 3). Minimum edge velocity is defined in a similar way.

A detailed investigation of the effect of flow and cavity geometry on the onset of the cavity oscillations was undertaken on the two inch diameter model. The test was done in the 6" free-jet tunnel. A family of three ojive nose shapes (with $\frac{\ell}{D} = 0.6,\ 1.12$ and 2.12) were employed. For a fixed nose shape and depth d, edge velocity U_e was determined for various widths b at which the cavity began to oscillate. For the same nose shape, the above experiment was repeated with five different depths. This gave one set of experimental data. Two other similar sets of data were obtained for the other two nose shapes. A total of ninety data points of known

U_e, δ, b, d and f at which oscillations began were obtained. When the data were non-dimensionalized and plotted as a non-dimensional width $\frac{b_{min}}{\delta_o}\sqrt{\frac{U_e \delta_o}{\nu}}$ against the non-dimensional depth $\frac{d}{\delta_o}$, all the experimental results fell on a single curve. Fig. 5 shows the results of the experiments. No cavity oscillations occur below these points. It is clear from these results that the depth has little effect on the non-dimensional width $\frac{b_{min}}{\delta_o}\sqrt{\frac{U_e \delta_o}{\nu}}$ when depth $\frac{d}{\delta_o} > 2$. There is a sharp increase in $\frac{b_{min}}{\delta_o}\sqrt{Re_{\delta_o}}$ when $\frac{d}{\delta_o} \sim O(1)$.

To investigate the effect of any pressure gradient before separation, the length of the ojive nose was varied by means of two cylindrical extensions. Relatively thick boundary layers, which were laminar at separation, were obtained. The minimum width for a particular depth was determined again by changing edge velocity U_e. These results are also shown in Fig. 5.

To verify the above results for minimum width, the three ojive nose shape models were tested at different edge velocities, so that the thickness of the shear layer for all these models at separation was constant. By keeping the depth constant, the minimum width b_{min} was determined. This experiment was repeated for five different shear layer thicknesses at separation. The results indicated that $b_{min}\sqrt{U_e}$ stayed constant for a fixed value of the depth $\frac{d}{\delta_o}$ for each of the five cases tested above. This is what one will expect from the universal curve $\frac{b_{min}}{\delta_o}\sqrt{Re_{\delta_o}}$ vs. $\frac{d}{\delta_o}$. Experimental results are tabulated in Table 1.

The effect of freestream conditions on cavity oscillations and, in particular, on the minimum width was investigated. For

this experiment, a one-inch cavity model was studied in the six-inch free jet. The model was moved along the axis of the jet within the potential core where the mean edge velocity stayed constant. The results obtained are shown in Fig. 6. The curve indicates freestream fluctuations in front of the cavity at different downstream stations from the jet exit. At x = 4", 8" and 12" where $\frac{\sqrt{\overline{u'^2}}}{U_\infty}$ was 0.26%, 0.77% and 1.64%, respectively, minimum width b_{min} for $U_\infty = 50$ ft/sec was determined. The results, as indicated on the curve, show that b_{min} is independent of the freestream fluctuation within the above range. The influence of freestream disturbances on cavity oscillations, out of the potential core, further shows that the phenomenon of cavity oscillation is independent of the freestream turbulence.

IV. b. Non-dimensional Frequency of Cavity Oscillations

For an axi-symmetric model, the non-dimensional frequency $\frac{fb}{U_e}$ for low subsonic flows can be expressed as

$$\frac{fb}{U_\infty} = F\left(\frac{U_\infty \ell}{\nu}, \frac{b}{D}, \frac{d'}{D}, \frac{\ell}{D}, \text{mean velocity profile at separation, etc.}\right)$$

Experimental results (shown later) indicate that non-dimensional frequency is independent of $\frac{\ell}{D}$ and the most important parameters defining cavity oscillations are U_e and δ_o instead of U_∞, D and ℓ. Therefore, one can write non-dimensional frequency $\frac{fb}{U_e}$ as a function

$$\frac{fb}{U_e} = F'\left(\frac{U_e \delta_o}{\nu}, \frac{b}{\delta_o}, \frac{d}{\delta_o}, \text{mean velocity profile at separation, etc.}\right)$$

To study the dependence on non-dimensional frequency of Reynolds number $Re_{\delta_o} = \frac{U_e \delta_o}{\nu}$, depth $\frac{d}{\delta_o}$ and width $\frac{b}{\delta_o}$, each

of them was varied separately, keeping others constant. To measure the frequency of cavity oscillations, hot-wire measurements of the longitudinal velocity fluctuations u' were analyzed.

IV. b. (i) Effect of Width

Fig. 7 shows the effect of width on cavity oscillations at Reynolds number $Re_{\delta_o} = 2.86 \times 10^3$ and depth $\frac{d}{\delta_o} = 10$ where non-dimensional frequency $\frac{fb}{U_e}$ is plotted against non-dimensional width $\frac{b}{\delta_o}$. No cavity oscillations occurred below $\frac{b}{\delta_o} = 5.25$ which represents the minimum width $(\frac{b}{\delta_o})_{min}$. First mode fluctuations occurred at a non-dimensional frequency of about 0.6. There was a slow increase in non-dimensional frequency as $\frac{b}{\delta_o}$ increased. As the critical value of $\frac{b}{\delta_o} = 8.15$ was reached, oscillations jumped to a higher mode. At this width two modes occurred alternately. The two modes never occurred simultaneously. Under certain flow conditions, switching between the two modes was audible. The second mode of cavity oscillations occurred at about a non-dimensional frequency of 0.95. As the width $\frac{b}{\delta_o}$ was increased slightly beyond the critical value of 8.15, the first mode disappeared and the flow began to oscillate in the second mode of cavity oscillation. As the width was decreased, the cavity oscillations jumped back to the first mode where the width $\frac{b}{\delta_o}$ was 8.15, and no significant hysterisis region was noticed. Beyond $\frac{b}{\delta_o} > 10$, the flow over the cavity became irregular and the periodic velocity fluctuations ceased to exist or were weaker than the turbulence fluctuations in the shear layer.

Fig. 8 shows another typical operation of cavity oscillations at a Reynolds number $Re_{\delta_o} = 0.92 \times 10^3$ and depth $\frac{d}{\delta_o} = 12.95$ in which the cavity began to oscillate in its second mode of oscillation. The second mode of oscillation occurred at a non-dimensional frequency $\frac{fb}{U_e} = 0.95$. The non-dimensional frequency slowly increased as the width was increased until a critical value of $\frac{b}{\delta_o} = 12.95$ was reached and the cavity oscillations jumped to a higher mode of oscillation. The third mode of cavity oscillation occurred around a non-dimensional frequency of about 1.4. As width $\frac{b}{\delta_o}$ increased beyond 18.10, periodic velocity fluctuations of the shear layer disappeared and turbulence was observed without the cavity flow switching to higher modes.

IV. b. (ii) Effect of Depth

Fig. 9 represents the effect of depth $\frac{d}{\delta_o}$ on non-dimensional frequency $\frac{fb}{U_e}$ at a fixed Reynolds number $Re_{\delta_o} = 0.96 \times 10^3$ and width $\frac{b}{\delta_o} = 11.0$. The minimum width $\frac{b_{min}}{\delta_o}$ for the onset of cavity oscillations was 9.40. The cavity began to oscillate in the second mode of oscillation with a non-dimensional frequency $\frac{fb}{U_e}$ of about 0.80. The results in Fig. 9 show that the non-dimensional frequency was independent of depth $\frac{d}{\delta_o} \leq 6$. In cavity flows with a depth $\frac{d}{\delta_o}$ less than 5, non-dimensional frequency dropped slowly as depth was decreased. The four points on the figure correspond to $\frac{d}{\delta_o} = 20.25$, 11.57, 5.78 and 2.87. At $\frac{d}{\delta_o} = 1.34$ oscillations disappeared. Therefore, somewhere between $1.34 < \frac{d}{\delta_o} < 2.87$ is the value of $(\frac{d}{\delta_o})_{o\ min}$ below which no cavity oscillations occur. Due to the limitations of the model, this minimum depth could not be determined precisely.

IV. b. (iii) Cavity Oscillations at Different Reynolds Numbers

Fig. 10 shows the results of the effect of Reynolds number Re_{δ_o} on non-dimensional frequency $\frac{fb}{U_e}$. During this experiment

$\frac{b}{\delta_o}$ was kept constant. Since the non-dimensional frequency is independent of depth for $\frac{d}{\delta_o} \geq 6$, depth $\frac{d}{\delta_o}$ was not constant though care was taken not to decrease the depth below the above limit. Experimental results for three ojive nose shapes with $\frac{\ell}{D} = 0.6$, 1.12 and 2.12 are plotted in Fig. 10. For any particular model, shear layer thickness at separation decreases as edge velocity increases. Therefore, to keep the non-dimensional width $\frac{b}{\delta_o}$ constant, the cavity width b was decreased accordingly when the edge velocity U_e was changed. Width $\frac{b}{\delta_o}$ was 12.76 throughout the experiment.

Within the range of Reynolds numbers $\frac{U_e \delta_o}{\nu}$ tested (0.6×10^3 to 1.5×10^3), cavity oscillations occurred in the second mode of oscillation with a non-dimensional frequency in the range of 0.8-0.9. Data points for different fineness ratios ($\frac{\ell}{D}$) fall on a single curve. It was stated in the beginning of this section that non-dimensional frequency $\frac{fb}{U_\infty}$ is a function of $\frac{U_\infty \ell}{D}$, $\frac{b}{D}$, $\frac{d'}{D}$, $\frac{\ell}{D}$ etc. Since $\frac{fb}{U_e}$ is independent of depth and for a fixed width $\frac{b}{\delta_o}$, is also independent of $\frac{\ell}{D}$, and it appears that the most appropriate parameters defining cavity oscillations are U_e and δ_o instead of U_∞, D and ℓ. This reduces the important non-dimensional parameters of cavity oscillations by one. Hence one can conclude that non-dimensional frequency $\frac{fb}{U_e}$ is only a function of Reynolds number $\frac{U_e \delta_o}{\nu}$, depth $\frac{d}{\delta_o}$ and width $\frac{b}{\delta_o}$.

IV. c. Mean Velocity Profiles in Shear Layer

The transverse coordinate y (measured positive upward from the edge of the cavity), is non-dimensionalized by the momentum

thickness θ, defined as

$$\theta = \int_{-\infty}^{\infty} \frac{U}{U_e}\left(1 - \frac{U}{U_e}\right) dy$$

where U_e is the velocity at the edge of the shear layer. Edge velocity U_e was almost constant along the cavity width. The mean velocity profiles at various downstream locations in non-dimensional form are plotted in Fig. 11 against $(y-y_{\frac{1}{2}})/\theta$, where $y_{\frac{1}{2}}$ corresponds to $\frac{U}{U_e} = 0.5$. The locus of $y_{\frac{1}{2}}/\theta$ is shown in Fig. 12. The cavity was oscillating in the first mode of oscillation with $\frac{fb}{U_e} = 0.67$. The downstream corner was located at $\frac{b}{\theta_o} = 60$. The depth and the Reynolds number at separation were $\frac{d}{\theta_o} = 100$ and $Re_{\theta_o} = 2.42 \times 10^2$.

As is clear from Fig. 11, in the early stages of shear layer growth, the velocity profile changes from a boundary layer profile to a shear layer profile. A similarity has been established at $\frac{x}{\theta_o} \simeq 15$. No measurements of mean velocity profile could be made beyond $\frac{x}{\theta} = 50$ because of the presence of the downstream corner. Velocity fluctuations $\sqrt{\overline{u'^2}}/U_e$ as high as 0.15 were noticed in the shear layer close to the downstream corner. Results of cavity flow visualization by smoke injection, discussed later, show that these large velocity fluctuations are attributed to large lateral motion of the cavity shear layer close to the downstream corner.

To study the effect of cavity oscillations on the growth of the shear layer, mean velocity profiles were measured for various

widths $\frac{b}{\theta_o}$ when edge Reynolds number $Re_{\theta_o} = 2.42 \times 10^2$ and depth $\frac{d}{\theta_o} = 100$ were kept constant. From these results, the momentum thickness as defined above was computed at various downstream locations $\frac{x}{\theta_o}$. Fig. 13 indicates the growth of the shear layer $\theta(x)/\theta_o$ as a function of $\frac{x}{\theta_o}$. Results for four cavity widths $\frac{b}{\theta_o}$ equal to 52.5, 60, 85 and 105.2 were analyzed. These correspond to cavity configurations when oscillations just appeared, oscillations in the first mode, cavity flow switching between the first and second modes of oscillation and finally, the cavity in its second mode of oscillation, respectively.

It is clear from these results that the growth of the shear layer was almost linear with x/θ_o in all modes of cavity oscillation. Growth rate $\frac{d\theta}{dx}$ increased in magnitude with increasing cavity widths but no sudden jump in growth rate occurred when cavity flow switched from one mode of oscillation to another. The growth rate $\frac{d\theta}{dx}$, which is a measure of rate of fluid mass entrained by the growing shear layer from inside the cavity, can be studied as a function of cavity width from results shown in Fig. 13. An entrainment rate $\frac{d\theta}{dx}$ as low as 0.006 was observed when the cavity began to oscillate. This increased to a value as high as 0.022 for large cavity widths when oscillations were in the second mode. Cavity oscillations are responsible for these large entrainment rates in the laminar shear layer. It should be noted that these entrainment rates are quite large for laminar shear layers and are comparable to the entrainment rate of the turbulent mixing layer which is $\frac{d\theta}{dx} \simeq 0.035$ (cf Ref. 22).

IV.d. Phase Measurements

Phase measurements of the shear layer velocity fluctuations were made by cross-correlating the hot-wire signals at different space locations. The reference hot-wire probe was brought from inside the cavity without disturbing the flow around the cavity. This probe was placed sufficiently downstream so that the shear layer velocity fluctuations were approximately sinusoidal. Throughout this experiment, the reference probe was kept fixed. Another probe, which could be moved relative to the reference probe, was brought from outside.

Before taking any phase measurement, axial symmetry of the shear layer flow around the cavity was tested. With respect to the reference probe, the second probe was moved circumferentially, while keeping their relative positions from the upstream corner constant. Phase measurements were made at different relative circumferential positions. This experiment was repeated with different spatial positions of the second probe from the upstream corner. Results showed that the flow around the cavity was axi-symmetric.

All the phase measurements were made relative to the phase at the upstream corner, $x = 0$, $y = 0$. Because of very small velocity fluctuations, no measurements could be made close to the upstream corner. Measurements close to the upstream cavity corner showed a linear phase distribution with downstream distance x/θ_o. These

results were extrapolated near this region to determine the phase of the disturbances at the upstream corner.

Typical phase-angle measurements at Reynolds number $Re_{\delta_o} = 2.86 \times 10^3$, width $\frac{b}{\delta_o} = 6$ and depth $\frac{d}{\delta_o} = 10$ are shown in Fig. 14. The flow was oscillating at a frequency $f = 625$ Hz, corresponding to a non-dimensional frequency $\frac{fb}{U_e} = 0.67$. The numbers in Fig. 14 represent the phase $\frac{\psi}{2\pi}$, (measured in terms of wave length) at various space locations by which the propagating disturbances lagged behind the upstream cavity corner. Fig. 15 shows constant phase lines of the propagating disturbances relative to their phase at $x = 0$ and $y = 0$. These lines have been drawn from experimental results in Fig. 14.

It is clear from Figs. 14 and 15 that the phase at a fixed location $\frac{x}{\delta_o}$ varies a great deal across the cavity flow. As one moves toward the cavity from outside ($\frac{x}{\delta_o}$ = constant) the measurements show that the phase of the disturbance decreases until one reaches the region denoted by the broken line in Fig. 14. In this region a sharp drop in phase occurs. As one moves further inside the cavity, the phase of the disturbance increases. Far outside the cavity, the phase shows a linear decrease with $\frac{y}{\delta_o}$ while far inside the measurements show a linear increase of phase.

Fig. 16 shows the oscilloscope traces of velocity fluctuations at $\frac{x}{\delta_o} = 4$ at various $\frac{y}{\delta_o}$ locations when the oscillations were in the first mode of oscillation. The flow and cavity configurations were the same as in Fig. 14. One clearly sees that the velocity fluctuations

are sinusoidal outside the cavity as well as inside the cavity with an intermediate region where velocity fluctuations of a higher harmonic occur. This region is denoted by dotted lines in the phase angle measurements of Fig. 14.

Phase-angle distribution of velocity fluctuations at $\frac{y}{\delta_o} = 0$ as a function of $\frac{x}{\delta_o}$ is shown in Fig. 17. The solid line on the wave is Powell's phase criterion, given by $\frac{h}{\lambda} = n + \frac{1}{4}$ where n is the integer representing the mode of jet edge-tone operation and h is the distance from the slit to the edge. According to Powell's theory,[50] the phase of the propagating disturbances varies linearly with distance x. For the first mode of oscillation, this formula gives a phase $\frac{\psi}{2\pi} = 1.25$ at the downstream corner relative to its phase at the upstream corner. As is clear from Fig. 17, the phase of the disturbances changes linearly with x but gives $\frac{\psi}{2\pi} \simeq 1.5$ instead of 1.25, as predicted by Powell's criterion.

Phase measurements of propagating disturbances through the shear layer were obtained for various cavity widths. From these measurements, the wave lengths of the disturbances were calculated. For these cavity configurations, the oscillating frequency f was known, hence the phase speed $U_c = \lambda f$ was computed. Present studies indicate that the disturbance in the shear layer propagates at a constant phase velocity if one moves along the line where $\frac{U}{U_e} = \text{constant}$. From the mean velocity and phase measurements, the phase velocity of the disturbances was computed as a function of width $\frac{b}{\delta_o}$.

Experimental results indicate that for a fixed depth $\frac{d}{\delta_o}$ and Reynolds number $\frac{U_e \delta_o}{\nu}$, as width $\frac{b}{\delta_o}$ was increased, the wave

length λ increased and the frequency of the disturbances dropped, but the product $f\lambda = U_c$ slowly increased in magnitude. This trend was maintained until a critical value of $\frac{b}{\delta_o}$ was reached when the oscillation jumped to a higher mode. This caused a sudden drop in wave length λ of the disturbances and a sudden increase in the frequency of the oscillations. But the phase velocity of the disturbance $U_c = \lambda f$ increased steadily as the width $\frac{b}{\delta_o}$ was further increased without any discontinuity as the oscillation switched modes.

Results of the phase velocity U_c/U_e as a function of width $\frac{b}{\delta_o}$ when the cavity was oscillating in its first and second modes of oscillation are indicated in Fig. 18. Throughout the above experiment, depth $\frac{d}{\delta_o} = 10$ and Reynolds number $Re_{\delta_o} = 2.86 \times 10^3$ were kept constant. As is clear from the results, the phase velocity of the disturbances increased with width until it reached a value of approximately $\frac{U_c}{U_e} \simeq 0.5$. No measurements could be made beyond $\frac{b}{\delta_o} > 10.5$ because of increased turbulence in the shear layer.

Fig. 19 shows the ratio of λ/b as a function of cavity width $\frac{b}{\delta_o}$ where Reynolds number $Re_{\delta_o} = 2.86 \times 10^3$ and depth $\frac{d}{\delta_o} = 10$ were fixed. Results for both first and second modes are shown. It should be noted that the wave lengths of the disturbances bear a nearly constant ratio to width b in any particular mode. This ratio jumps to a lower value as the cavity goes to a higher mode. This is an important experimental result indicating that the wave lengths of the propagating disturbances have a definite integral relation to the cavity width, for each mode of cavity oscillation.

IV.e. Effects of Cavity Geometry on Oscillations

All measurements so far were made using a model with a rectangular cavity. In order to assess the significance of the details of the flow field inside the cavity, a thin disc was mounted inside the cavity as shown in Fig. 20(A). The parameters b' and D' were varied in steps. The main observations were that the frequency of oscillations remained independent of the disk location as long as $b' < b_{min}$ and D' was not large enough to interact significantly with the free shear layer near the top of the cavity. From this experiment one can conclude that the details of the flow inside the cavity are not of importance for the periodic oscillation phenomenon.

In a second experiment, a lip was added to the downstream corner as shown in Fig. 20(B). It was found that b' and not b was the important dimension with which the frequency is scaled. The scaling is the same as in Fig. 7. Hence the volume of the cavity has little effect on the frequency of oscillations. This indicates that the shallow cavity oscillation phenomenon is not a cavity resonance phenomenon as it is for deep cavities (Cf Ref. 15).

To verify the above conclusion further, holes were drilled circumferentially as shown on Fig. 20(B) to allow an exchange of mass between the cavity and the outer flow. The effect of closing and opening these holes on the frequency of cavity oscillations was investigated. These results indicate that the phenomenon of cavity oscillations based on the interaction between the shear layer deflection and internal pressure is inadequate to explain the mechanism

of oscillations in the flows over cavities.

IV. f. Flow Visualization

Fig. 21a is a typical spark shadowgraph of the cavity flow. This shadowgraph picture was taken on a one-inch diameter model with free stream velocity U_∞ = 50 ft/sec, b = 0.425" and d = 0.25". The flow was visualized by heating the model above room temperature. As a result air close to the model became hot as it flowed around it. This resulted in a density gradient which deflected the light rays and created a shadow effect. A high-intensity point spark source was placed at the focus of an 18" concave mirror to get an intense parallel light beam. This parallel light beam was passed over the heated model and shadowgraphs were photographed on a high speed film.

The spark shadowgraph picture shown in Fig. 21a indicated that vortices were formed by the interaction of the shear layer with the downstream edge and were shed downstream at the frequency of cavity oscillations. As mentioned above, to get a good shadowgraph effect, excessive heating was required. Too much heating may change the mean boundary layer profile and hence the stability characteristics of the cavity shear flow. To avoid this problem, the shear layer was visualized by injecting smoke into it. Continuous white smoke was injected from inside the cavity. Care was taken not to disturb the shear layer. The model was lighted from above and both instant and motion smoke pictures were taken from the side. What one sees in such a photograph are the instant streaklines. Figs. 21 (b), (c), (d) and (e) are typical smoke pictures of cavity

flow. All of these pictures were taken on the two inch diameter model at a freestream velocity of 20 ft/sec. For all these smoke pictures flow was from left to right.

Figs. 21(b) and (c) show a non-oscillating cavity, i.e., width $b < b_{min}$. As stated before, the above pictures showed that for width b less than b_{min}, the shear layer bridged the gap smoothly and attached close to the downstream corner. The flow remained laminar and without large oscillations until b_{min} was reached. At b_{min}, violent cavity oscillations appeared which persisted as width b was further increased. This condition is shown in Fig. 21(d). Fig. 21(e) shows cavity flow for width $b > b_{min}$.

Figs. 22(a) show the effect of depth d on the development of a separated shear layer. The width b in these pictures was 2.0", which was much larger than b_{max} at which the cavity oscillations existed. The shear flow near separation was independent of the downstream corner. Fig. 22a(i) has a depth d = 0.425". The smoke picture shows that transition of the laminar shear layer occurred very close to the upstream corner. On the other hand, Fig. 22a(ii), for which depth d = 0.05", shows that the transition from a laminar flow to a turbulent one was delayed quite far beyond the upstream cavity corner. This indicates that shallow cavities have a stabilizing effect on the separated shear layer and consequently require a longer b_{min} for the onset of cavity oscillations, as compared to deep cavities (cf Fig. 5).

Fig. 23 shows two sets of four consecutive frames of motion pictures taken on a one-inch diameter model. The flow is from

right to left. The freestream velocity was 30 ft/sec with cavity width b = 0.70" and depth d = 0.425". Due to lack of a very intense steady light source, one could only go as high as 500 frames/sec. The oscillations occurred at a frequency f = 300 Hz. Results of the motion pictures are summarized below:

(A) Strong interaction with the downstream corner occurred when the cavity oscillations began at $b = b_{min}$.

(B) When the cavity was oscillating, the mean streakline did not oscillate much until it was very close to the downstream corner. Strong oscillations of the shear layer occurred in the vicinity of the downstream corner.

(C) At the downstream corner, the mean streakline oscillated in and out at cavity oscillation frequency. As the streakline entered the cavity, the shear layer rolled up into a vertex which was shed as it deflected out of the cavity. Fig. 23 1(i) shows the most inward position of the shear layer with a vortex, shed a little earlier, at the downstream corner. In Fig. 23 1(ii), the shear layer is in its most outward position and is ready to shed a vertex. The process continues at the frequency of cavity oscillations.

Fig. 23(2) shows a similar sequence of cavity oscillations.

IV. g. Effect of Mass Injection on Cavity Oscillations

The influence of the addition of mass on the cavity flow when it begins to oscillate was investigated experimentally. Results indicated that cavity oscillations could be delayed with the introduction of a small quantity of air. To understand the flow, smoke was injected at the upstream cavity corner. Results obtained are shown

in Figs. 22(b). Study of the smoke pictures indicated that the shear layer was effectively blown out of the cavity with the continuous addition of a finite mass. This reduced the interaction with the downstream corner and consequently cavity oscillations were postponed. Oscillations reappeared when either width or the edge Reynolds number Re_θ were increased. One can, in principle, delay the cavity oscillations with a further addition of mass, but the present experiments indicated that an excess amount of mass injection spoiled the cavity shear flow. This may be attributed to excessive radial momentum imparted to the cavity shear layer. No quantitative measurements of mass addition were undertaken in this study.

IV. f. Some Miscellaneous Observations About Cavity Flow

(1) To measure the frequency of cavity oscillations, the fluctuating component of the mean velocity was analyzed. On surveying the shear layer with the hot wire probe, it was found that the u' fluctuations were almost sinusoidal in the shear layer except close to the downstream corner. In this region the wave form of the u' fluctuations was quite complex. Due to rolling up of vortices in the vicinity of the downstream corner, the non-linear effects became predominant. Higher harmonics of the fundamental frequency of cavity oscillations were noticed because of superimposed non-linear velocity fluctuations. These higher harmonics should not be confused with the higher modes of the cavity oscillations. To avoid this difficulty, most of the frequency measurements were made at the outer edge of the shear layer, slightly in front of the downstream corner.

(2) On carefully analyzing the cavity flow before intense oscillations occurred, i.e., $b < b_{min}$, it was noticed that periodic fluctuations of very small magnitude were present and their frequency scaled with the cavity width (Cf Figs. 3 and 4). The energy associated with such fluctuations was very small compared to cavity fluctuations when width $b > b_{min}$. Fig. 3 indicates experimental results for both oscillating and non-oscillating cavities.

Results in Fig. 4 show hot-wire output signals of u' fluctuations in cavity shear flow for $b \leq b_{min}$. The flow of non-oscillating cavities with $b < b_{min}$ was studied under the influence of artificial excitation. The present study shows that the cavity could be put into intense oscillation when excited at a frequency which lay on the curve f vs. $\frac{1}{b}$ when extended beyond $b < b_{min}$ (Fig. 3). Cavity flow did not respond to artificial excitation away from this frequency. On turning off the external excitation, the cavity flow came back to its original non-oscillating state. Careful study of the hot-wire signal, when acoustic energy was turned on and off, showed that the cavity flow took a finite time to come to its equilibrium state of oscillation. These results suggest that the cavity oscillation system has some kind of inherent damping in it which has to be overcome by the strong interaction of the cavity shear layer with the downstream corner.

(3) The visualization of cavity flow with a one-inch diameter model with a semi-hemispherical nose showed that the shear layer blew out of the cavity and reattached behind the downstream cavity corner. This might have been caused by the separation of the boundary layer ahead of the upstream cavity corner. As the cavity

width b was increased, this reattachment point moved closer to the upstream corner until a critical value of width b''_{min} was reached which resulted in strong cavity oscillations. Experiments showed that cavity oscillations could be delayed for quite large widths $b''_{min} > b_{min}$. This seems to be a practical way of designing a non-oscillating cutout in which an interaction of the cavity shear layer and the downstream cavity corner is avoided.

V. RELATION OF CAVITY-FLOW OSCILLATIONS TO SHEAR LAYER STABILITY

V.a. Inferences Drawn from the Results Compared with Existing Models

In this section, the experimental results will be reviewed in relation to existing cavity oscillation models. To emphasize the results, the key features of the present study are summarized below:

(1) The experiments show that oscillations in shallow cavities are independent of the volume of the cavity. Oscillation frequency remains unchanged even when an exchange of mass between the cavity and the outer flow is allowed. Therefore, a mechanism of cavity oscillations based on the interaction between the shear layer deflection and internal pressure, as emphasized in the shear layer deflection model (cf section II. c.), seems inadequate to explain flow oscillations in cavities.

(2) Phase measurements for a given cavity flow indicate that the phase speed of the disturbances stays constant over the whole length of the shear layer (i.e., the width of the cavity) in magnitude as the width is increased. It is further noticed that during any particular mode of oscillation, the wave length λ of the disturbances bears nearly a constant relationship to the width b of the cavity. The spacing of the periodic vortices which are shed from the downstream corner at the frequency of cavity oscillations further confirms such an integral relationship between b and λ. The present results suggest that $b \simeq \lambda(N+\frac{1}{2})$ where N can be 0, 1, 2, 3, --- etc.

(3) Measurement of the longitudinal velocity component u in the cavity shear layer (except close to the upstream and the downstream corner) indicates a similarity in the mean velocity profile.

The experimental results indicate that the integral relation between the cavity width b and the wave length λ of the disturbances is not $N+\frac{1}{4}$ or N where N can be 1, 2, 3, --- etc., depending upon the mode of oscillation, as has been predicted by Powell's phase criteria and wave interaction model. As stated above, this study suggests a phase relation given by $\frac{b}{\lambda} \simeq (N+\frac{1}{2})$ where N can be 0, 1, 2, 3, --- etc. During the present study, oscillations in the cavity's fundamental mode with $b \simeq \frac{\lambda}{2}$ were never noticed, as it had been observed in edge-tones by Karamcheti[21] and Bauer. It should be noted that in the experimental results presented above, the first mode of cavity oscillation corresponds to an integral relation between the wave length of the disturbance and the cavity width $b \simeq \frac{3}{2}\lambda$ (Fig. 17). It has been further observed that, under certain flow conditions, oscillations began in the second mode of oscillation, ($b \simeq \frac{5}{2}\lambda$) with absence of oscillations in the first mode. The reasons for the selection of a particular mode of oscillation remained obscure during the earlier part of this study. It is clear from the present experiments that definite criteria exist for the cavity to oscillate in a certain mode. To try to obtain insight into these criteria and clarify the conditions which cause a shift in the cavity mode, a stability analysis of the self-similar experimental mean velocity

profile was undertaken. This is described in Appendix II. Experiments by Karamcheti [21, 50, 51] et al. on the edge-tone flow field showed that the disturbances in the jet do not convect at a constant phase speed. Their study further showed that the amplification of the disturbances is not exponential, as has been predicted by the linearized stability theory of parallel shear flows. In order to explain such behavior, they conclude that the jet should be treated as a non-parallel flow field. In light of their experiments on the edge-tone system, Woolley[54] and Karamcheti extended their arguments to cavity flows and suggested that the cavity shear layer should also be treated as non-parallel shear flow. They speculate that the frequency which receives the maximum total integrated amplification over the length of non-parallel shear layer spanning a cavity of width b should be the one at which the cavity is most likely to oscillate. A review of the existing literature does not reveal any experimental evidence to justify the above arguments. In contrast to edge-tone flow measurements, the present experiments indicate that the disturbances propagate at a constant phase velocity. As a first approximation, therefore, a calculation of the integrated amplifications of different frequencies and their phases along the shear layer (whose profiles and growth rate $\theta = \theta(x)$ are known a priori) was undertaken.

To evaluate the phase and the integrated amplification of a disturbance of a fixed frequency, as it propagates through the growing cavity shear layer, the results of the stability characteristics of the mean cavity shear flow are required. If the variation of the shear layer momentum thickness over the wave length λ of the disturbances

is small, the flow, as a first approximation, can be treated as a quasi-parallel shear flow. The results are, therefore, more accurate when applied to cavity flows oscillating in higher modes of cavity oscillation.

Appendix II gives the derivation of the equations of motion for stability analysis of the inviscid, and parallel shear flows. For numerical computations, the undisturbed mean velocity profile $\bar{U}(\bar{y}) = 0.5\ (1+\tanh 0.52\ \bar{y})$ was chosen. This profile agrees quite well with the measurements, as Fig. 24 shows. Close to the inner edge of the shear layer, the measurements do not agree well with the assumed mean velocity profile. At these points the velocity fluctuations are comparable with the mean velocity. Therefore, the accuracy of hot-wire velocity measurements is very doubtful. Stability of both temporally and spatially propagating disturbances was studied. Fig. 25 shows the amplification rates of temporally and spatially growing small disturbances, as a function of non-dimensional frequency $\frac{f\theta}{U_e}$ for the assumed mean velocity profile. The effect of non-dimensional frequency on phase speed $\frac{U_c}{U_e}$ is indicated on Fig. 26. The results of Figures 25 and 26 were used to calculate the integrated amplification and the phase of various disturbances along the cavity shear layer, as described in sections V.b. and V.c. These results were used to predict possible cavity modes and the frequencies the cavity shear layer is most likely to select (cf section V.d.).

V. b. Theoretical Basis for Computing Integrated Amplification of a Propagating Disturbance Through the Cavity Shear Flow

Assume that for the two-dimensional, inviscid, and parallel flow, the small propagating disturbances are given by the stream function

$$\psi' = \phi(y)\, e^{i(\alpha x - \omega t)}$$

and $$\frac{\partial \psi'}{\partial y} = \phi'(y) e^{i(\alpha x - \omega t)}$$

$$u' = \text{Real}\left[\frac{\partial \psi'}{\partial y}\right] = \text{Real}\left[\phi'(y) e^{i(\alpha x - \omega t)}\right]$$

Let $\phi'(y) = |\phi'(y)| e^{i\psi}$, then

$$u' = |\phi'(y)|\ \text{Real}\left[e^{i(\alpha x - \omega t + \psi)}\right] \qquad (1)$$

Consider the spatially growing disturbances where wave number α is complex and frequency ω is real, then

$$\alpha = \alpha_r + i\,\alpha_i$$

Define $\theta \equiv \alpha_r x - \omega t + \psi$

Substituting for α in (1), one gets

$$u' = |\phi'(y)| e^{-\alpha_i x} \cos\theta$$

$$\overline{u'^2} = |\phi'(y)|^2 e^{-2\alpha_i x} \cdot \frac{1}{2\pi} \int_0^{2\pi} \cos^2\theta\, d\theta$$

$$= \tfrac{1}{2} |\phi'(y)|^2 e^{-2\alpha_i x}$$

$$\text{Let} \quad \frac{\sqrt{\overline{(u')^2}}_{max}}{\sqrt{\frac{1}{2}\left|\phi'(y)\right|^2}_{max}} \equiv a = e^{-\alpha_i x}$$

where a is a measure of the maximum amplitude of the u' disturbances. Differentiating the above expression with respect to x and on multiplying both sides by θ, one gets

$$\theta \cdot \frac{1}{a} \cdot \frac{da}{dx} = -\alpha_i \theta = F(S) \qquad (2)$$

$$S \equiv \frac{f\theta}{U_e}$$

F(S) is the spatial amplification rate of the disturbance of non-dimensional frequency S (cf Fig. 25). If the shear layer growth is small over the wave length λ of the disturbance, stability analysis of parallel shear flows can be used to calculate the amplification rate of a disturbance propagating through a slowly growing shear layer. One can express a disturbance of fixed frequency propagating through a growing shear layer as

$$\frac{dS}{S} = \frac{d\theta}{\theta} \qquad (3)$$

$$U_e = \text{constant}$$

From expressions (2) and (3), one gets

$$\frac{1}{a}\frac{da}{dS} = \frac{1}{\theta'(x)}\frac{F(S)}{S} \quad \text{where } \theta'(x) = \frac{d\theta}{dx}$$

which on integration results in

$$\log\left(\frac{a}{a_o}\right) = \int_{S_o}^{S} \frac{1}{\theta'(x)} \frac{F(S)}{S}\, dS \qquad (4)$$

$$= K(f)/\theta'(x) \quad \text{for } \theta'(x) = \text{constant}$$

where K(f) is the integrated amplification of the disturbance frequency f from $S_o = \frac{f\theta_o}{U_e}$ to $S = \frac{f\theta}{U_e}$ and $F(S) = -\alpha_i \theta$.

Total integrated amplification K(f) of the disturbance frequency can be computed for a given cavity flow whose growth rate $\frac{d\theta}{dx}$ and amplification rate F(S) as a function of S, are known.

V.c Phase Computation of a Disturbance Through the Cavity Shear Flow

The phase of any disturbance which is propagating through the cavity shear layer with a frequency f and a phase velocity U_c at any downstream location x is given by

$$\psi(x) = \frac{2\pi f x}{U_c} + \psi_o$$

where ψ_o is the phase of the disturbance at x = 0. In the following analysis, the phase of the disturbance is measured relative to the phase at x = 0.

(A) For temporally growing disturbances, the phase speed is independent of non-dimensional frequency and is related to edge velocity U_e as $\frac{U_c}{U_e} = 0.5$. Therefore the phase of the disturbance at a station x below the downstream corner relative to the phase at x = 0 is given by

$$\psi(x)_{\text{temporal}} = \frac{4\pi f x}{U_e}$$

(B) For spatially growing disturbances, the phase speed of the disturbances is a function of non-dimensional frequency $\frac{f\theta(x)}{U_e}$ (Fig. 26). To calculate the phase of a propagating disturbance through the cavity flow, one has to know the shear layer growth rate so as to compute the local propagation speed $U_c = U_c\left(\frac{f\theta)x)}{U_e}\right)$. Therefore, one can write

$$\underset{\text{spatial}}{\psi(x)} = \alpha_r x - \omega t + \text{const}$$

$$\frac{d\psi}{dx} = \alpha_r = \frac{1}{\theta} \cdot \bar{\alpha}_r(S) \quad \text{where } S = \frac{f\theta}{U_e},\ \bar{\alpha}_r = \alpha_r \theta$$

$$\psi - \psi_o = \frac{U_e}{f\theta'} \int_{S_o}^{S} \frac{\bar{\alpha}_r(S)}{\theta}\, dS = \frac{1}{\theta'} \int_{S_o}^{S} \bar{\alpha}_r(S)\, \frac{dS}{S}$$

where $\theta' = \frac{d\theta}{dx}$ = constant.

The phase of the spatially growing disturbances relative to the phase at x = 0 is given by

$$\underset{\text{spatial}}{\psi(x)} = \frac{2\pi}{\theta'} \int_{S_o}^{S} \frac{U_e}{U_c}\, dS$$

where $\alpha_r = \frac{2\pi f}{U_c}$, $S_o = \frac{f\theta_o}{U_e}$ and $S = \frac{f\theta(x)}{U_e}$.

V.d. Prediction of the Mode and the Frequency of Cavity Oscillations

The experimental results indicate that, out of various possible modes of cavity oscillation, cavity flow chooses to oscillate in one particular mode. On changing either the geometry or the flow, the cavity oscillations may switch from one mode of oscillation to another. Existing cavity models fail to predict the particular mode which the cavity flow is most likely to select. Results presented in this section will shed some light on this matter.

All the experimental results presented in this section were carried out at a fixed cavity depth $\frac{d}{\theta_o}$ = 100 and Reynolds number $Re_{\theta_o} = 2.42 \times 10^2$ at separation. The predicted results of cavity

oscillations for three cavity widths $\frac{b}{\theta_o}$ = 52.5, 85.0 and 105.2 are presented. These correspond to oscillations in the first mode, cavity flow switching between the first and second mode of oscillations and finally, the cavity in its second mode of oscillation respectively.

Fig. 27 shows computed results of phase distribution of spatially growing disturbances of various frequencies, as a function of downstream location $\frac{x}{\theta_o}$. The phase of the disturbance frequencies has been measured relative to their phase at the upstream cavity corner. In order to investigate the integrated amplification associated with these frequencies, calculated total integrated amplification has been plotted as a function of disturbance frequency on the same plot. The experimental results of shear layer growth rate with x for various cavity widths (Fig. 13) were used in these computations. For computation of phase and integrated amplification rate, linear shear layer growth was assumed throughout the cavity flow.

The results in Fig. 27 show that out of various possible modes of cavity oscillation, given by the integral relation $b \simeq \lambda(N+\frac{1}{2})$, cavity flow chooses to oscillate in a mode which corresponds to N = 1. Results indicate that the disturbance frequency, which gives a phase 3π at x = b relative to the upstream cavity corner, lies close to the one which receives maximum integrated amplification through the shear layer. The frequency associated with the N = 0 cavity mode receives quite small amplification compared to one which receives the maximum total integrated amplification. Again, the frequencies corresponding to N=2, 3, 4 --- etc. are too large in magnitude compared to the one which received maximum integrated amplification, and are not amplified as they propagate along the cavity shear layer. The simultaneous requirement of cavity oscillation frequency to have the right phase and near maximum total integrated amplification through the cavity flow, does not allow the cavity to respond to frequencies associated with modes other than N = 1. The observed cavity oscillation frequency of 705 Hz as indicated on Fig. 27 is in reasonable

agreement with the predicted frequency, which gets maximum integrated amplification and has an approximate phase 3π at the downstream cavity corner, relative to the upstream corner.

Results for the cavity flow, which was oscillating alternately in its first and second mode of oscillation are indicated in Fig. 28. The cavity was oscillating at frequencies of 550 and 735 Hz. As is clear from Fig. 28, these observed frequencies are close to the predicted frequencies, corresponding to N = 1 and 2 modes and lie close to the one which receives the maximum integrated amplification through the cavity shear flow. As argued above, the cavity does not respond to cavity oscillation modes associated with either N = 0 or N = 3, 4, 5 --- etc.

Results for cavity oscillation, in its second mode of oscillation are studied in Fig. 29. The experiments did not show cavity oscillations corresponding to the N = 1 mode, which might be possible according to Fig. 29.

Figs. 30, 31 and 32 compare the experimental results of the three cavity configurations studied above with the theory of temporally growing disturbances. Since the propagation speed is independent of non-dimensional frequency, the phase of various disturbance frequencies varies linearly with the downstream distance x. Similar conclusions as for spatially growing disturbances can be drawn from such a comparison.

On the basis of the above results, it is asserted that:

(A) When cavity oscillations appear, the frequency at which the cavity flow chooses to oscillate is such that

(i) it satisfies the phase criteria $\psi-\psi_o = (2N+1)\pi$ where N can be 0, 1, 2, 3 --- etc.

(ii) and receives the maximum integrated amplification through the cavity flow.

The mode which the cavity shear flow selects for oscillations is one in which both these conditions are satisfied simultaneously.

(B) The cavity jumps from one mode to another when frequencies corresponding to these modes lie close to the one which receives the maximum integrated amplification through the cavity flow.

V. e. Comparison of Numerical Results with Experiments

In this section, a comparison is made between the theoretical prediction and the experimental measured quantities in the self-similar region of the cavity flow. The effect of non-dimensional frequency on phase speed U_c/U_e is indicated on Fig. 26, along with four sets of experimental results. Because of the growth of the shear layer along the cavity width, one does not have a unique momentum thickness θ to scale the frequency of cavity oscillations. In fact, the non-dimensional frequency $\frac{f\theta(x)}{U_e}$ increases monotonically with distance x, as the disturbance of frequency f propagates through the shear layer at phase velocity U_c/U_e. On Fig. 26, the non-dimensional frequencies $\frac{f\theta(x=0)}{U_e}$ and $\frac{f\theta(x=b)}{U_e}$, corresponding to the initial and final momentum thicknesses, respectively, have been joined by a straight line. As apparent in Fig. 26, the measurements correlate well with calculated results when the cavity oscillates in its second mode of oscillation.

Measured amplitude distribution of longitudinal velocity fluctuations u' has been compared with the numerical results in Fig. 33 for the non-dimensional frequency $\frac{f\theta}{U_e} = 0.01648$. Normalization of the measured amplitude was done with spatially growing disturbances such that their maxima have the same value. No attempt was made to compare measurements with calculations for flow far inside the cavity, because of the violation of the boundary conditions as $y \to -\infty$ in the present flow configurations. As one would expect, quite large velocity fluctuations were measured in this region as compared to the calculated ones.

Fig. 34 shows the phase distribution given by the spatial and temporal stability theory at non-dimensional frequency $\frac{f\theta}{U_e} = 0.01648$, and the observed results. The experimental results are in better agreement with the theory of spatially growing disturbances than with the temporal one. Variation of phase for spatially growing disturbances is a linear function of $|\bar{y}|$ at distances far away from $\bar{y} = 0$. The slope of the phase $\frac{\partial \psi}{\partial \bar{y}}$ has an opposite sign for $\bar{y} \to \pm \infty$ with a phase reversal, whose location is a function of non-dimensional frequency $\frac{f\theta}{U_e}$, occurring somewhere within the shear layer. This kind of behavior of the amplified disturbances is verified by the present experimental investigation as shown in Fig. 34. These calculated and experimental results for the phase distribution are in disagreement with Freymuth's interpretation of the phase for $\bar{y} \to -\infty$ (Ref. 16, Fig. 34). For details of the asymptotic behavior of the phase as $\bar{y} \to \pm \infty$, the reader may refer to Appendix I.

Fig. 35 shows results of longitudinal velocity fluctuations $\left(\sqrt{\overline{u'^2}}\right)_{max}/U_e$ in the cavity shear layer as a function of the downstream location $\frac{x}{\theta_o}$, when the cavity was in the first mode of oscillation with $\frac{fb}{U_e} = 0.67$, $Re_{\theta_o} = 2.42 \times 10^2$, $\frac{b}{\theta_o} = 60$ and $\frac{d}{\theta_o} = 100$. The calculated results for both temporally and spatially growing disturbances (cf equation 4, section V.b) are shown on the same Figure. The results of the computed growth rates of Fig. 25 have been used in these computations. As is clear from Fig. 35, the amplification of the disturbances is not exponential as one would expect because of changing local non-dimensional frequency $\frac{f\theta(x)}{U_e}$ which results in different amplification rates.

In comparing the experimental and theoretical results in Figures 33-35, it must be kept in mind that the latter are obtained from a local approximation of the parallel-flow theory, whereas the actual oscillation is a result of the complete cavity interaction. That is, the oscillation frequency which actually exists is not the one that would be approximate to the local profile if the shear layer was freely developing as, for example, in Freymuth's experiments.

VI. CONCLUSION AND DISCUSSION

In this section, a summary of the results and the inferences drawn from the present study are presented. Certain experimental results suggest the need for further investigation of oscillations in flow over cavities. These are discussed briefly in this section.

VI.a. Minimum Cavity Width

The experimental results for laminar flows over a cavity indicate that the non-dimensional width $\frac{b_{min}}{\delta_o}\sqrt{Re_{\delta_o}}$ is independent of depth $\frac{d}{\delta_o}$ for $\frac{d}{\delta_o} \geq 2$. For $\frac{d}{\delta_o} > 2$, the value of the width $\frac{b_{min}}{\delta_o}\sqrt{Re_{\delta_o}}$ below which no cavity oscillations occur is 0.29×10^3. This result can be used in designing non-oscillating cavities with laminar separation. It should be noted, that for a fixed edge velocity U_e and kinematic viscosity ν, minimum width $b_{min} \sim \sqrt{\delta_o}$. Furthermore, for laminar boundary layers without a pressure gradient, the edge velocity U_e and boundary layer thickness at separation (for a fixed forebody shape), are related as $\delta_o \sim \frac{1}{\sqrt{U_e}}$. Then the minimum width $b_{min} \sim \delta_o^{\frac{3}{2}}$. It is thus concluded that increasing the shear layer thickness at the upstream cavity corner tends to delay the onset of cavity oscillations.

There is a sharp increase in the non-dimensional minimum width $\frac{b_{min}}{\delta_o}\sqrt{Re_{\delta_o}}$ for $\frac{d}{\delta_o} < 2$, below which no oscillations occur. Smoke pictures (Fig. 22a) show that the effect of decreasing cavity depth $\frac{d}{\delta_o}$ is to stabilize the laminar shear flow of the cavity. It is concluded that one requires longer cavities for the onset of cavity oscillations for cavities with a smaller depth $\frac{d}{\delta_o}$, compared to those with a larger depth. This effect is very pronounced in very

shallow cavities. In these a strong lateral constraint on the cavity shear flow may avert the growth of three-dimensional disturbances which contribute to the transition from a laminar flow to a turbulent one.[41]

VI. b. Oscillation Frequency

The overall features of cavity oscillations are given by the effect of the width $\frac{b}{\delta_o}$, the depth $\frac{d}{\delta_o}$ and the Reynolds number $Re_{\delta_o} = \frac{U_e \delta_o}{\nu}$, on the non-dimensional frequency $\frac{fb}{U_e}$. East[15] studied oscillations in rectangular cavities with a turbulent boundary layer separation. His results fall into two bands of frequencies $\frac{fb}{U_e}$ of about 0.3 to 0.4 and others between 0.6 to 0.9 with a few results around 1.3. Similar bands of frequencies are noted in edge-tone generation.[21] Present results fall into three bands of frequencies of 0.5 to 0.6, 0.8 to 0.95 and 1.3 to 1.5. It is concluded that one gets a lower non-dimensional frequency for a given mode of oscillation for a turbulent boundary layer separation, compared to one with a laminar boundary layer separation. Similar results have been reported by Karamcheti[20] for high speed flows over rectangular cutouts.

The results for the effects of the width $\frac{b}{\delta_o}$ and the Reynolds number $\frac{U_e \delta_o}{\nu}$ on the non-dimensional frequency are very significant. In a particular mode of cavity oscillation, the non-dimensional frequency increases gradually in magnitude as the width or the Reynolds number is increased. The present study shows that wave length λ of the disturbances bears an approximate integral relation with the width $b \simeq \lambda(N + \frac{1}{2})$ in any particular mode of oscillation. Therefore, the non-dimensional frequency can be written as

$\frac{fb}{U_e} = \frac{U_c}{U_e}(N+\frac{1}{2})$. Thus, an increase in the propagation speed of disturbances, with an increase of width (cf Fig. 18) for a fixed Reynolds number, results in an increase in non-dimensional frequency $\frac{fb}{U_e}$, in each mode of cavity oscillation.

VI. c. Free Shear-Layer Regions

On the basis of flow visualization and hot-wire measurements of laminar cavity shear flows, one can divide cavity shear flows into the following main regions, viz.,

(a) Close to the upstream cavity corner, flow transformation from a boundary layer profile to a shear layer profile occurs. Present studies indicate that this region extends as far as 10 to 15 momentum thicknesses θ_o downstream from the point of separation. For width $b < b_{max}$, velocity fluctuations of very small magnitude at the frequency f of cavity oscillations were noticed in this region.

(b) The second region occupies the greater part of the cavity flow. Here pure sinusoidal velocity fluctuations of frequency f of cavity oscillations occur. This disturbance, at frequency f, propagates at a constant phase speed.

(c) In this region, which lies very close to the downstream cavity corner, the shear layer deflects in and out of the cavity at the frequency f of cavity oscillations. This gross lateral motion of the shear layer causes large velocity fluctuations and results in a periodic shedding of vortices at a frequency f from the downstream corner. Hot-wire output close to the downstream corner shows a non-linear signal superimposed on the periodic one having a frequency f.

Mean and fluctuating velocity measurements further show that the effect of the downstream cavity corner on cavity shear flow is to postpone the transition of the separated laminar layer to turbulence. The experiments show that the cavity shear layer remains laminar until a maximum width b_{max} is reached. At b_{max}, the periodic signal could not be measured due to increased turbulence in the shear layer. Maximum width $\frac{b_{max}}{\theta_o} \geq 100$ was observed over a range of Reynolds number at separation $Re_{\delta_o} = 5 \times 10^2$ to 2×10^3. The stabilizing effect may be attributed to these large self-sustained oscillations induced in the cavity shear layer by the presence of the downstream corner. Presence of these oscillations seems to delay the rolling up of the laminar shear layer into vortices. As suggested by Roshko,[41] these periodic oscillations may avert the growth of the three-dimensional disturbances which contribute to the production of irregular fluctuations and result in a turbulent flow.

The experiments show that the presence of cavity oscillations in the flow induces a large increase in the shear layer growth rate. For a given cavity flow, growth rate $\frac{d\theta}{dx}$ increases continuously as the cavity width is increased. This process is terminated when the maximum width b_{max} is reached. For width $b > b_{max}$ the cavity shear flow for $x/\theta_o \geq 50$ is irregular in nature. Growth rates as high as $\frac{d\theta}{dx} \simeq 0.022$ have been observed. These large growth rates may be caused by increased 'Reynolds stresses' $\overline{u'v'}$ due to the presence of large amplitude oscillations in the cavity shear layer.

VI. d. Criterion for the Oscillation Mode

The measurements of phase $\frac{\psi}{2\pi}$ (which is a measure of how much velocity fluctuations lag behind the upstream cavity corner) show that phase increases almost linearly with distance $\frac{x}{\delta_o}$ as has been predicted by Powell's and Rossiter's models. The results further suggest that for shallow cavities an approximate phase relation between the wave length of the propagating disturbance λ and width b given by $\frac{b}{\lambda} \simeq (N+\frac{1}{2})$ exists, where N can be 0, 1, 2 --- etc. depending upon the mode of the cavity oscillations. This phase relation does not agree with Powell's criterion for edge-tones, given by $\frac{h}{\lambda} = (N+\frac{1}{4})$, where h is the distance from the edge to the slit and N = 1, 2, 3 --- etc. depending upon the mode of oscillation.

The present study shows that the phase velocity $\frac{U_c}{U_e}$ is a function of width $\left(\frac{b}{\delta_o}\right)$ for a fixed depth $\frac{d}{\delta_o}$ and Reynolds number Re_{δ_o}. It increases in magnitude as width is increased. The measurement further shows that the non-dimensional frequency $\frac{fb}{U_e}$ is a function of width $\frac{b}{\delta_o}$ and Reynolds number Re_{δ_o}.

From the present experiments, it is concluded that oscillations in shallow cavities at low subsonic speeds are due to disturbances which grow as they propagate through the shear layer. The frequency of the disturbance for a given cavity flow corresponds to the one which receives the maximum integrated amplification along the cavity shear layer, as suggested by Woolley and Karamcheti.[54] The experiments further show that the wave length of these propagating disturbances bears an integral relation

to width $\frac{b}{\lambda} \simeq (N+\frac{1}{2})$ in each mode of cavity oscillation. By studying the integrated amplification and phase distribution of disturbance frequencies, in light of the phase criterion $\frac{b}{\lambda} \simeq (N+\frac{1}{2})$, one can predict the mode in which a cavity flow will oscillate (cf section V.d.).

VI.3. Summary and Conclusions

(1) The phenomenon of oscillations in low speed flows over cavities is not an acoustic resonance phenomenon in the longitudinal direction. These oscillations result from propagating disturbances which get amplified along the cavity shear layer.

(2) The present experiments show that the onset of cavity oscillations is accompanied by a large lateral motion of the cavity shear layer close to the downstream corner. A detailed investigation by flow visualization and measurement of the fluctuating quantities close to the downstream corner will further help to understand the mechanism of the onset of cavity oscillations.

(3) It is observed that the effect of depth for $\frac{d}{\delta_o} \simeq O(1)$ is to delay the transition of the free laminar shear layer flow to a turbulent one. This may be due to spanwise constraint imposed on the shear layer by the depth and may delay the growth of three-dimensional disturbances which contribute to turbulence.

(4) It is further observed that the transition of the laminar cavity shear flow to turbulence is postponed by the presence of large amplitude oscillations in cavity flow until a maximum width b_{max} is reached. No rolling up of the laminar cavity shear layer into vortices occurs for cavity widths as large as $\frac{b}{\theta_o} > 100$. The transition phenomenon which occurs for widths $b > b_{max}$ is quite complex and needs further experimental investigation.

(5) The results show that for shallow cavities, an approximate integral relation between the wave length of the propagating disturbance λ of the cavity oscillations and width b given by $\frac{b}{\lambda} \simeq (N+\frac{1}{2})$ exists, where N can be 0, 1, 2, 3 --- etc. depending upon the mode of cavity oscillation.

(6) The experiments show that the frequency that receives the maximum integrated amplification along the cavity shear layer is approximately the frequency at which the cavity flow oscillates. The particular mode a cavity flow selects for oscillation can be predicted by applying the mode criterion $\frac{b}{\lambda} \simeq (N+\frac{1}{2})$ to the disturbance frequency, which receives the maximum integrated amplification along the cavity shear flow.

(7) The presence of strong cavity oscillations contributes to a large growth of the shear layer. Growth rates $\frac{d\theta}{dx} \simeq 0.022$ in laminar cavity flows are noticed. Because of rapid growth of the cavity shear layer, the stability analysis of the self-similar velocity profile should be undertaken by treating the

cavity shear flow as a non-parallel flow. A stability of such a flow, satisfying the boundary conditions imposed by the downstream cavity corner, should be undertaken. Such an analysis will shed more light on the possible frequencies and modes of oscillation in cavity flows.

APPENDIX I

Phase Distribution as $\bar{y} \to \pm \infty$ for Spatially Growing Disturbances in an Inviscid Parallel Shear Flow

Let us assume periodic disturbances travelling in the streamwise direction with the mean velocity profile U(y) given by

$$u(x, y, t) = \phi(y)\, e^{i(\alpha x - \beta t)}$$

where wave number $\alpha = \alpha_r + i\alpha_i$ is complex. For an unbounded velocity profile, the disturbances must vanish at infinite, i.e.,

$$\phi(y) \to 0 \quad \text{as} \quad y \to \pm \infty \qquad \text{(see Appendix II)}$$

Let $\phi(y)$ behave asymptotically as $e^{-\alpha|y|}$ as $y \to \pm \infty$, then

$$u(x, y, t) \sim e^{-\alpha|y|}\, e^{i(\alpha x - \omega t)}$$

$$\text{phase } [u] = -\alpha_i |y| + \alpha_r x - \omega t$$

Thus, the asymptotic behavior of phase with y has an opposite slope depending on whether $y \to \pm \infty$.

APPENDIX II

Derivation of the Equations of Motion for Stability Analysis of Inviscid and Parallel Shear Flows

For the two-dimensional shear layer, let x represent the distance along the axis of the shear layer from the upstream corner, and y the distance from the shear layer axis. The inviscid Navier-Stokes equations for two-dimensional incompressible flow can be written as

$$\begin{aligned} u_x + v_y &= 0 \\ u_t + u\,u_x + v\,u_y &= -\frac{1}{\rho} p_x \\ v_t + u\,v_x + v\,v_y &= -\frac{1}{\rho} p_y \end{aligned} \qquad (1)$$

The mean velocity is regarded as steady and can be described by cartesian components U and V, and their pressure P. It is further assumed that $U = U(y)$ and $V \equiv 0$, i.e., flow is parallel. The flow is divided into a mean part independent of time and a fluctuating part, i.e.,

$$\begin{aligned} u(x, y, t) &= U(y) + u'(x, y, t) \\ v(x, y, t) &= v'(x, y, t) \\ p(x, y, t) &= P(x, y) + p'(x, y, t) \end{aligned} \qquad (2)$$

Substituting (2) into (1) and assuming that the mean flow itself satisfies the Navier-Stokes equations, then, on neglecting higher order terms, one gets

$$\frac{\partial u'}{\partial x} + \frac{\partial v'}{\partial y}$$

$$\frac{\partial u'}{\partial t} + U\frac{\partial u'}{\partial x} + \frac{dU}{dy}v' + \frac{1}{\rho}\frac{\partial p'}{\partial x} = 0 \qquad (3)$$

$$\frac{\partial v'}{\partial t} + U\frac{\partial v'}{\partial x} + \frac{1}{\rho}\frac{\partial p'}{\partial y} = 0$$

The reference quantities chosen for non-dimensionalization are the freestream conditions and physical length δ, i.e., the shear layer thickness. Then the various non-dimensional quantities are:

$$\bar{y} = y/\delta$$

$$\bar{U}(y) = U/U_e \qquad (4)$$

$$\bar{t} = U_e t/\delta$$

where δ is the shear layer thickness.

Assume a solution of the form

$$u' = U_e Z_1(\bar{y})\exp[i(\bar{\alpha}\bar{x} - \bar{\omega}\bar{t}]$$

$$v' = U_e Z_2(\bar{y})\exp[i(\bar{\alpha}\bar{x} - \bar{\omega}\bar{t}] \qquad (5)$$

$$p' = \rho U_e^2 Z_3(\bar{y})\exp[i(\bar{\alpha}\bar{x} - \bar{\omega}\bar{t}]$$

On substituting (5) into (3), the governing equations of motion in non-dimensional form can be written as

$$i\bar{\alpha} Z_1 + \frac{dZ_2}{d\bar{y}} = 0$$

$$i\bar{\alpha}(\bar{U} - \bar{c})Z_1 + \frac{d\bar{U}}{d\bar{y}} Z_2 + i\bar{\alpha} Z_3 = 0 \qquad (6)$$

$$i\bar{\alpha}(\bar{U} - \bar{c})Z_2 + \frac{dZ_3}{d\bar{y}} = 0$$

$$\bar{c} \equiv \bar{\omega}/\bar{\alpha}$$

On elimination of Z_1 from equations (6), the governing equations in Z_2 and Z_3 are

$$(\bar{U} - \bar{c}) \frac{dZ_2}{d\bar{y}} - \frac{d\bar{U}}{d\bar{y}} Z_2 - i\bar{\alpha} Z_3 = 0 \qquad (7)$$

$$i\bar{\alpha}(\bar{U}-\bar{c})Z_2 + \frac{dZ_3}{d\bar{y}} = 0 \qquad (8)$$

with boundary conditions

$$\bar{y} \to +\infty \begin{cases} \bar{U} \to 1 \\ \dfrac{d\bar{U}}{d\bar{y}} \to 0 \end{cases}$$

$$\bar{y} \to -\infty \begin{cases} \bar{U} \to 0 \\ \dfrac{d\bar{U}}{d\bar{y}} \to 0 \end{cases}$$

Satisfying the boundary conditions at $\bar{y} \to +\infty$, equations (7) and (8) reduce to

$$(1-\bar{c}) \frac{dZ_2}{d\bar{y}} - i\bar{\alpha} Z_3 = 0$$

$$i\alpha(1-\bar{c})Z_2 + \frac{dZ_3}{d\bar{y}} = 0 \qquad (9)$$

Assume further that as $\bar{y} \to +\infty$, $Z_2 \simeq C_2 e^{m\bar{y}}$ and $Z_3 \simeq C_3 e^{m\bar{y}}$. On substituting this into equations (9), one gets

$$m = \pm \bar{\alpha}$$

For $Z_2 \to 0$ and $Z_3 \to 0$ as $\bar{y} \to +\infty$, $m = -\bar{\alpha}$

$$\text{For } \bar{y} \to +\infty \begin{cases} Z_2 \simeq C_2 e^{-\bar{\alpha}\bar{y}} \\ Z_3 \simeq i(1-\bar{c})C_2 e^{-\bar{\alpha}\bar{y}} \end{cases}$$

where C_2 and C_3 are arbitrary constants.

Similarly, on satisfying boundary conditions at $\bar{y} \to -\infty$, one must have

$$\text{For } \bar{y} \to -\infty \begin{cases} Z_2 \simeq B_2 e^{\bar{\alpha}\bar{y}} \\ Z_3 \simeq i\,\bar{c}\,B_2 e^{\bar{\alpha}\bar{y}} \end{cases}$$

where B_2 is an arbitrary constant.

Thus the eigenvalue problem is

$$\begin{aligned} (\bar{U}-\bar{c})\frac{dZ_2}{d\bar{y}} - \frac{d\bar{U}}{d\bar{y}} Z_2 - i\bar{\alpha} Z_3 &= 0 \\ \frac{dZ_3}{d\bar{y}} + i\bar{\alpha}(\bar{U}-\bar{c})Z_2 &= 0 \end{aligned} \qquad (10)$$

with boundary conditions

$$\frac{Z_3}{Z_2} \to i(1-\bar{c}) \qquad \text{as } \bar{y} \to +\infty$$

$$\frac{Z_3}{Z_2} \to i\,\bar{c} \qquad \text{as } \bar{y} \to -\infty$$

For the temporal mode:

$\bar{\alpha}$ is real, $\bar{c}$ is complex

For the spatial mode:

$\bar{\alpha}$ is complex, $\bar{\omega} \equiv \bar{\alpha}\,\bar{c}$ is real.

Computational Technique

The computation of the eigenvalue problem can be simplified by eliminating the term $\frac{d\bar{U}}{d\bar{y}}$ with the substitution

$$Z_4 \equiv \frac{Z_2}{\bar{U} - \bar{c}}$$

Then the equations (10) reduce to

$$\begin{aligned} \frac{dZ_3}{d\bar{y}} &= -i\bar{\alpha}(\bar{U}-\bar{c})^2 Z_4 \\ \frac{dZ_4}{d\bar{y}} &= i\bar{\alpha}\frac{Z_3}{(\bar{U}-\bar{c})^2} \end{aligned} \qquad (11)$$

with boundary conditions:

$$\frac{Z_3}{Z_4} \to i(1-\bar{c})^2 \qquad \text{as } \bar{y} \to +\infty$$

$$\frac{Z_3}{Z_4} \to -i\bar{c}^2 \qquad \text{as } \bar{y} \to -\infty$$

Mack[30] studied the inviscid stability of the laminar compressible boundary layers extensively by integrating the governing equations of motion numerically. His method of computation has

been adapted to evaluate the eigenfunctions and eigenvalues of the two-dimensional, incompressible and inviscid stability equations (11) for arbitrary shear layer profile.

REFERENCES

1. Betchov, R. and Criminale, W. O. Jr., "Stability of Parallel Flows," Academic Press, New York, London, 1967.
2. Brown, G. B., "The Vortex Motion Causing Edge Tones," Proceedings Physical Society (London) 49, pp. 493-507, 1937.
3. Brown, G. L. and Roshko, A., "The Effect of Density Difference on Turbulent Mixing Layer," AGARD-CP-93, AGARD Conference Proceedings No. 93 on Turbulent Shear Flows, 13-15, Sept. 1971.
4. Browand, F. K., "An Experimental Investigation of the Instability of an Incompressible Separated Shear Layer," J. F. M., Vol. 26, Pt. 2, pp. 281-307, 1966.
5. Brazier, J. G., "The Hydrostatic Channel and A3D-1 Bomb Bay Buffeting Tests," Douglas Aircraft Co. Report No. ES 17825, Dec. 27, 1954.
6. Boeing Airplane Co., "Investing of B-47 Bomb Bay Buffeting," Report D-12675, Feb. 15, 1952.
7. Bilanin, A. J. and Covert, E. E., "Estimation of Possible Excitation Frequencies for Shallow Rectangular Cavities," AIAA Journal, Vol. 11, No. 3, pp. 347-351, March 1973.
8. Bradshaw, P., "The Effect of Initial Conditions on the Development of a Free Shear Layer," J. F. M., Vol. 26, Pt. 2, pp. 225-236, 1966.
9. Chapman, D. R., Kuehn, D. M. and Larson, H. K., "Investigation of Separated Flows in Supersonic and Subsonic Streams with Emphasis on 'Effect of Transition'," NACA TR 1356, 1958.

10. Charwat, A. F., Roos, J. N., Dewey, F. C. and Hitz, J. A., "An Investigation of Separated Flows. Part 1. The Pressure Field," J. Aerospace Sciences, Vol. 28, No. 6, pp. 457-470, 1961.

11. Covert, E. E., "An Approximate Calculation of the Onset Velocity of Cavity Oscillations," AIAA Journal, Vol. 8, No. 12, pp. 2189-2194, Dec. 1970.

12. Curle, N., "The mechanism of edge-tones," Proceedings of the Royal Society (A), 216, pp. 412-424, 1953.

13. Drazin, P. G. and Howard, L. N., "Hydrodynamic Stability of Parallel Flow of Inviscid Fluid," Advances in Applied Mechanics 9, pp. 1-89, 1966.

14. Dunham, W. H., "Flow-induced Cavity Resonance in Viscous Compressible and Incompressible Fluids," Fourth Symposium on Naval Hydrodynamics, Ship Propulsion and Hydrodynamics, Rept. ARC-73, Vol. 3, Office of Naval Research, Washington, D. C., 1962.

15. East, L. F., "Aerodynamic induced resonance in rectangular cavities," J. Sound Vibration, Vol. 3, pp. 277-287, 1966.

16. Freymuth, P., "On transition in a separated laminar boundary layer," J. F. M., Vol. 26, Pt. 4, pp. 683-704, 1966.

17. Gaster, M., "The role of spatially growing waves in the theory of hydrodynamic stability," Progress in Aeronautical Sciences, Vol. 6, pp. 251-270, 1965.

References (Cont'd)

18. Helmholtz, H., "Über diskontinuierliche Flüssigkeits-bewegungen," Monatsberichte Königliche Akademi Wissenschaften Berlin, S. 215-228, 1868.

19. Heller, H. H., Holmes, D. G. and Covert, E. E., "Flow Induced Pressure Oscillations in Shallow Cavities," J. of Sound and Vibrations, Vol. 18, No. 4, pp. 545-552, 1971.

20. Karamcheti, K., "Sound Radiated from Surface Cutouts in High-Speed Flows," Ph.D. Thesis, California Institute of Technology, June 1956.

21. Karamcheti, K. and Bauer, A. B., "Edgetone Generation," Stanford University, Dept. of Aero. and Astro., Rept. SUDAER 162, July 1963.

22. Liepmann, H. W. and Laufer, J., "Investigation of Free Turbulent Mixing," NACA Tech. Note No. 1257, 1947.

23. Landau, L. D., "Stability of tangential discontinuities in compressible fluids," Dokl, Akad. Nank, SSSR44, pp. 139-141, 1944.

24. Lin, C. C., "On the Stability of Laminar Mixing Region between Two Parallel Streams of Gas," NACA TN 2887, 1953.

25. Lin, C. C., "The Theory of Hydrodynamic Stability," Cambridge University Press.

26. Lessen, M., Fox, T. A., Zien, H. M., "On the inviscid stability of the laminar mixing of two parallel streams of compressible fluid," J.F.M. 25, pp. 737-742, 1966.

References (Cont'd)

27. Lewis, J. E. and Behrens, W., "Fluctuation Measurements in the Near Wake of a Wedge With and Without Base Injection," AIAA J. Vol. 7, No. 4, pp. 664-670, April 1969.

28. Lord Rayleigh, "On the Stability of Jets," Scientific papers, 1, pp. 361-371, 1878. Cambridge Univ. Press.

29. Lord Rayleigh, "On the stability or instability of certain fluid motion," Scientific Papers 1, pp. 474-487, 1880. Cambridge Univ. Press.

30. Mack, L. M., "Computation of the Stability of the Laminar Compressible Boundary Layer," Methods in Computational Physics, Vol. 4, 1965.

31. Michalke, A., "The Instability of Free Shear Layers," Progress in Aerospace Sciences, pp. 213-239, Pergamon Press, Oxford and New York, 1972.

32. Michalke, A., "On the Inviscid Instability of Hyperbolic-tangent Velocity Profile," J. F. M. 19, pp. 543-556, 1964.

33. Michalke, A., Freymuth, P., "The instability and the formation of vortices in a free boundary layer," AGARD Conference Proc. No. 4, "Separated Flows," pt. II, pp. 575-595, 1966.

34. Michalke, A., "The influence of the vorticity distribution on the inviscid instability of a free shear layer," Fluid Dynamics Transactions, Vol. 4, pp. 751-760, 1969.

35. Miksad, R. H., "Experiments on the non-linear stages of free-shear layer transition," J. F. M. Vol. 56, Pt. 4, pp. 695-719, 1972.

References (Cont'd)

36. Miles, J. W., "On the disturbed motion of a plane vortex sheet," J.F.M. 4, pp. 538-552, 1958.

37. McGregor, W. and White, R. A., "Drag of rectangular cavities in supersonic and transonic flows including the effects of cavity resonance," AIAA Journal, Vol. 8, No. 11, pp. 1959-1964, Nov. 1970.

38. Nyborg, W. L., "Self-Maintained Oscillations of the Jet in a Jet-Edge System," The J. of the Acoustical Society of America, Vol. 26, No. 2, pp. 174-182, March 1954.

39. Plumblee, H.E., Gibson, J.S. and Lassiter, L.W., a theoretical and experimental investigation of the acoustic response of cavities in an aerodynamic flow," WADD-TR-61-75, March 1962.

40. Powell, A., "On the Edgetone," J. of Acoustical Society of America, Vol. 33, p. 395, 1961.

41. Roshko, A., "Transition in Incompressible Near-Wakes," The Physics of Fluids, Supplement, 1967.

42. Roshko, A., "On the Development of Turbulent Wakes from Vortex Streets," NACA Tech. Note 2913, March 1953.

43. Roshko, A., "Some measurements of flow in a rectangular cutout," NACA TN-3488, 1955.

44. Roshko, A., "Experiments on the Flow Past a Circular Cylinder at Very High Reynolds Numbers," J.F.M., Vol. 10, pp. 345-356, 1961.

References (Cont'd)

45. Rossiter, J. E., "Wind Tunnel Experiments on the Flow Over Rectangular Cavities at Subsonic and Transonic Speeds," Communicated by the Deputy Controller Aircraft (Research and Development) Ministry of Aviation, R & M No. 3438, Oct. 1964. (Replaces R. A. E. Tech. Rept. No. 64037 - A. R. C. 26621).

46. Rossiter, J. E. and Kurn, A. G., "Wind tunnel measurement of unsteady pressures in and behind a bomb bay," (Canberra) A. R. C. C. P. 728, Oct. 1962.

47. Sato, H., "Experimental investigation on the transition of laminar separated layer," Journal of the Physical Society of Japan 11, No. 6, pp. 702-709, 1956.

48. Sato, H., "The Stability and Transition of a Two-Dimensional Jet," J. F. M. 7, pp. 53-80, 1960.

49. Spee, B. M., "Wind tunnel experiments on flow over rectangular cavities at subsonic and transonic speeds," AGARD Conference Proceedings No. 4, Separated Flows, Pt. 2, 1966.

50. Shields, W. L. and Karamcheti, K., "An experimental investigation of the edgetone flow field," Stanford Univ., Dept. of Aero. and Astro., Rept., SUDAAR, 304, Feb. 1967.

51. Stegen, G. R. and Karamcheti, K., "On the structure of an edgetone flow field," Stanford Univ., Dept. of Aero. and Astro., Rept. SUDDAR 303, Feb. 1967.

References (Cont'd)

52. Stull, F. D., Curran, E. T. and Velkoff, H. R., "Investigation of two-dimensional cavity diffusers," AIAA Paper No. 73-685, AIAA 6th Fluid and Plasma Dynamic Conference, Palm Springs, California, July 16-18, 1973.

53. Tani, I., Iuchi, M. and Komoda, H., "Experimental investigation of flow separation associated with a step or a groove," Aero Research Institute, Univ. of Tokyo Rept. No. 364, April 1961.

54. Woolley, J. P. and Karamcheti, K., "A study of narrow band noise generation by flow over ventilated walls in transonic wind tunnels," Nielsen Engineering and Research, Inc. (NEAR) TR 50, Feb. 1973.

55. Woolley, J. P. and Karamcheti, K., "The role of jet stability in edgetone generation," AIAA Paper No. 73-628, AIAA 6th Fluid and Plasma Dynamics Conference, Palm Springs, Calif., July 16-18, 1973.

Table I

Table for $b_{min}\sqrt{U_e}$ for fixed value of shear layer thickness δ_o

δ_o	Model	U_e(ft/sec)	b_{min}(inches)	$b_{min}\sqrt{U_e}$ ($\sqrt{ft^3/sec}$)
0.035"	#1	62.00	0.316"	0.207
	#2	82.00	0.277"	0.209
0.04"	#1	41.00	0.442"	0.235
	#2	52.00	0.380"	0.228
	#3	94.50	0.285"	0.230
0.045"	#1	28.50	0.562"	0.250
	#2	39.00	0.481"	0.250
	#3	59.50	0.384"	0.247
0.05"	#2	33.00	0.570"	0.273
	#3	43.50	0.503"	0.276
0.055"	#2	27.50	0.705"	0.308
	#3	35.00	0.592"	0.292

#1 Model with $\frac{\ell}{D} = 0.6$; #2 Model with $\frac{\ell}{D} = 1.12$; #3 Model with $\frac{\ell}{D} = 2.12$

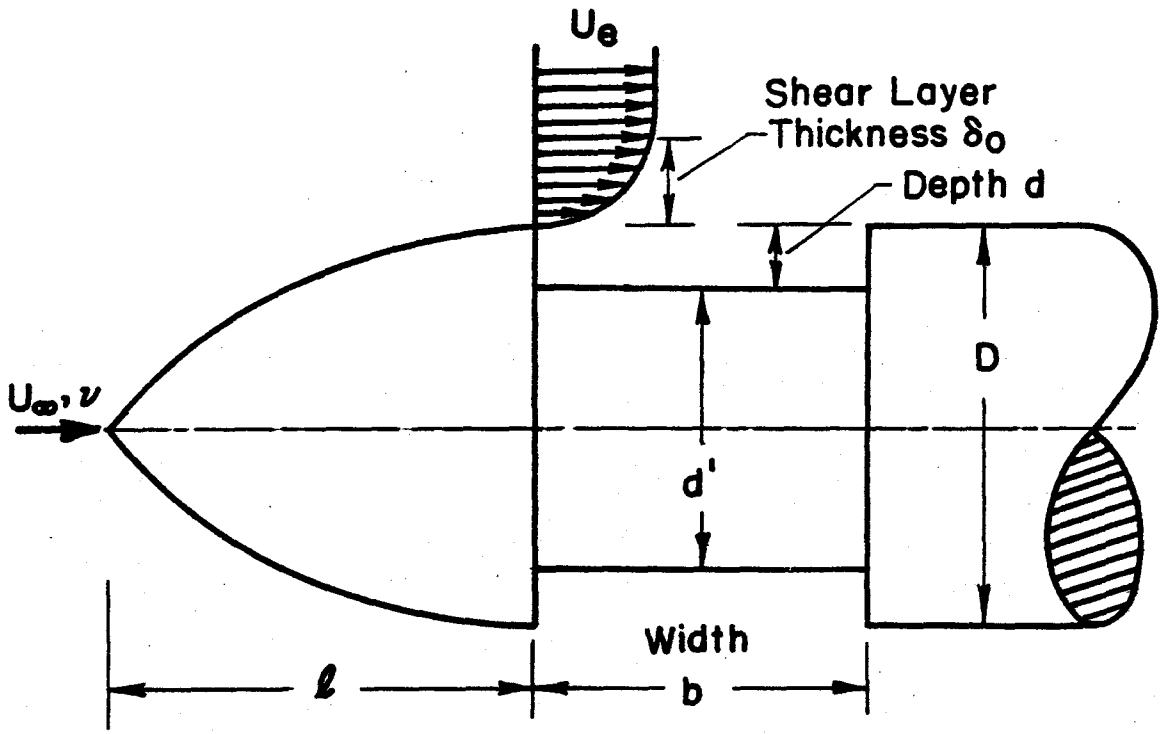

D = 1.0", 2.0" and 6.0"

b and d are variable

U_e: 0-80 ft/sec

Re_D: 2×10^4-10^5 (laminar boundary layer at separation)

Free stream turbulence at 50 ft/sec ~ 0.3% $\frac{\sqrt{\overline{u'^2}}}{U_\infty}$

Nose shape

D = 1.0" Hemispherical nose

D = 2.0" I ogive with $\frac{\ell}{D} = 0.6$

II ogive with $\frac{\ell}{D} = 1.12$

III ogive with $\frac{\ell}{D} = 2.12$

D = 6.0" Ellipsoid with ratio of major to minor axis = 3.

FIG. 1 Model of Cavity Oscillations with Pertinent Nomenclature

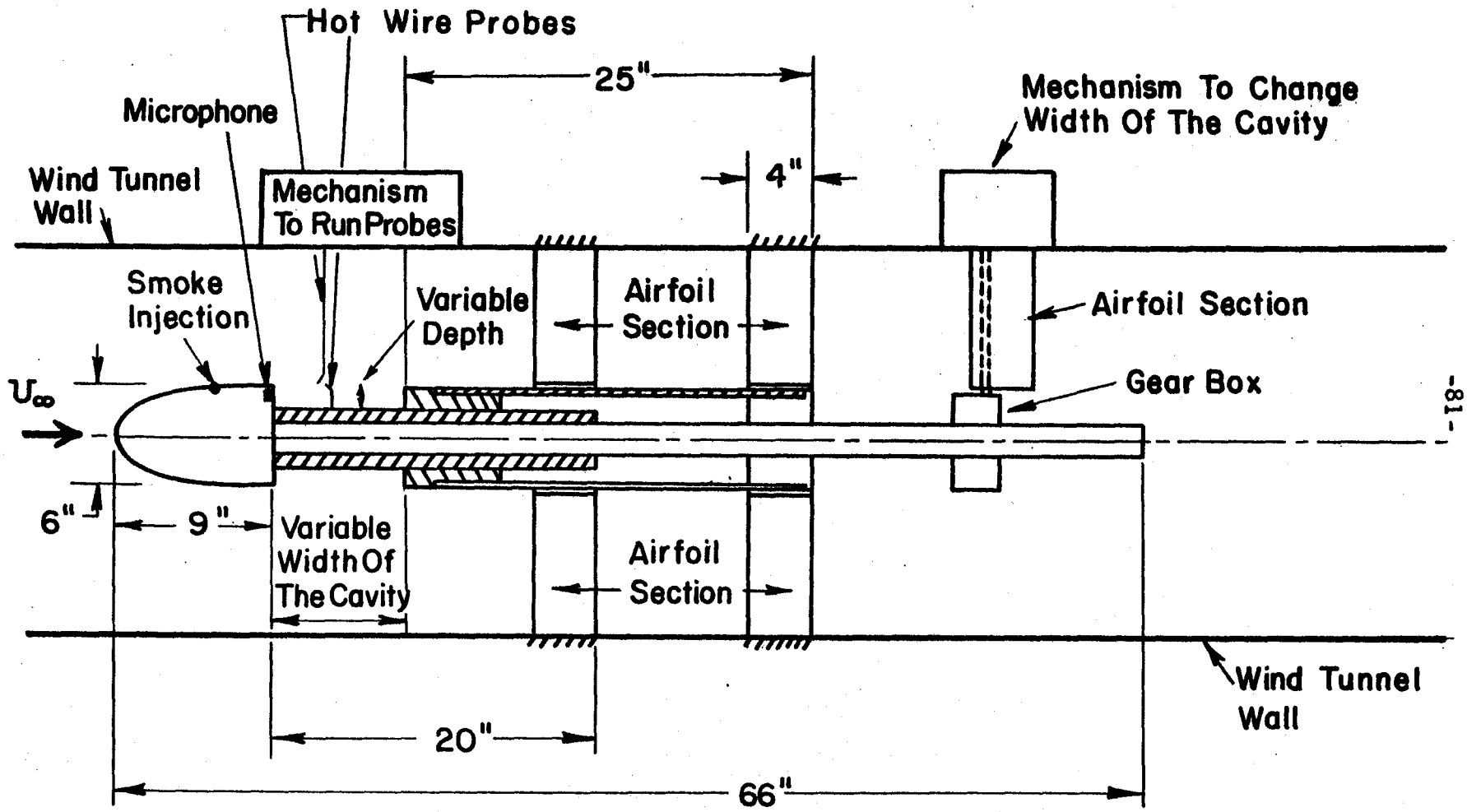

FIG. 2 Six Inch Cavity Oscillation System

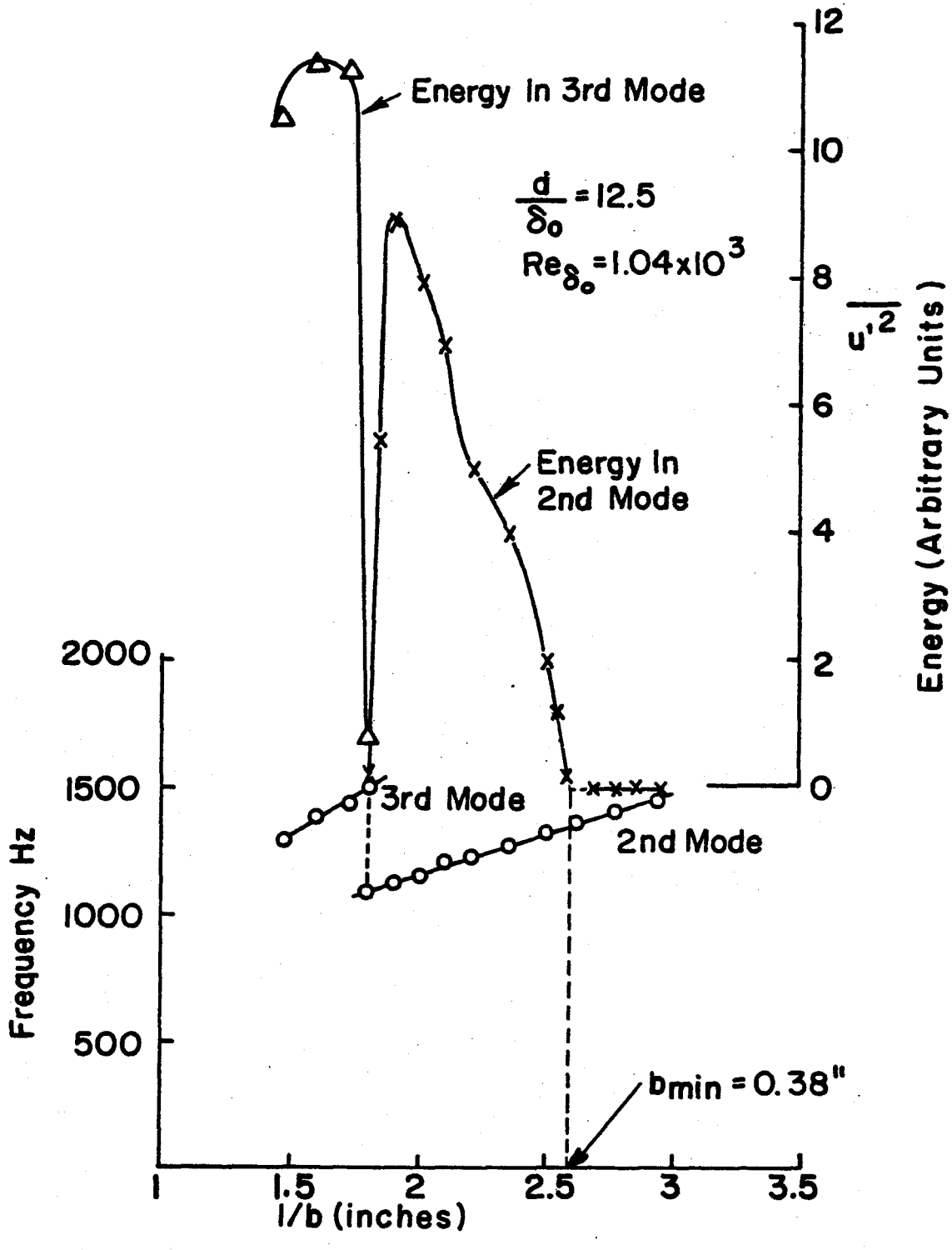

FIG. 3 Discrete Energy in Various Modes of Cavity Oscillation

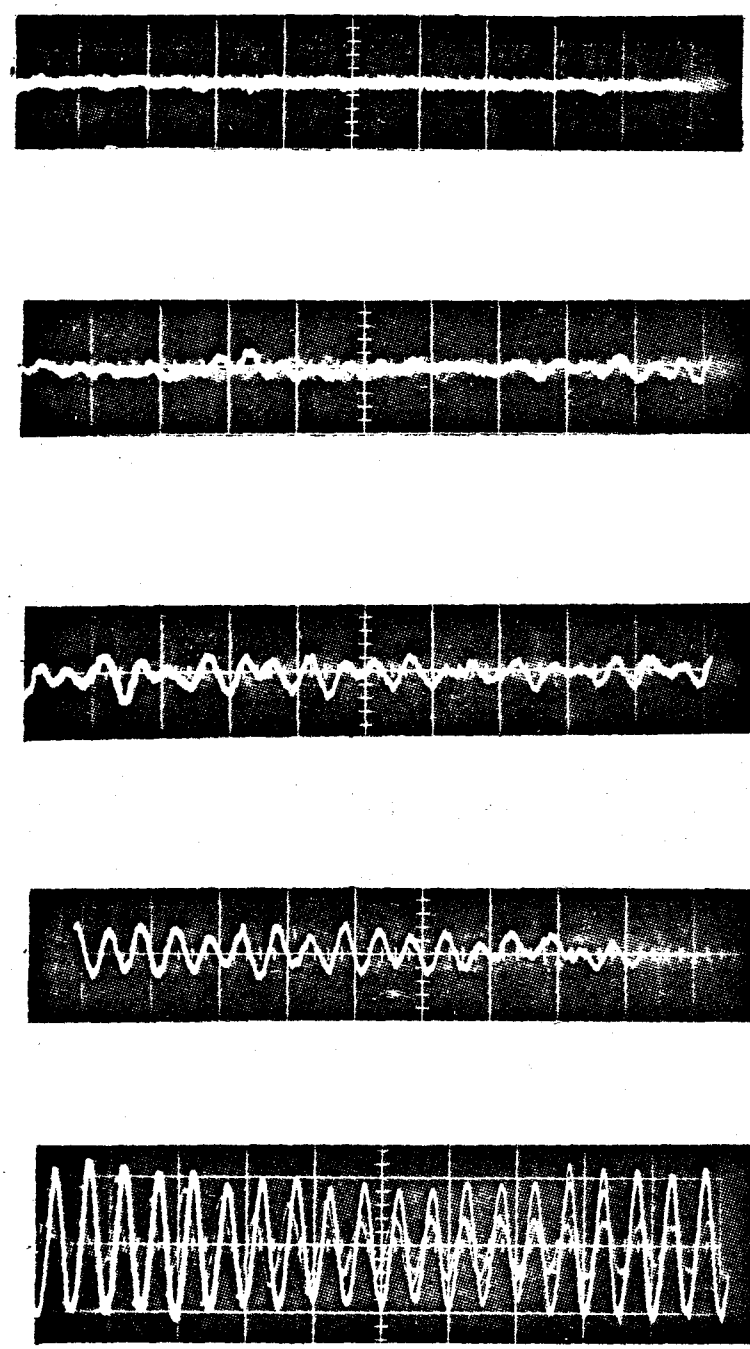

FIG. 4 Oscilloscope Traces of Cavity Oscillations for $b \leq b_{min}$, $D = 1.0"$, $U_\infty = 50$ ft/sec, $d = 0.5"$, and $b_{min} = 0.275"$

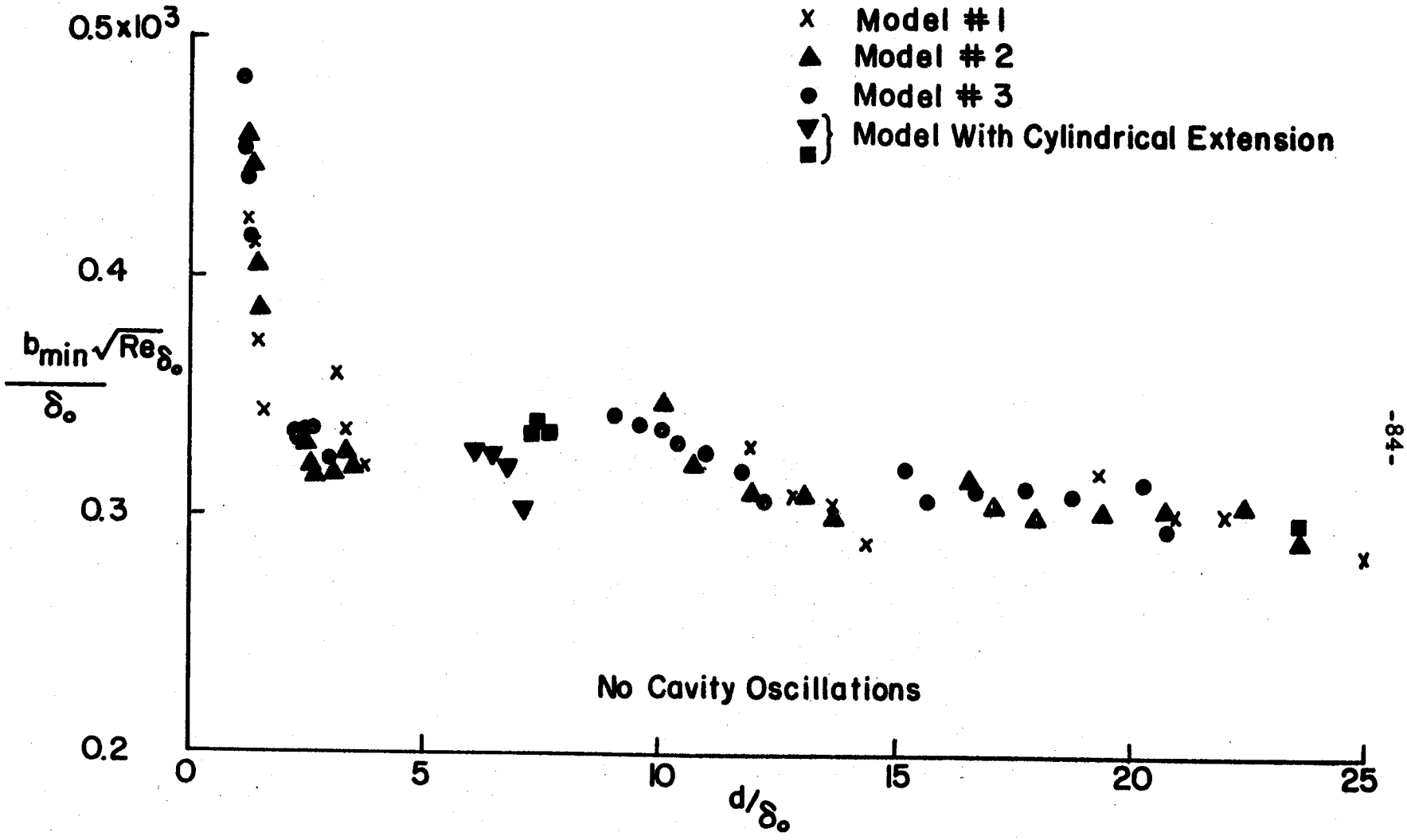

FIG. 5 Region of Cavity Oscillation

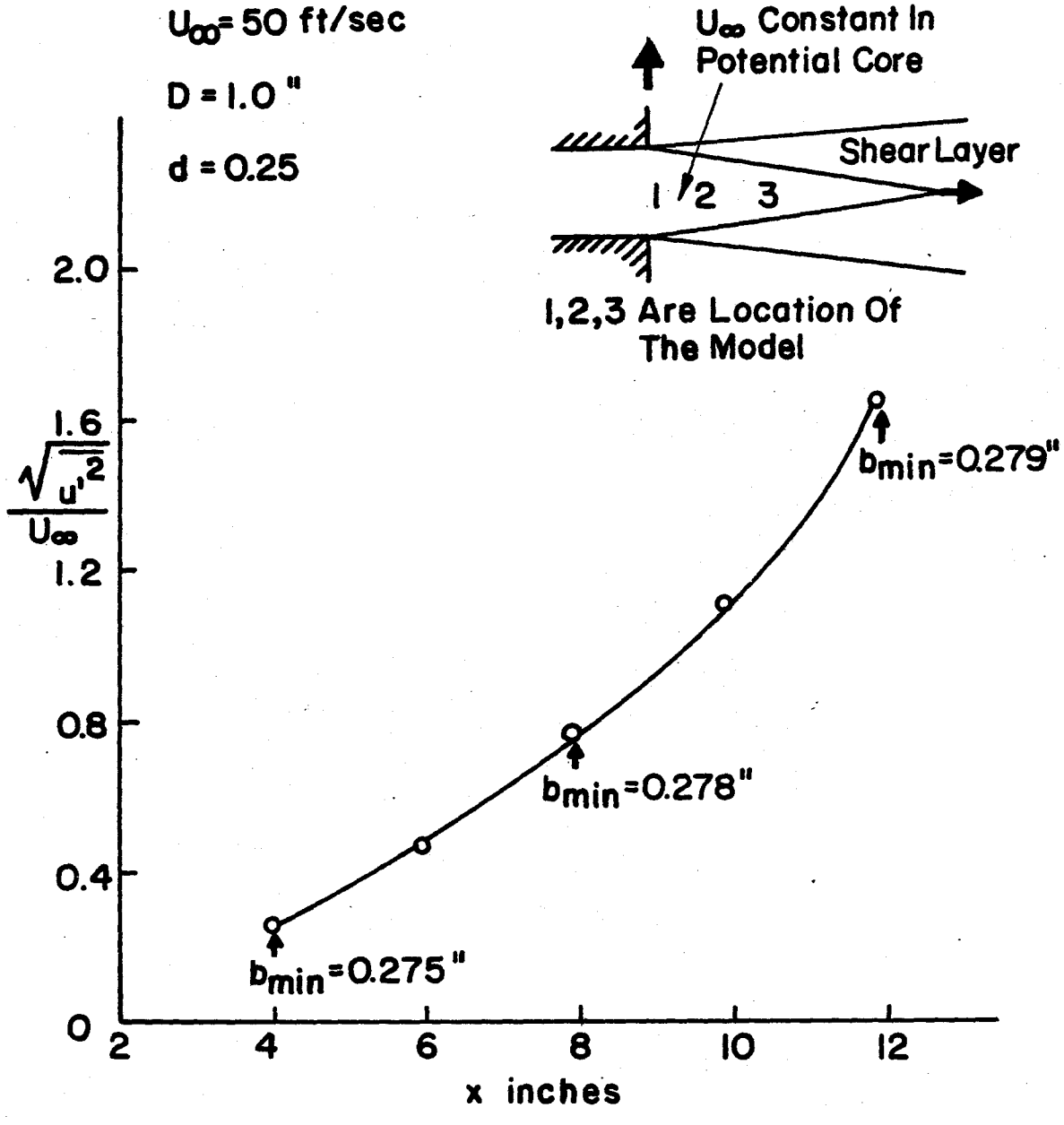

FIG. 6 Effect of Freestream Turbulence on Minimum Cavity Width

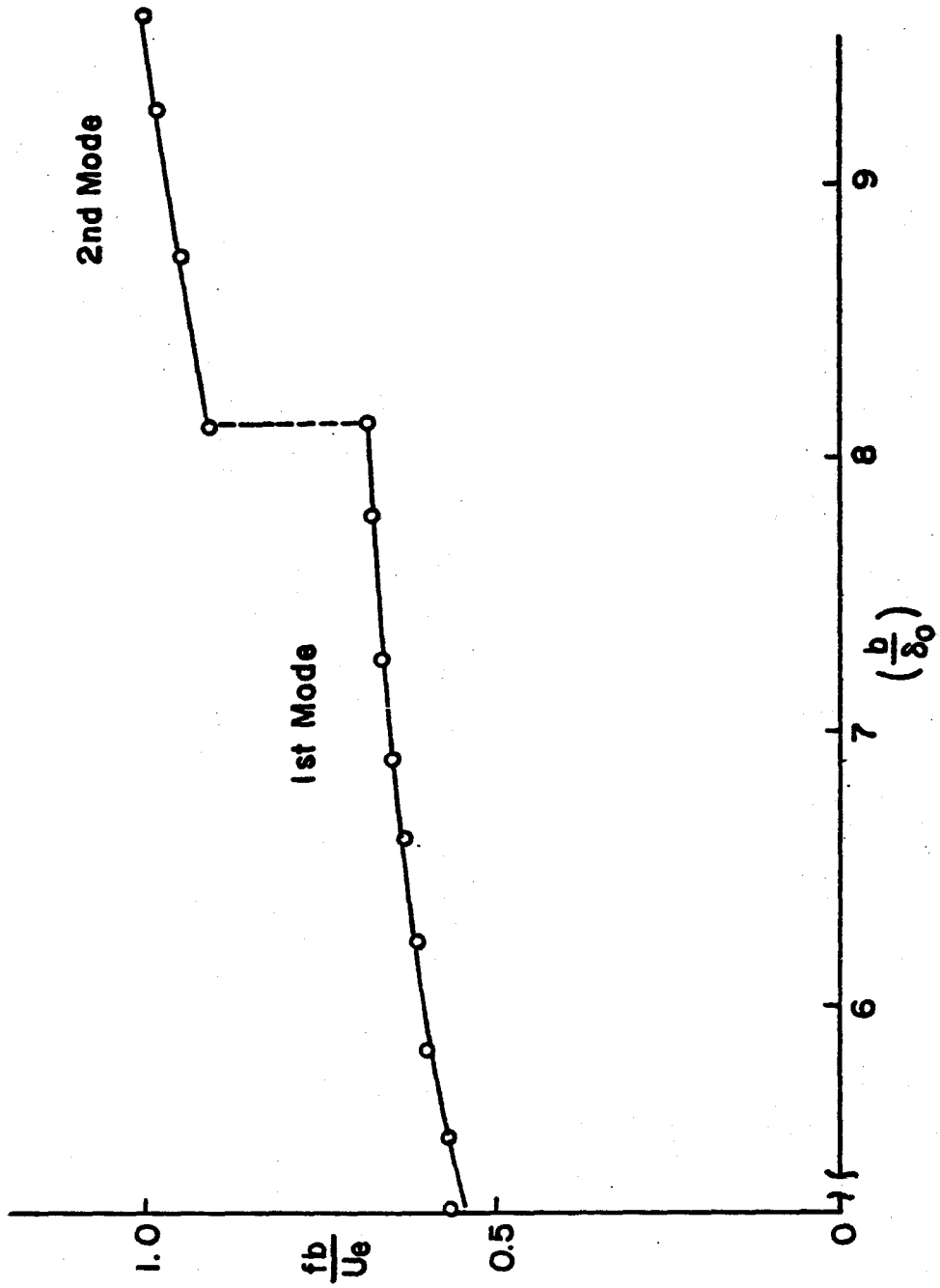

FIG. 7 Effect of Width on Non-dimensional Frequency at $Re_{\delta_o} = 2.86 \times 10^3$ and $\frac{d}{\delta_o} = 10$

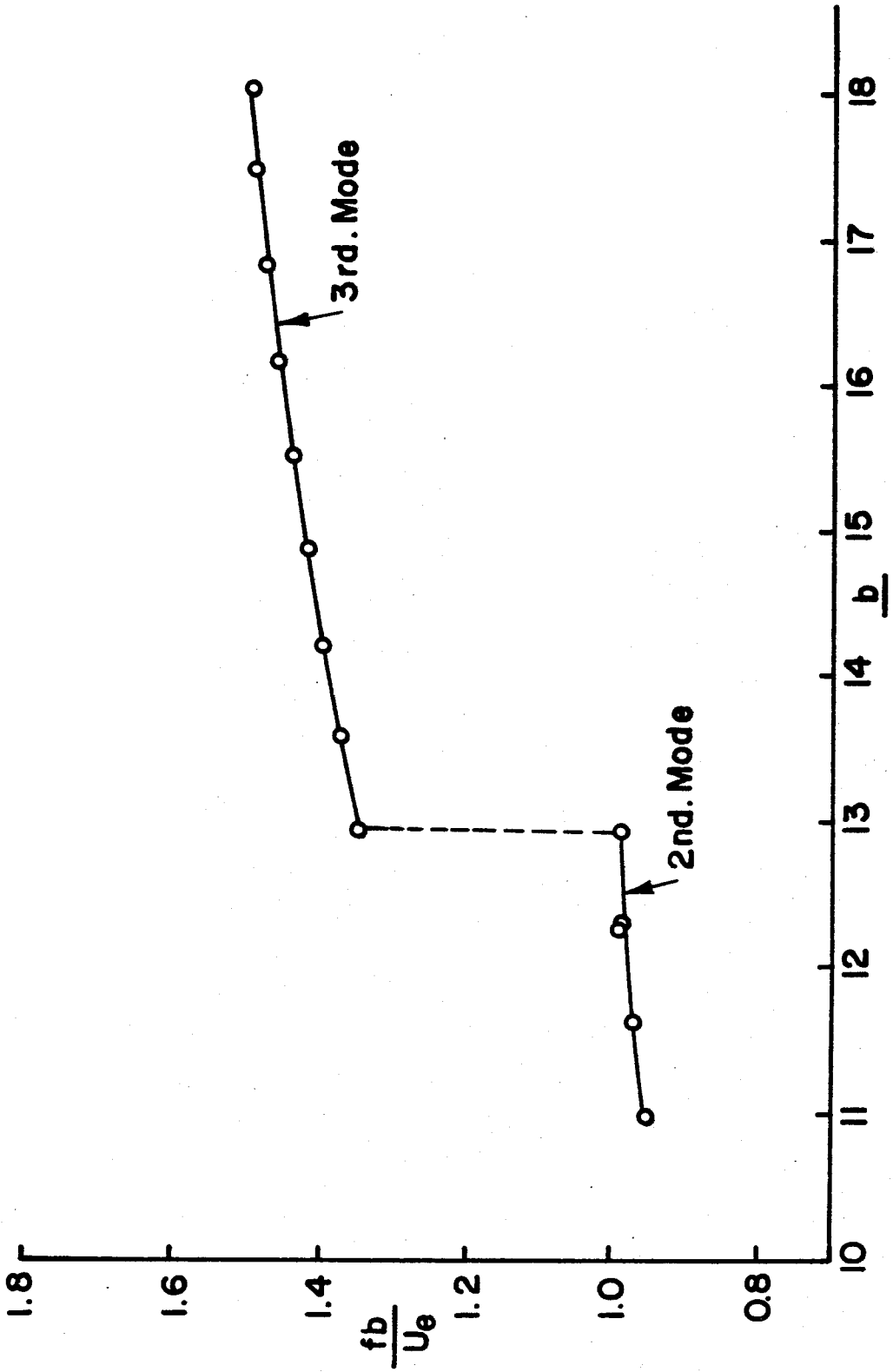

FIG. 8 Effect of Width on Non-dimensional Frequency at $Re_{\delta_o} = 0.92 \times 10^3$ and $\frac{d}{\delta_o} = 12.95$

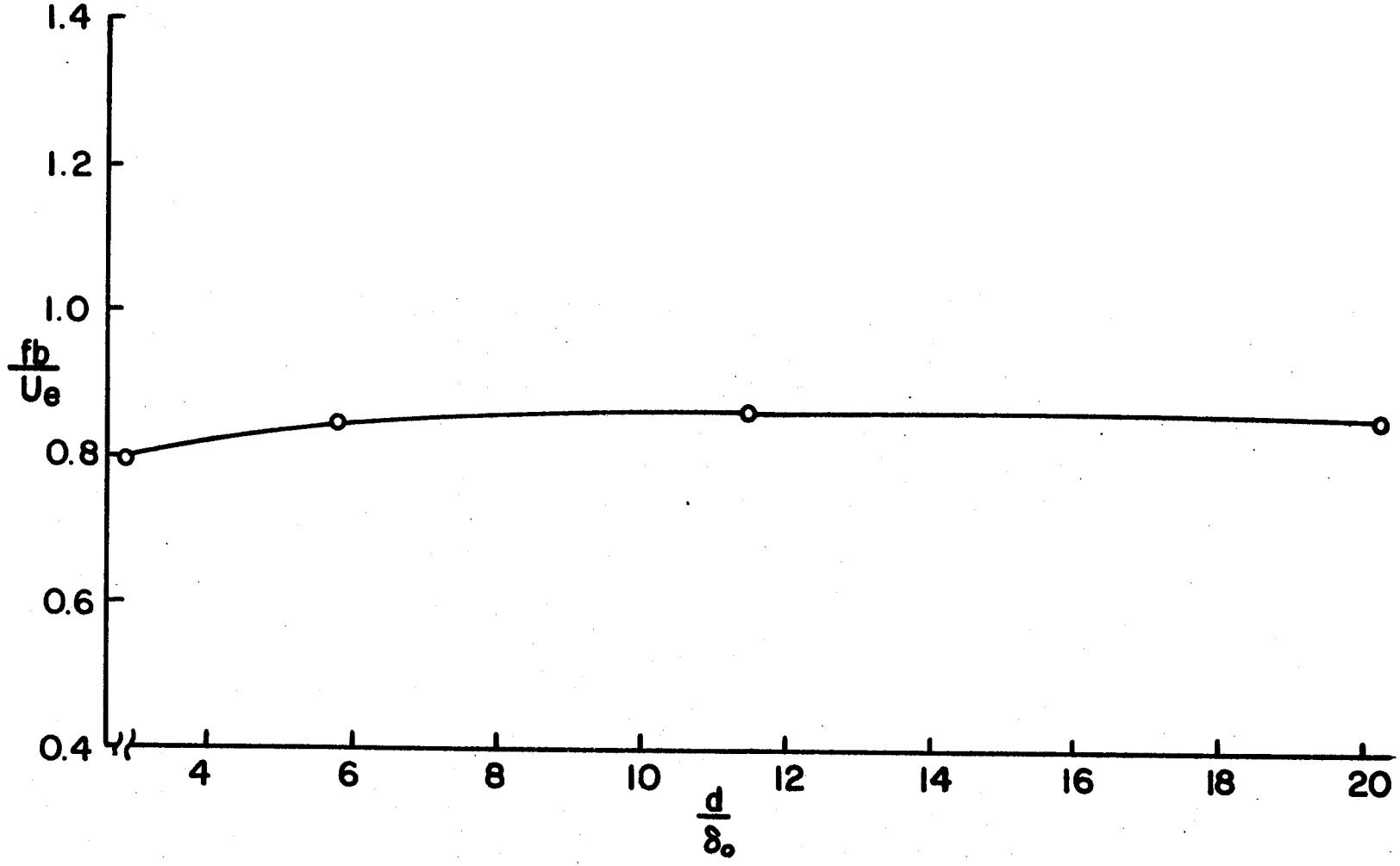

FIG. 9 Effect of Depth on Non-dimensional Frequency at $Re_{\delta_o} = 0.96 \times 10^3$ and $\frac{b}{\delta_o} = 11.00$

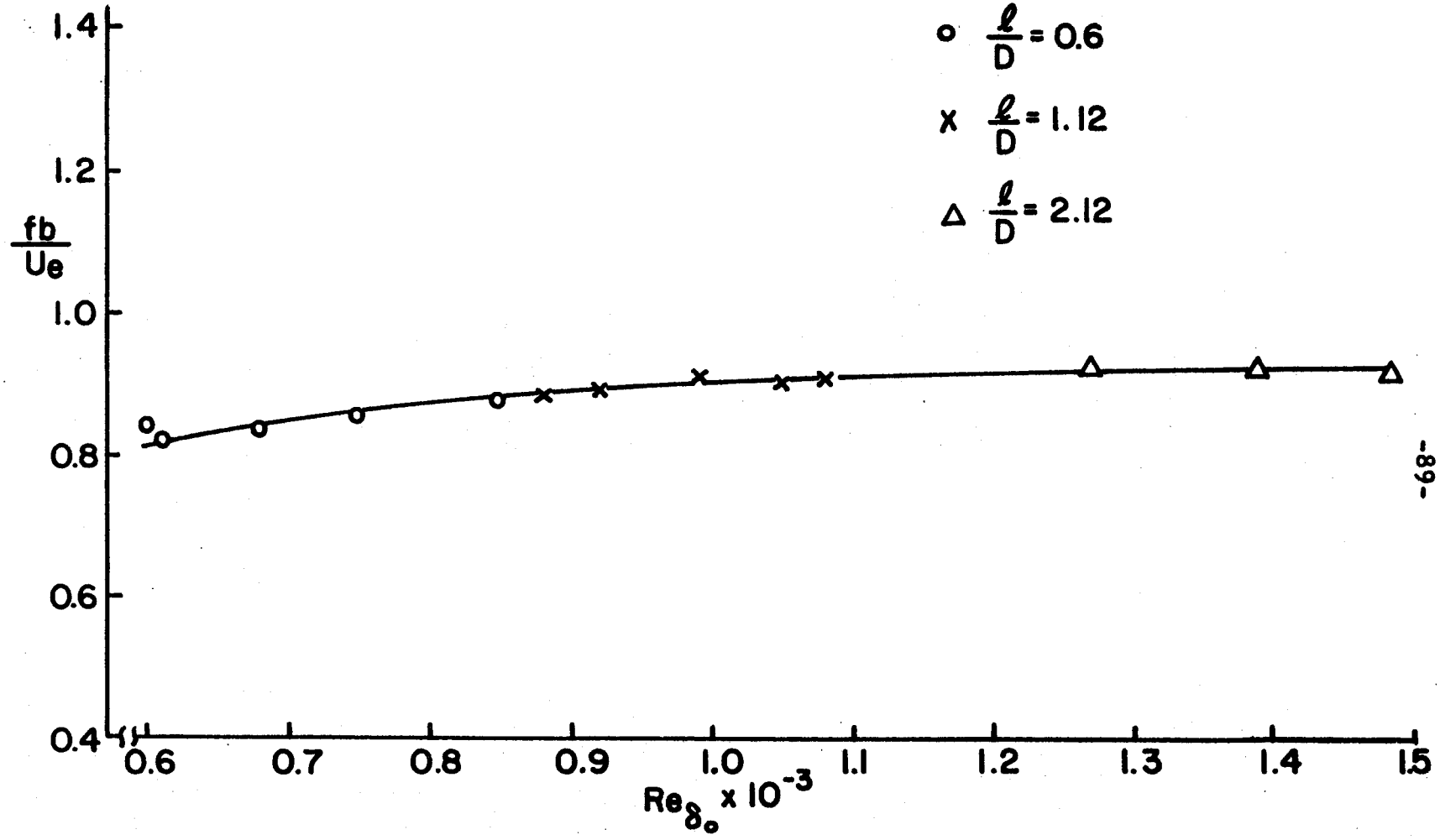

FIG. 10 Effect of Reynolds Number on Non-dimensional Frequency at $\frac{b}{\delta_o} = 12.76$

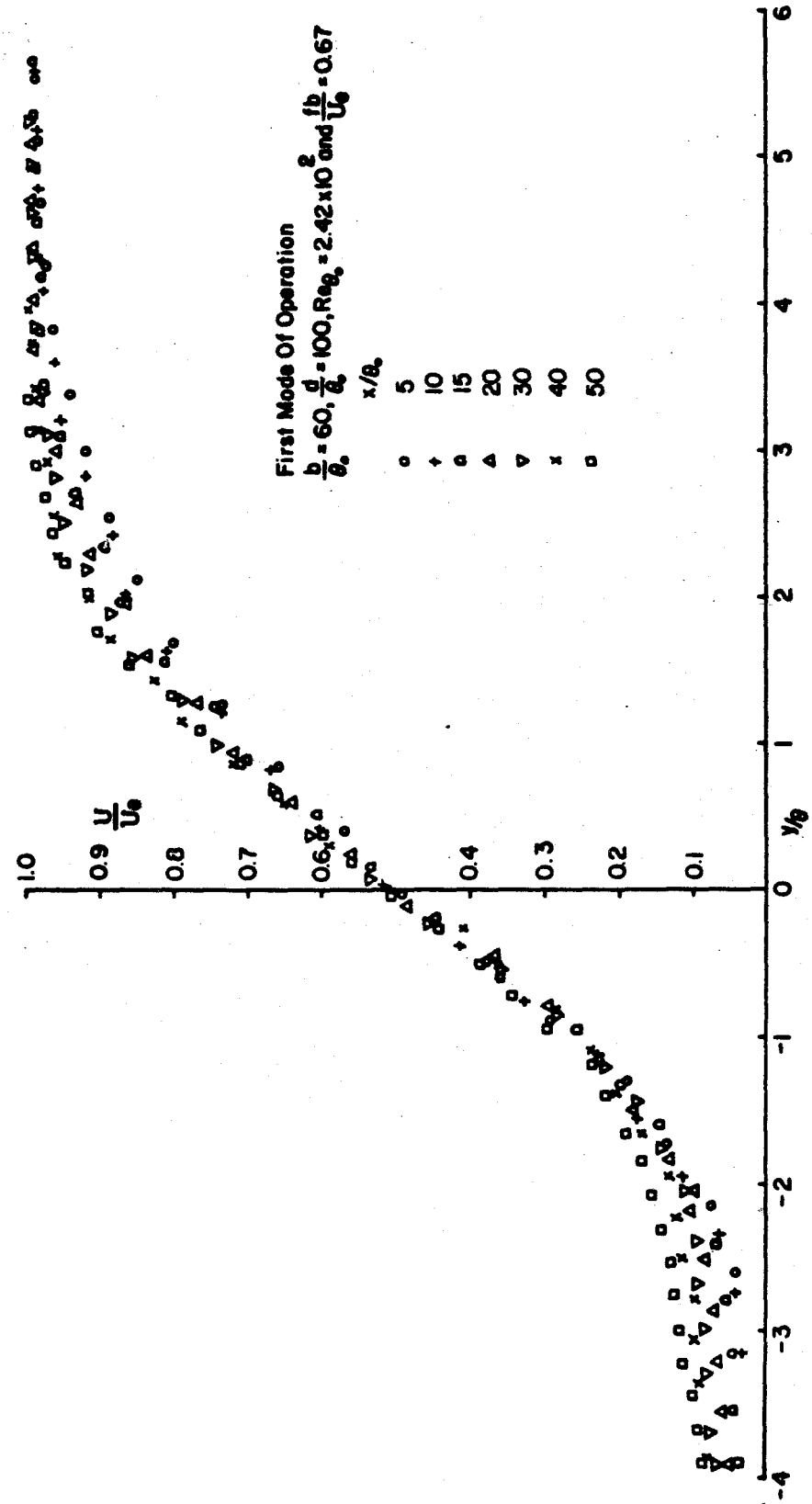

FIG. 11 Non-dimensional Mean Velocity Profiles in Shear Layer at Different Downstream Locations. Cavity Oscillation in 1st Mode of Oscillation with $\frac{fb}{U_e} = 0.67$, $\frac{b}{\theta_o} = 60$, $\frac{d}{\theta_o} = 100$ and $Re_{\theta_o} = 2.42 \times 10^2$

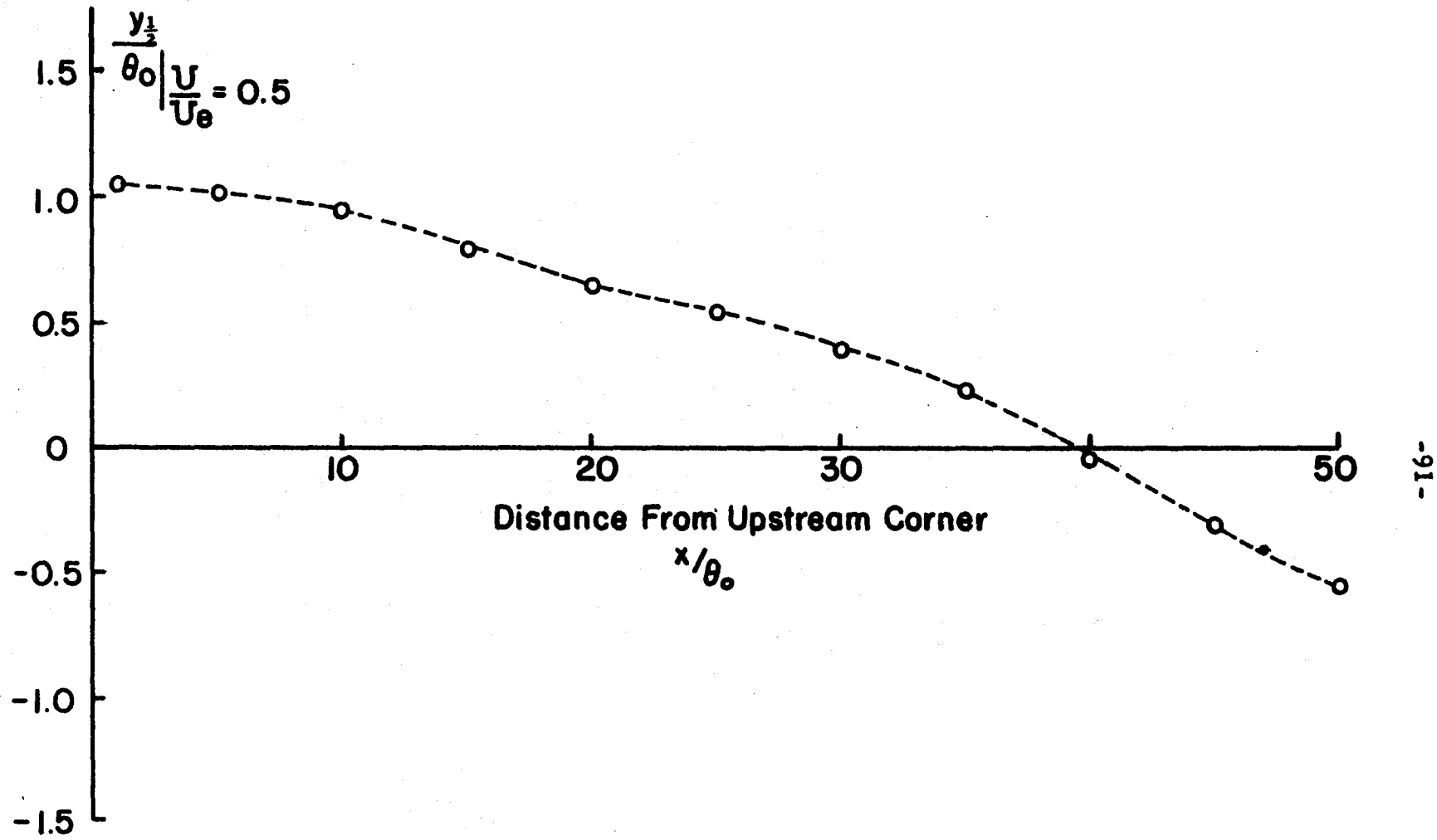

FIG. 12 Locus of $y_{\frac{1}{2}}/\theta$

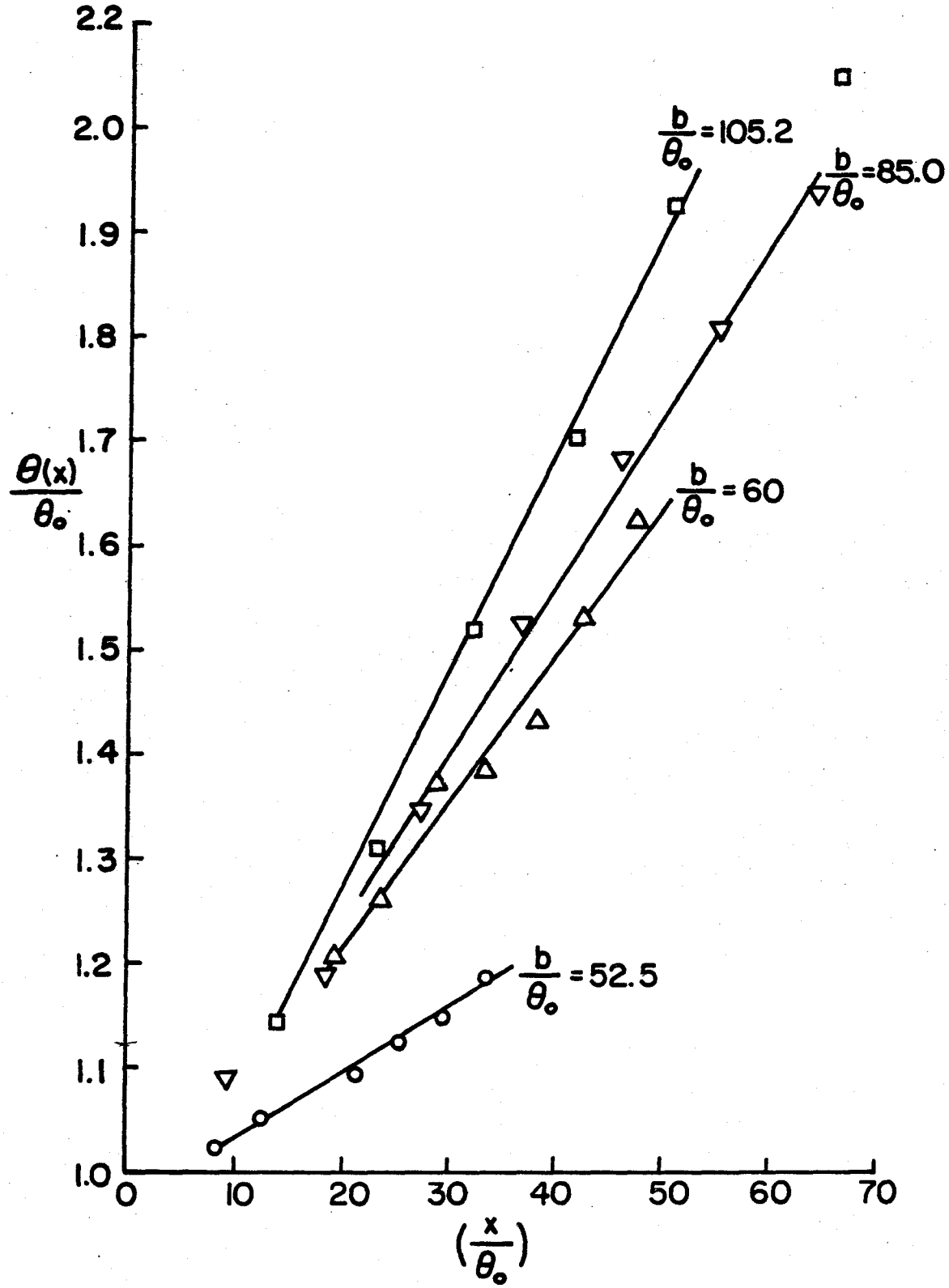

FIG. 13 Effect of Cavity Width on Shear Layer Growth at $Re_{\theta_o} = 2.42 \times 10^2$ and $\frac{d}{\theta_o} = 100$

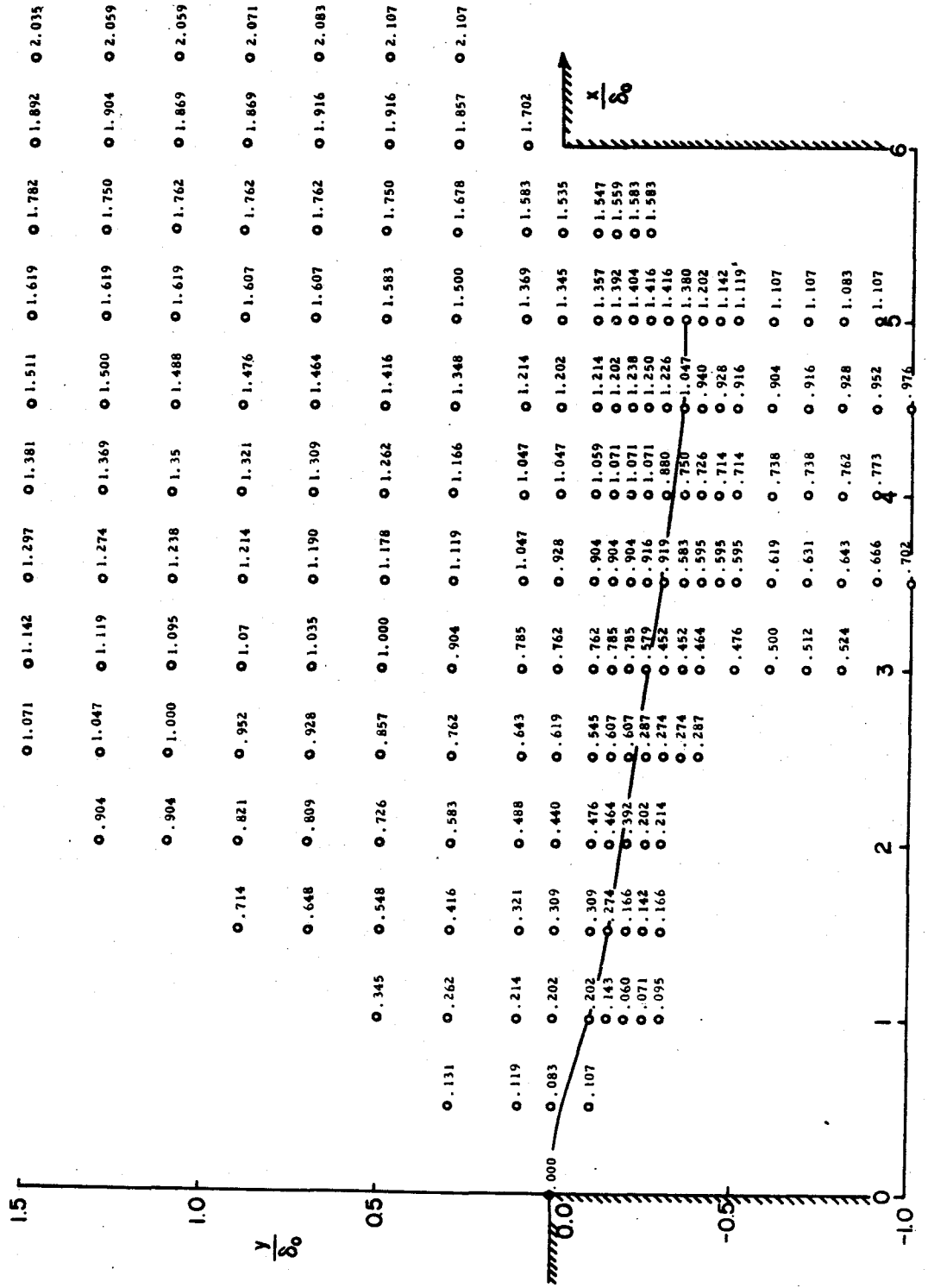

FIG. 14 Cavity Oscillation Phase Angles in First Mode of Oscillation at $Re_{\delta_o} = 2.86 \times 10^3$, $\frac{b}{\delta_o} = 6$, $\frac{d}{\delta_o} = 10$ and $\frac{fb}{U_e} = 0.67$

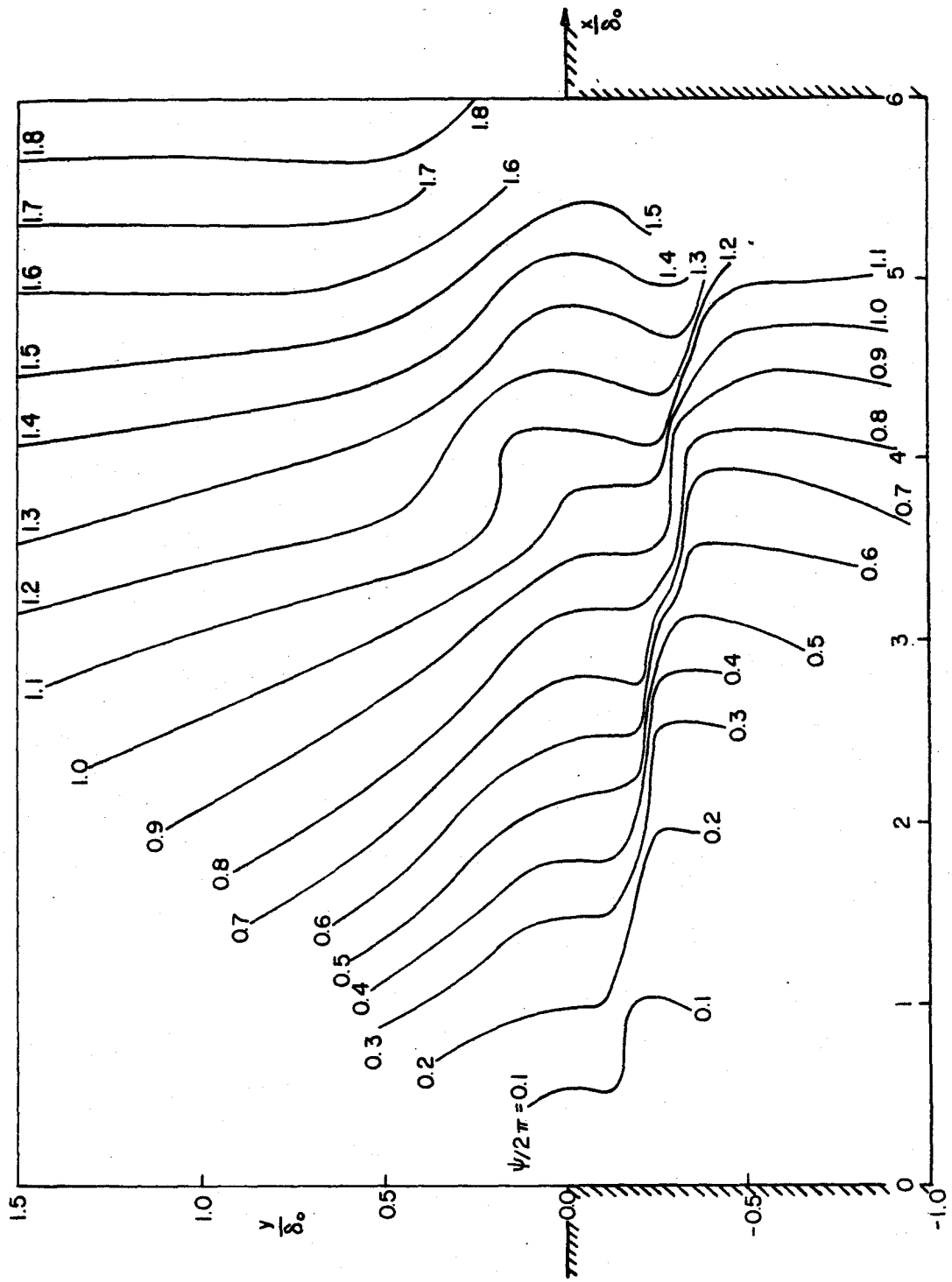

FIG. 15 Lines of Constant Phase in First Mode of Cavity Oscillation at $Re_{\delta_o} = 2.86 \times 10^3$, $\frac{b}{\delta_o} = 6$, $\frac{d}{\delta_o} = 10$ and $\frac{fb}{U_e} = 0.67$

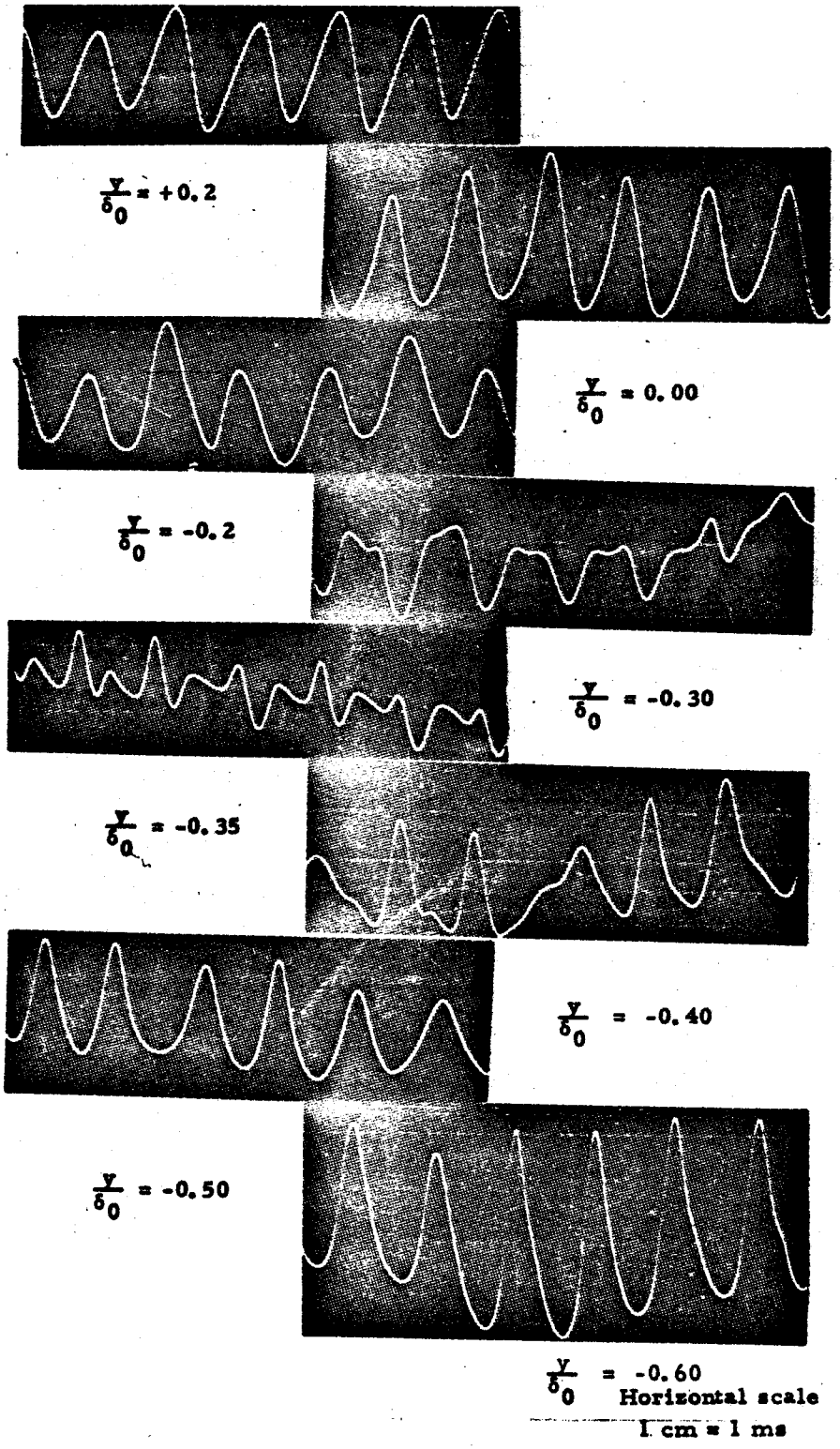

FIG. 16 Oscilloscope Traces of Velocity Fluctuations at $x/\delta_0 = 4.0$, 1st Mode, $d/\delta_0 = 10.00$, $b/\delta_0 = 6$, and $Re_{\delta_0} = 2.86 \times 10^3$

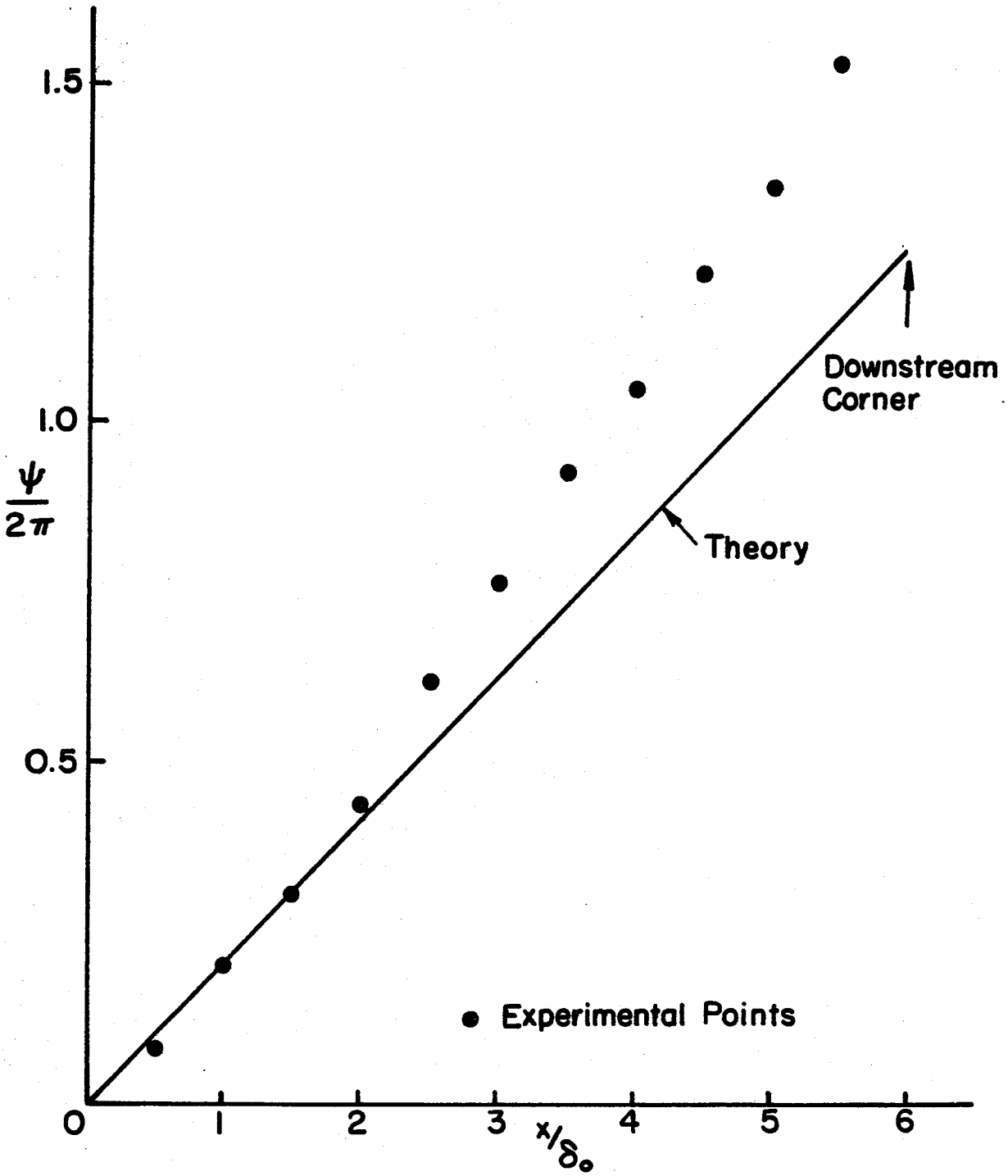

FIG. 17 Phase Angles at Various Downstream Locations for the First Mode of Cavity Oscillations at $Re_{\delta_o} = 2.86 \times 10^3$, $\frac{b}{\delta_o} = 6$, $\frac{d}{\delta_o} = 10$ and $\frac{fb}{U_e} = 0.67$

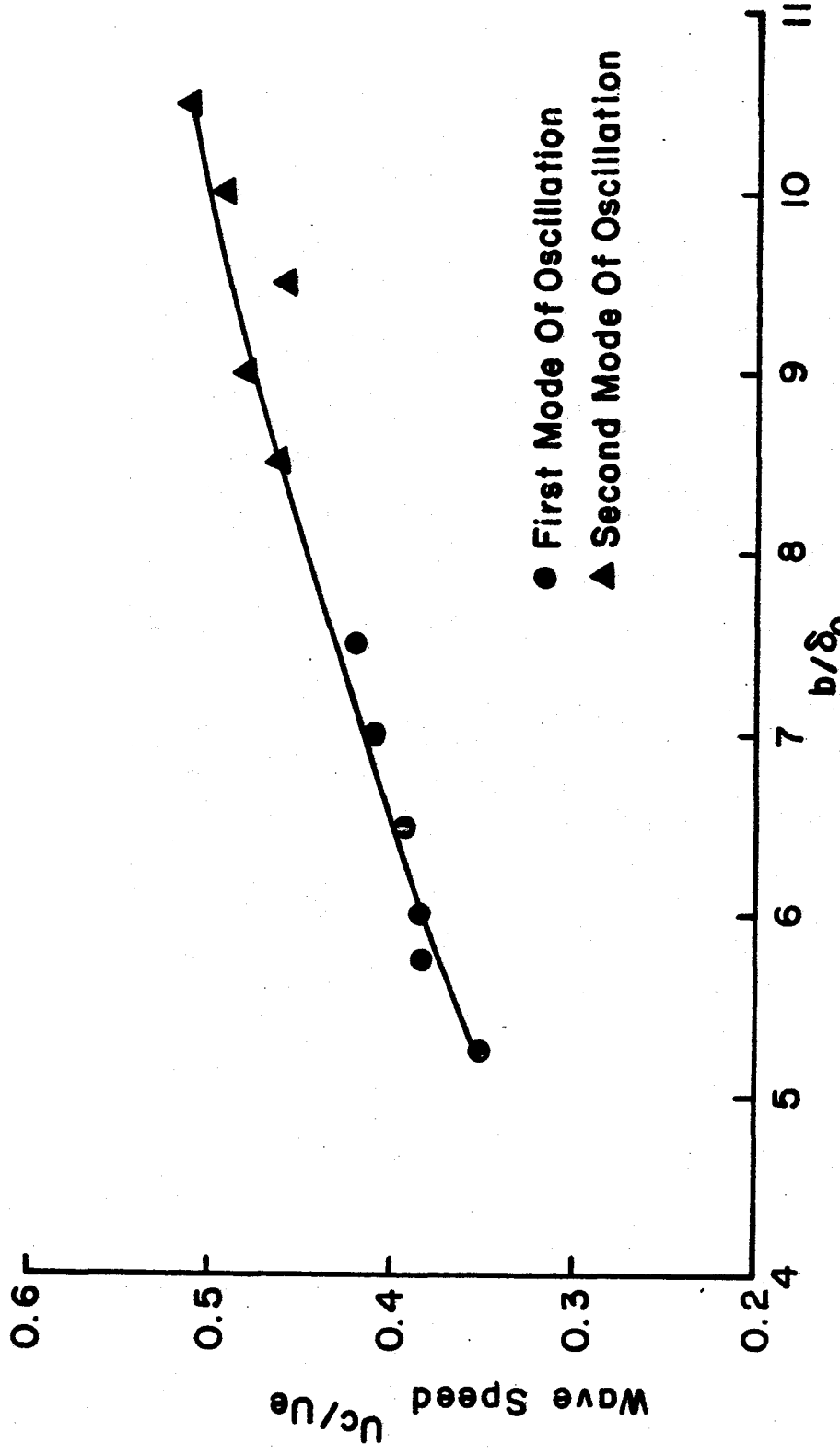

FIG. 18 Effect of Width on Propagation Speed in the First and Second Modes of Cavity Oscillations at $Re_{\delta_o} = 2.86 \times 10^3$ and $\frac{d}{\delta_o} = 10$

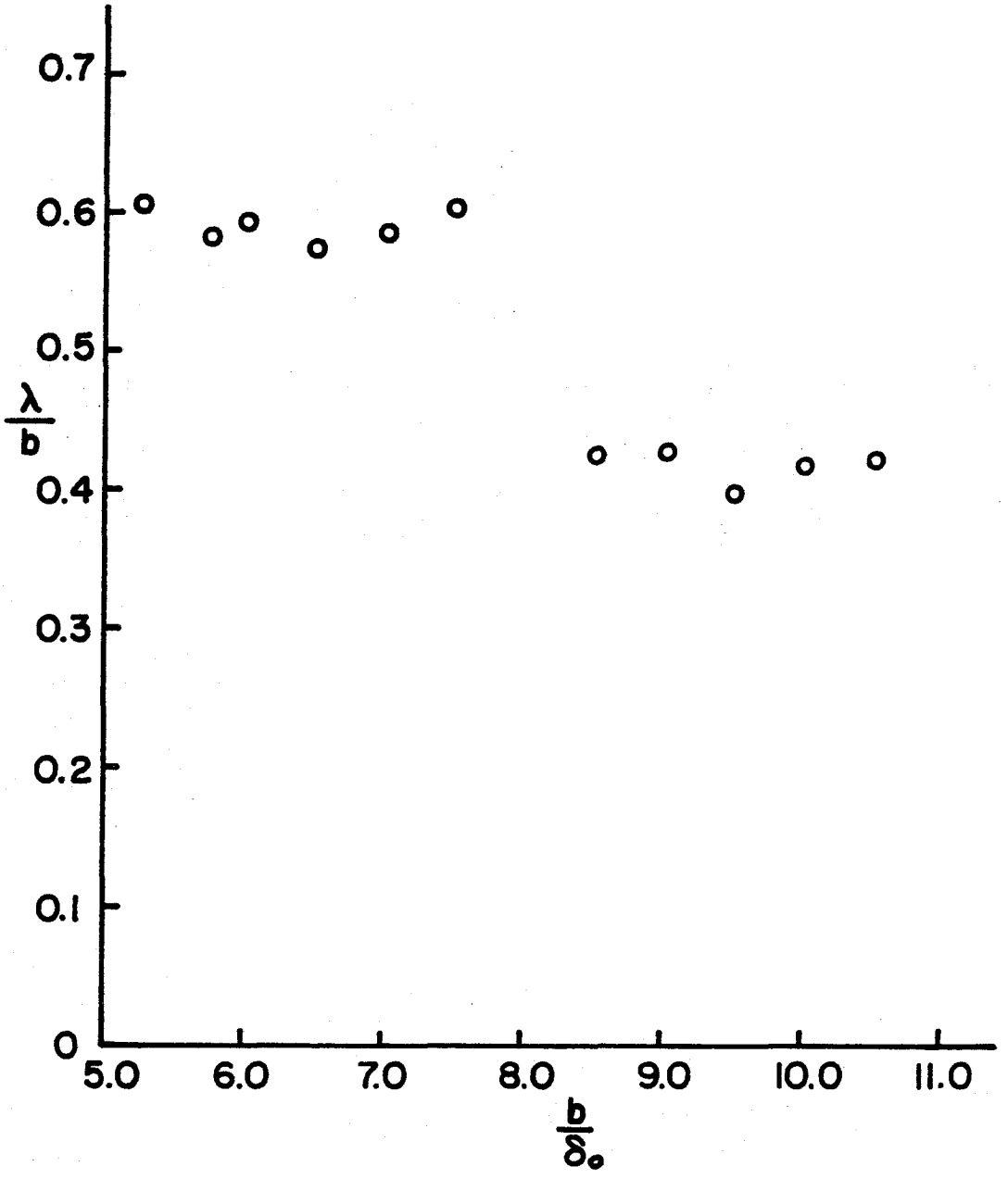

FIG. 19 Effect of Cavity Width on Wave Length of Disturbance at $Re_{\delta_o} = 2.86 \times 10^3$ and $\frac{d}{\delta_o} = 10$

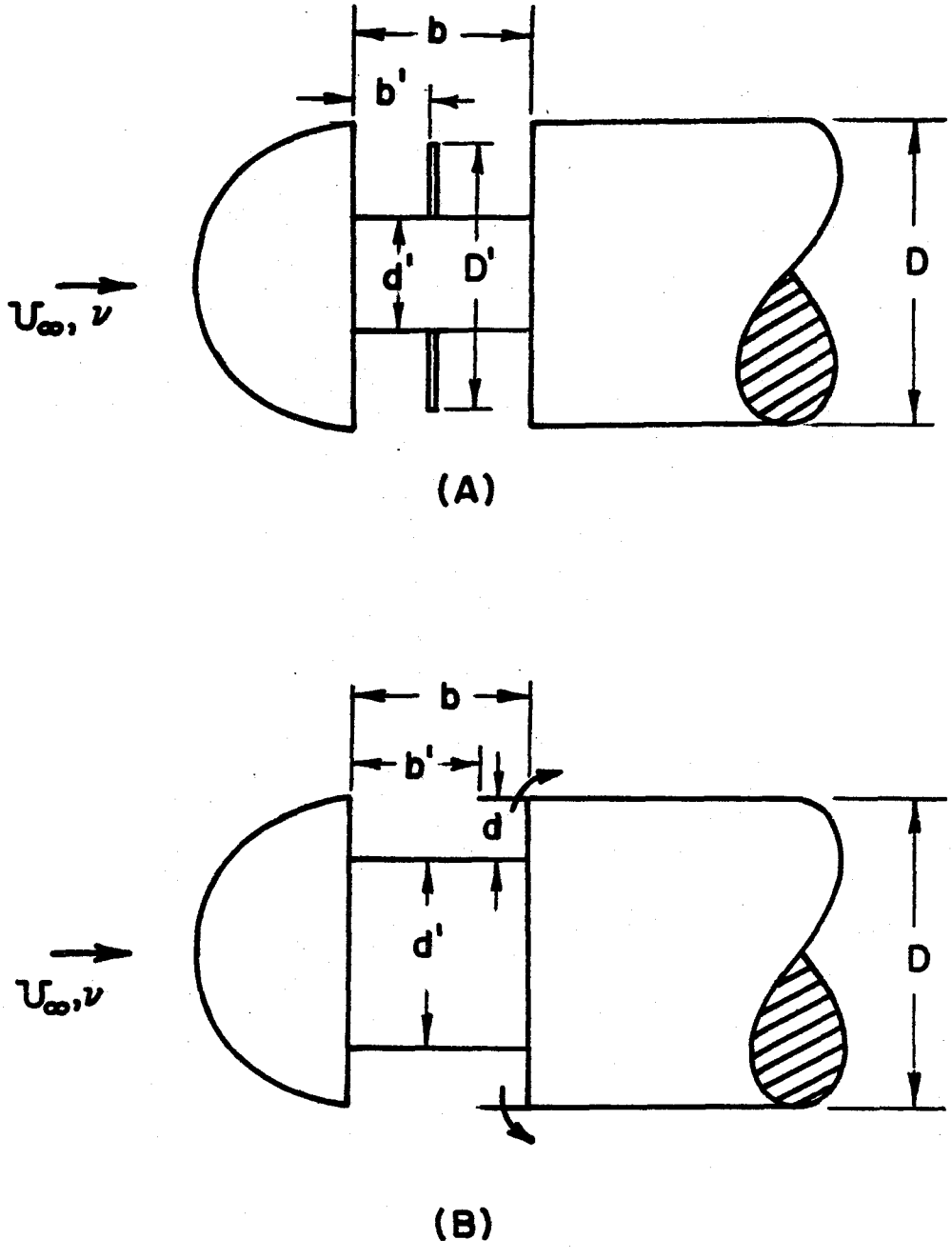

FIG. 20 Effect of Geometry on Cavity Oscillations

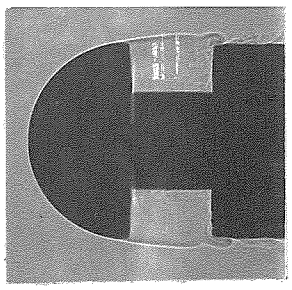

a) Spark Shadowgraph

U_∞ = 50 ft/sec, d = 0.25", b = 0.425"

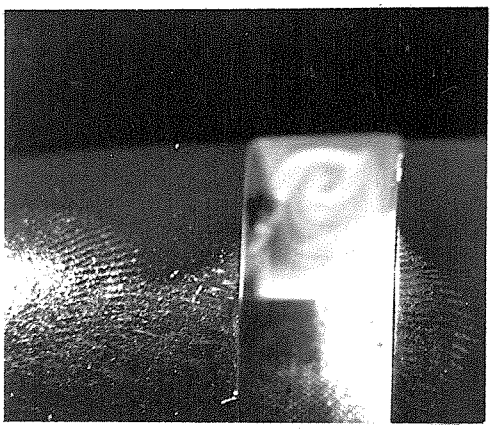

b) Smoke Picture

Width b = 0.35" < b_{min}

U_∞ = 20 ft/sec, d = 0.5"

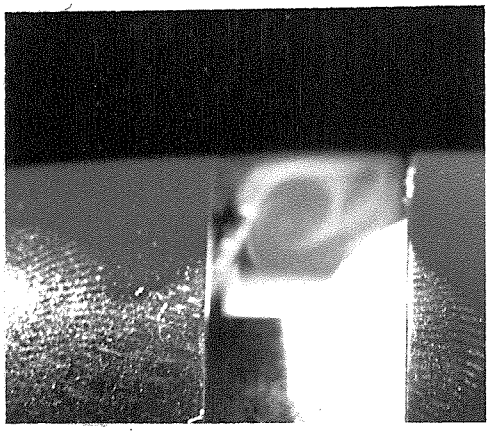

c) Smoke Picture

Width b = 0.5" < b_{min}

U_∞ = 20 ft/sec, d = 0.5"

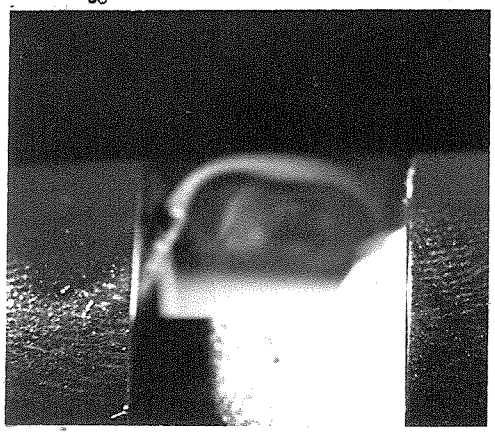

d) Smoke Picture

Width b = 0.675" = b_{min}

U_∞ = 20 ft/sec, d = 0.5"

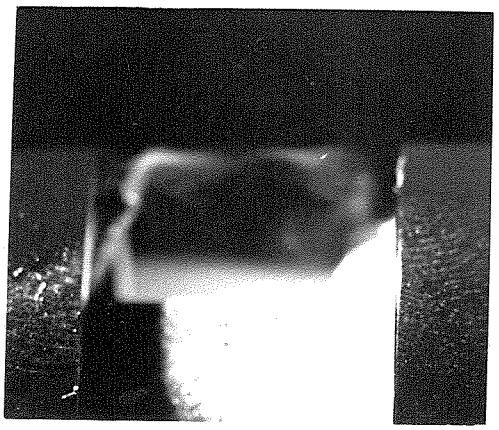

e) Smoke Picture

Width b = 0.8" > b_{min}

U_∞ = 20 ft/sec, d = 0.5"

Fig. 21. Visualization of Cavity Flow

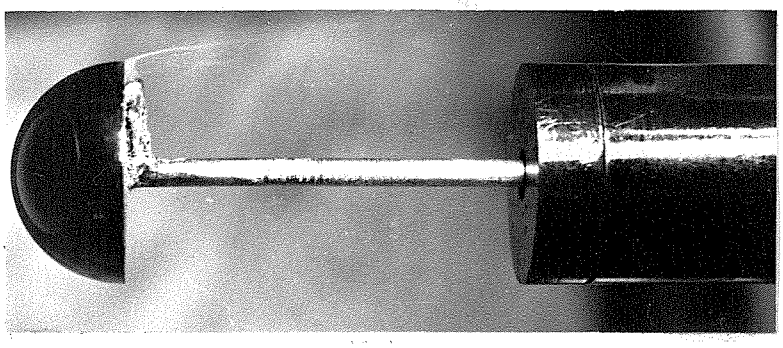

(i)

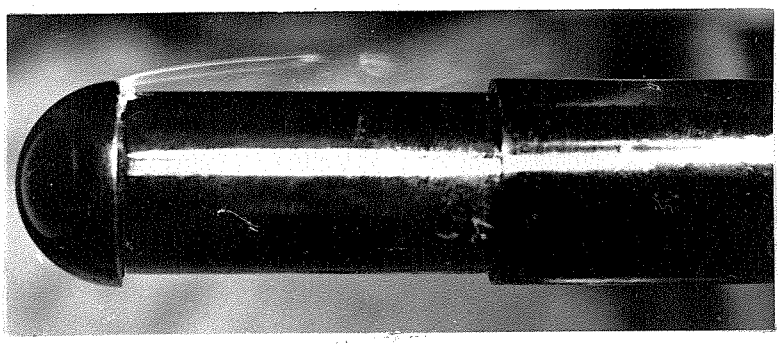

(ii)

a) Smoke Pictures

U_∞ = 20 ft/sec

b = 2.0"

(i) depth d = 0.425"

(ii) depth d = 0.05"

(i)

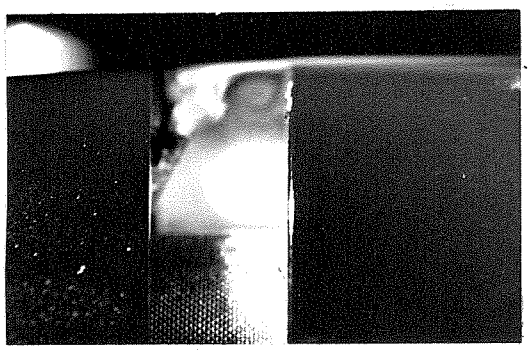

(ii)

b) Smoke Pictures

U_∞ = 20 ft/sec

d = 0.5"

(i) Cavity Oscillations, b = 0.5" > b_{min}, no mass addition

(ii) No Cavity Oscillations, b = 0.5" > b_{min}, with mass addition

Fig. 22. Visualization of Cavity Flow

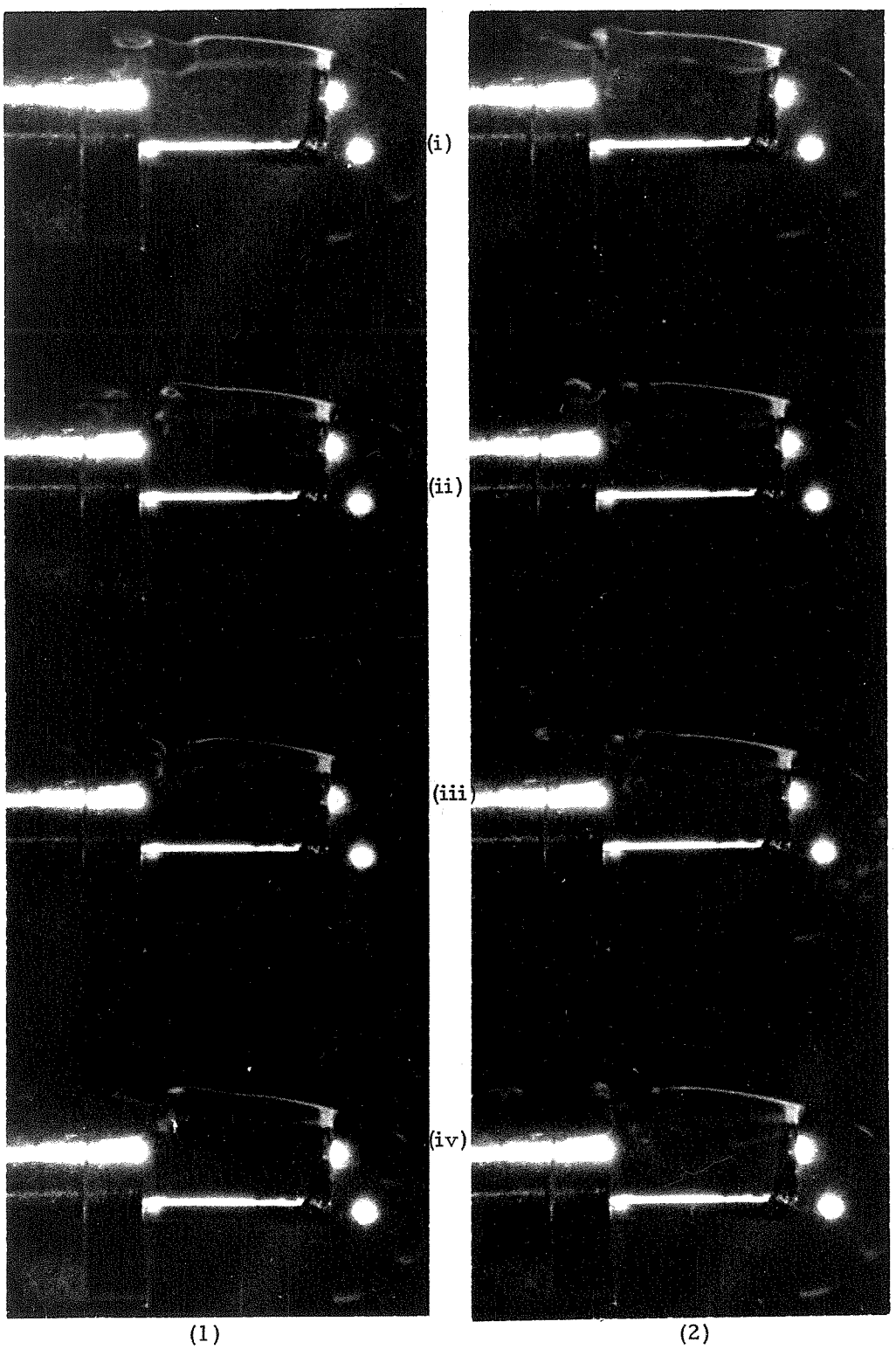

Fig. 23. Motion Pictures of Cavity Oscillations at 500 frames/sec, f = 300 Hz, b = 0.70" and d = 0.425"

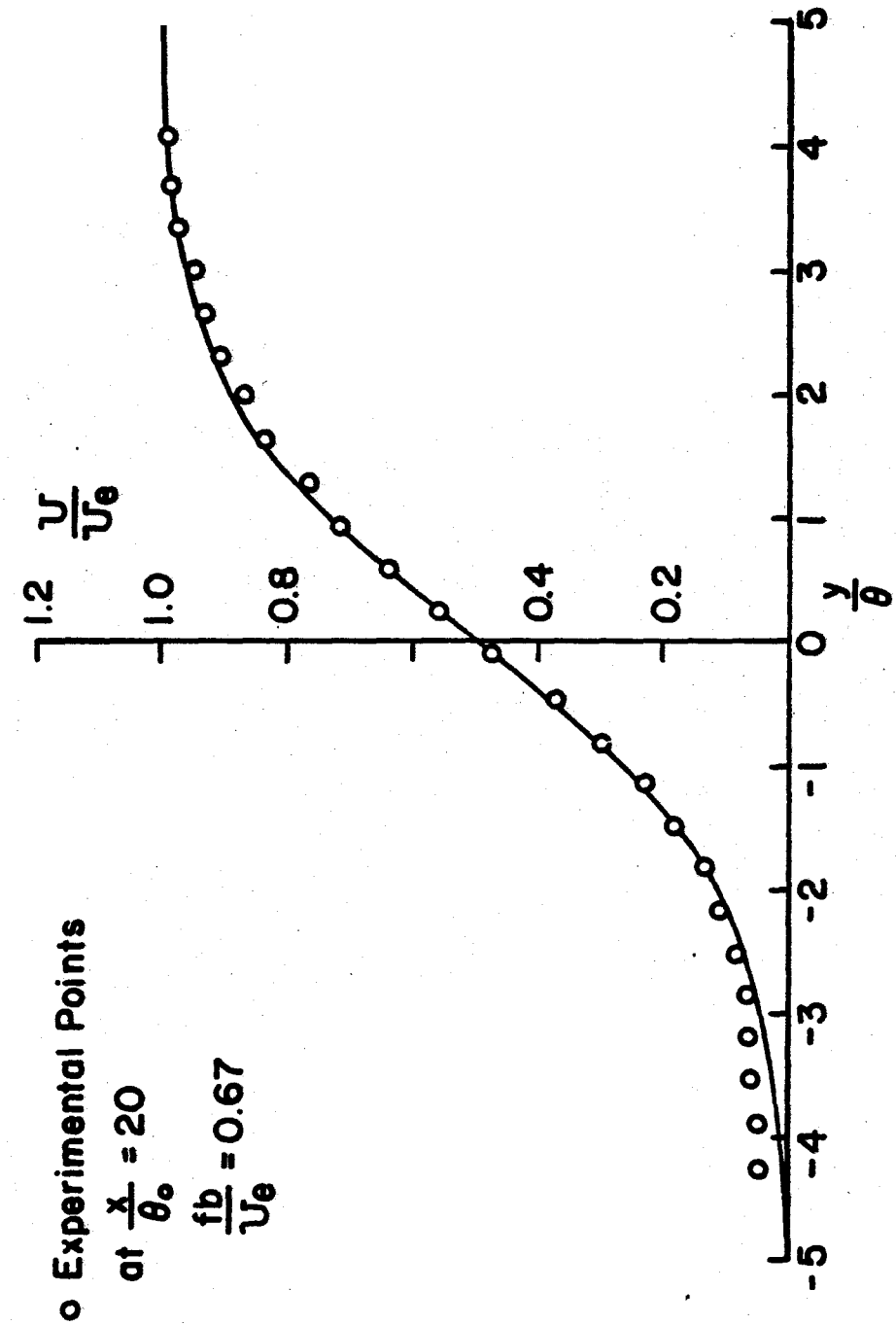

FIG. 24 Tangent Hyperbolic Profile and Measured Velocity Profile in Dimensionless Form

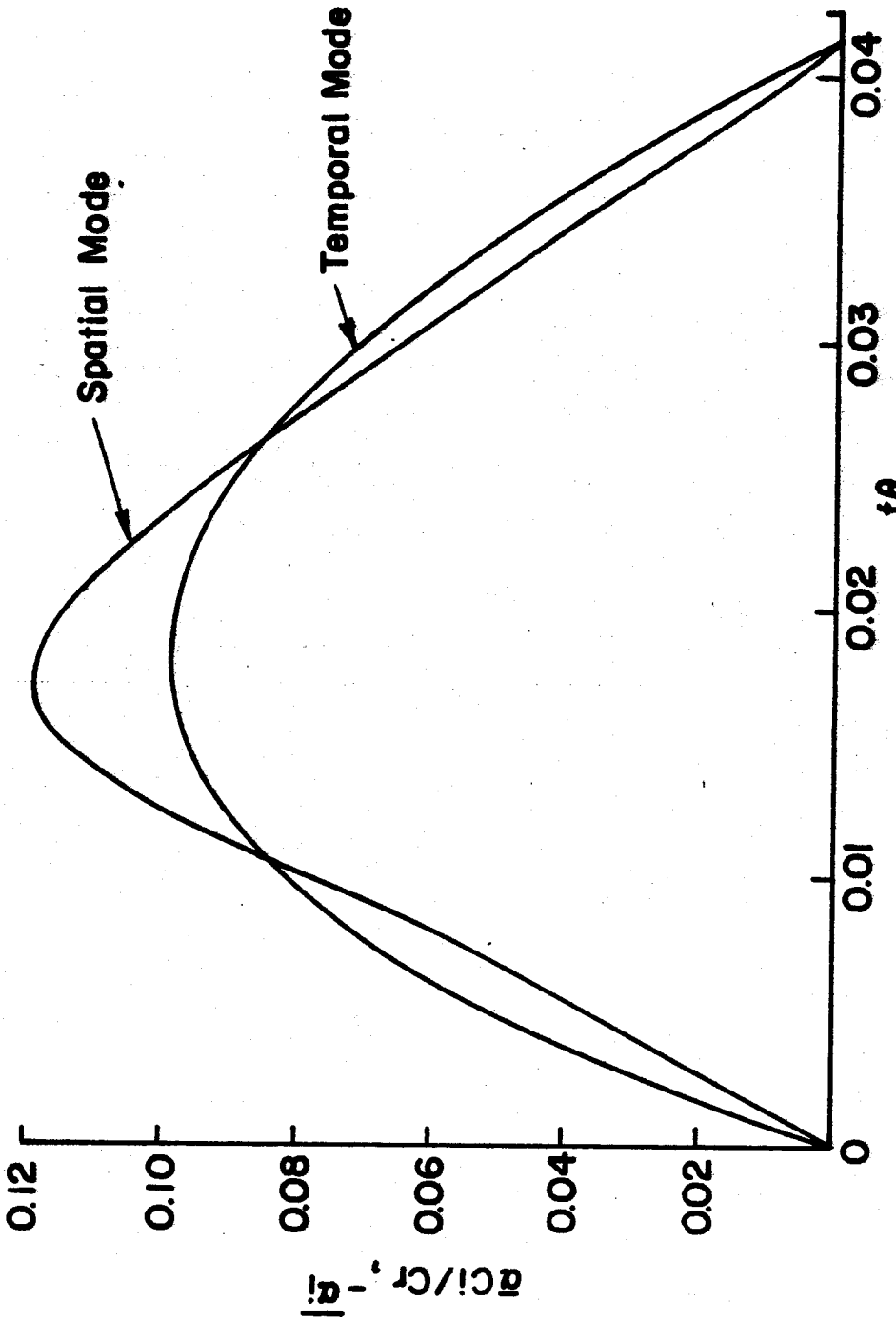

FIG. 25 Growth Rate as a Function of Non-dimensional Frequency for Spatially and Temporally Growing Disturbances

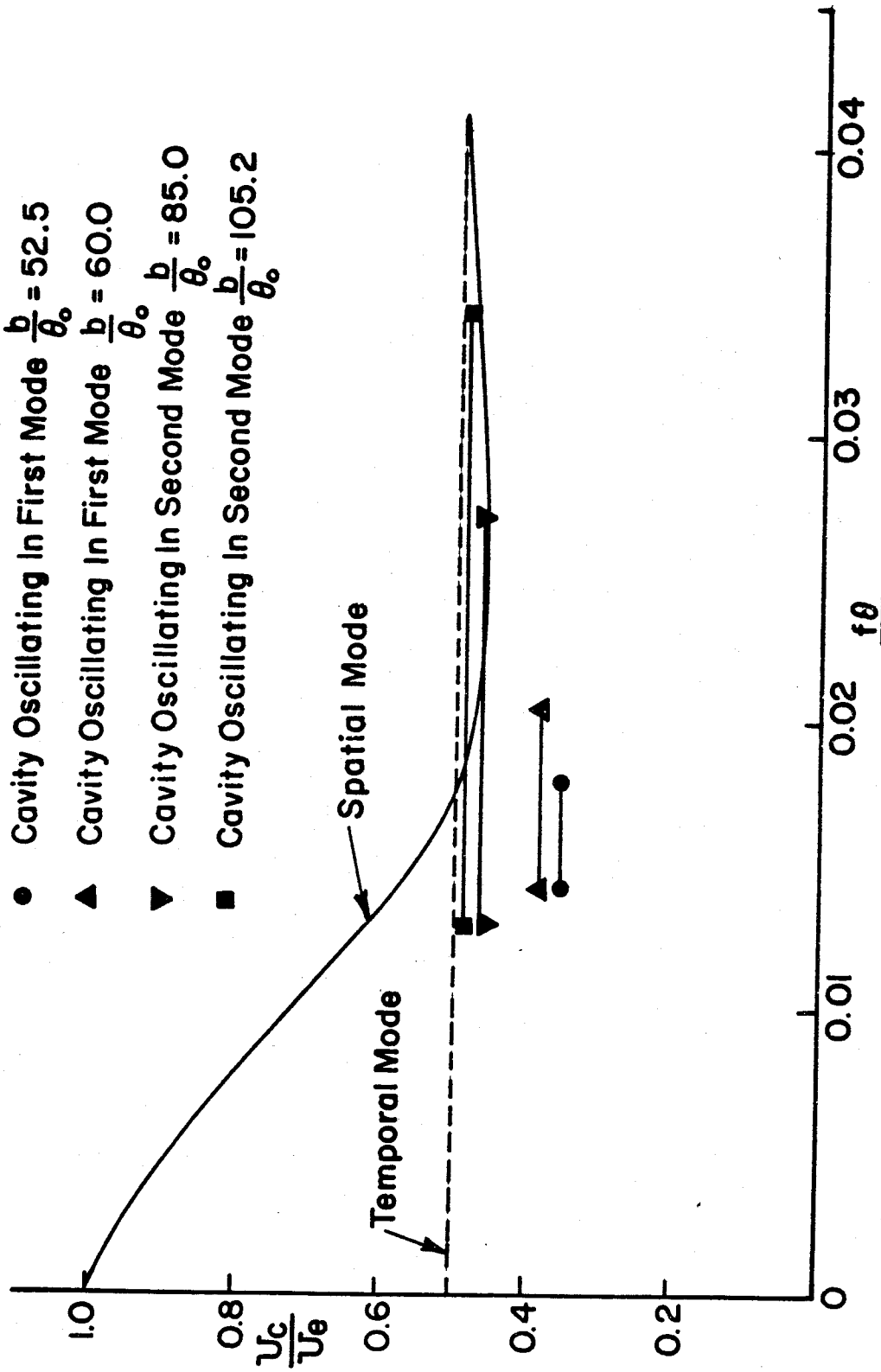

FIG. 26 Comparison of Calculated and Measured Phase Velocity as a Function of Non-dimensional Frequency

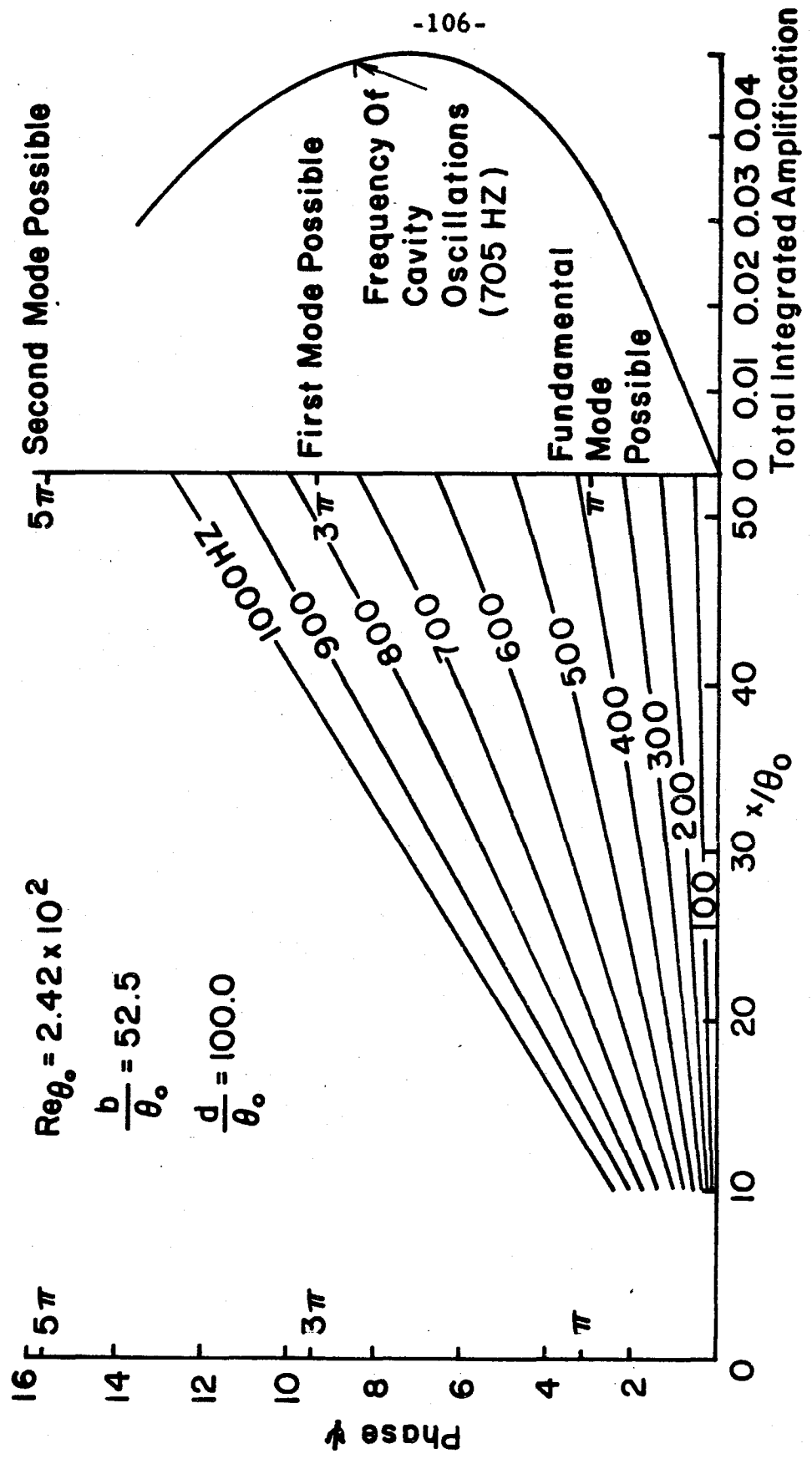

FIG. 27 Comparison Experimentally Measured Frequency of Cavity Oscillations with Predicted Frequencies of Spatially Growing Disturbances in the First Mode of Cavity Oscillation

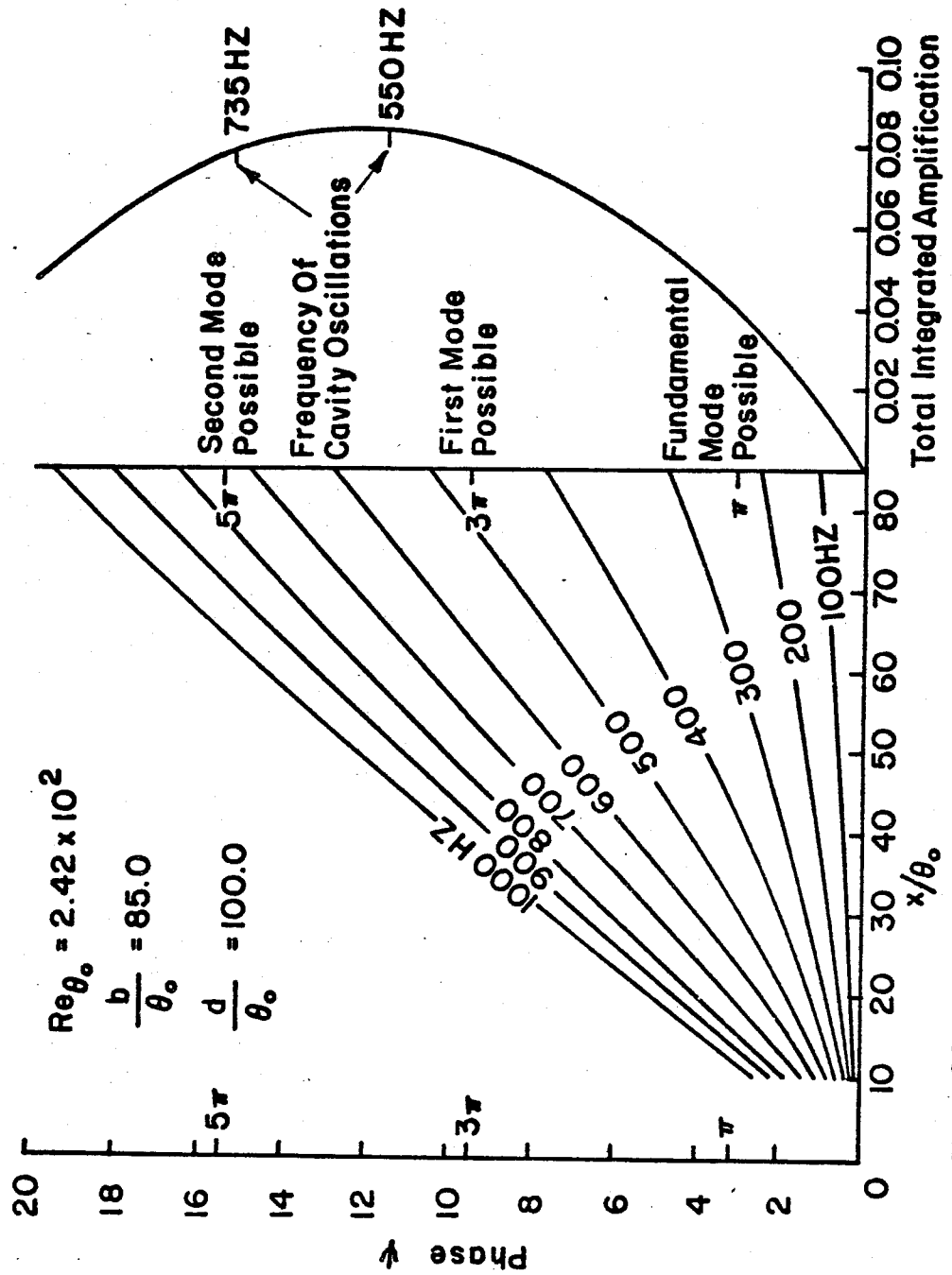

FIG. 28 Comparison of Experimentally Measured Frequency of Cavity Oscillations with Predicted Frequencies of Spatially Growing Disturbances with Cavity Flow Switching Between the First and Second Mode of Cavity Oscillation

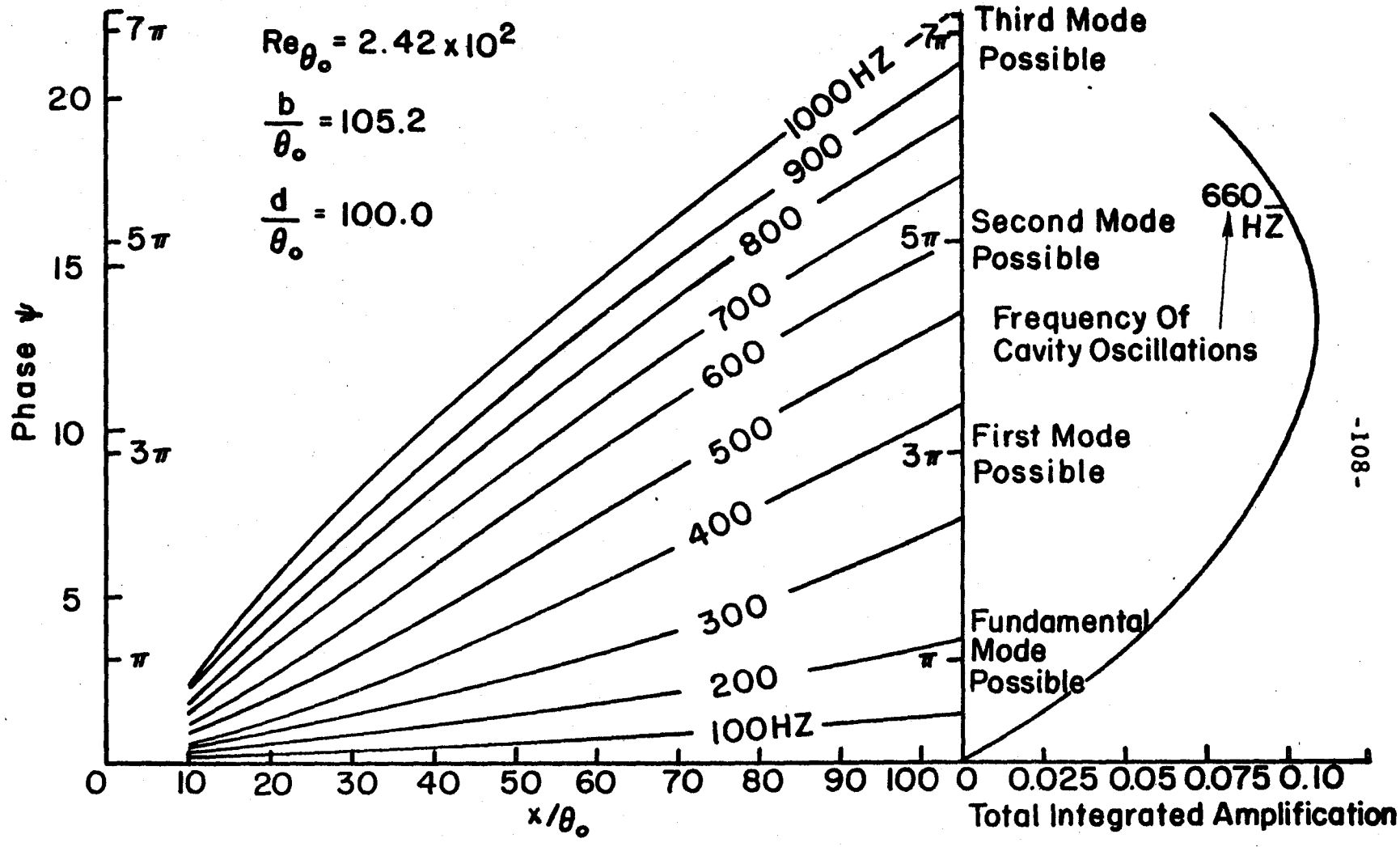

FIG. 29 Comparison of Experimentally Measured Frequency of Cavity Oscillations with Predicted Frequencies of Spatially Growing Disturbances in the Second Mode of Cavity Oscillation

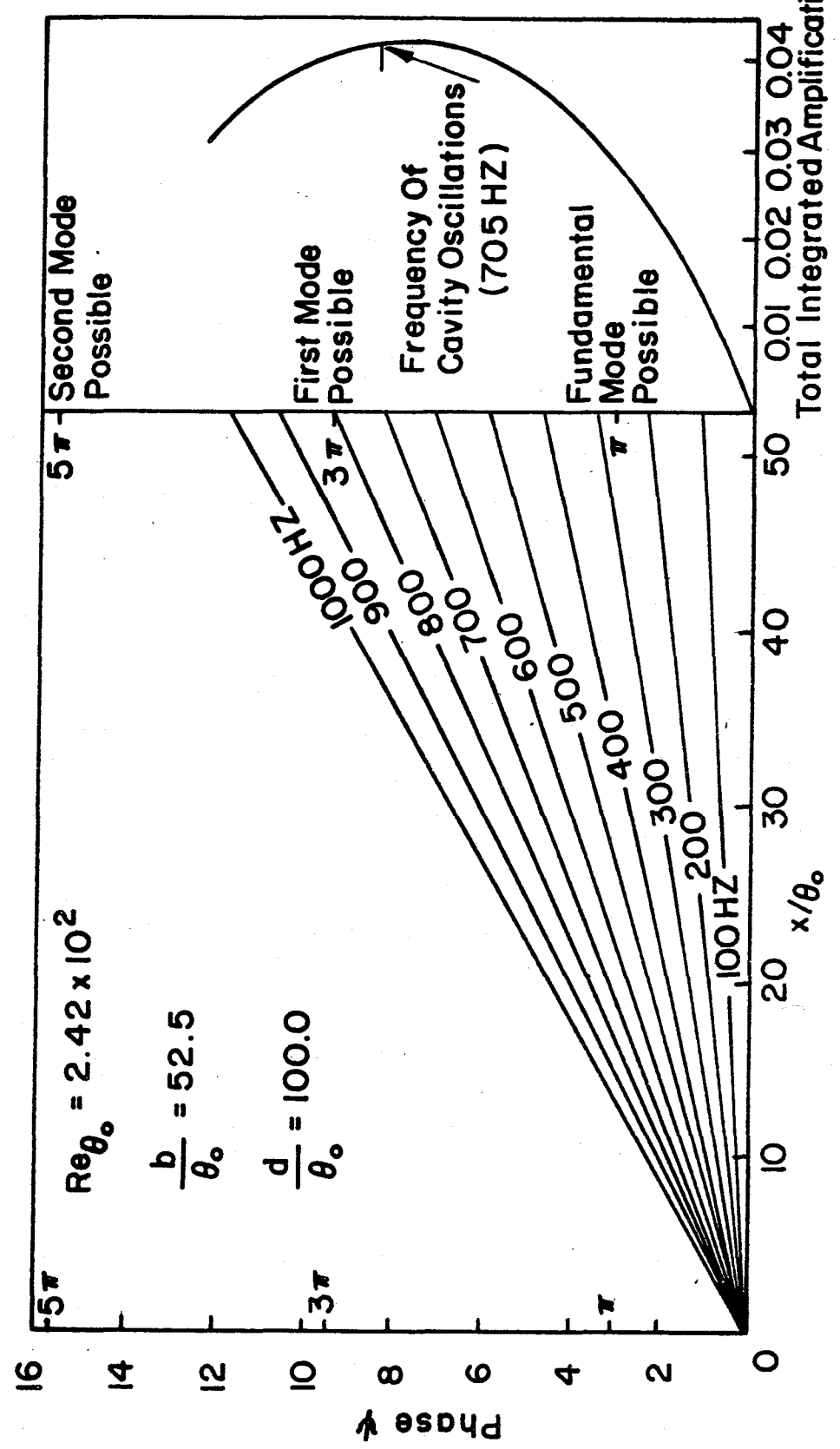

FIG. 30 Comparison of Experimentally Measured Frequency of Cavity Oscillations with Predicted Frequencies of Temporally Growing Disturbances in the First Mode of Cavity Oscillation

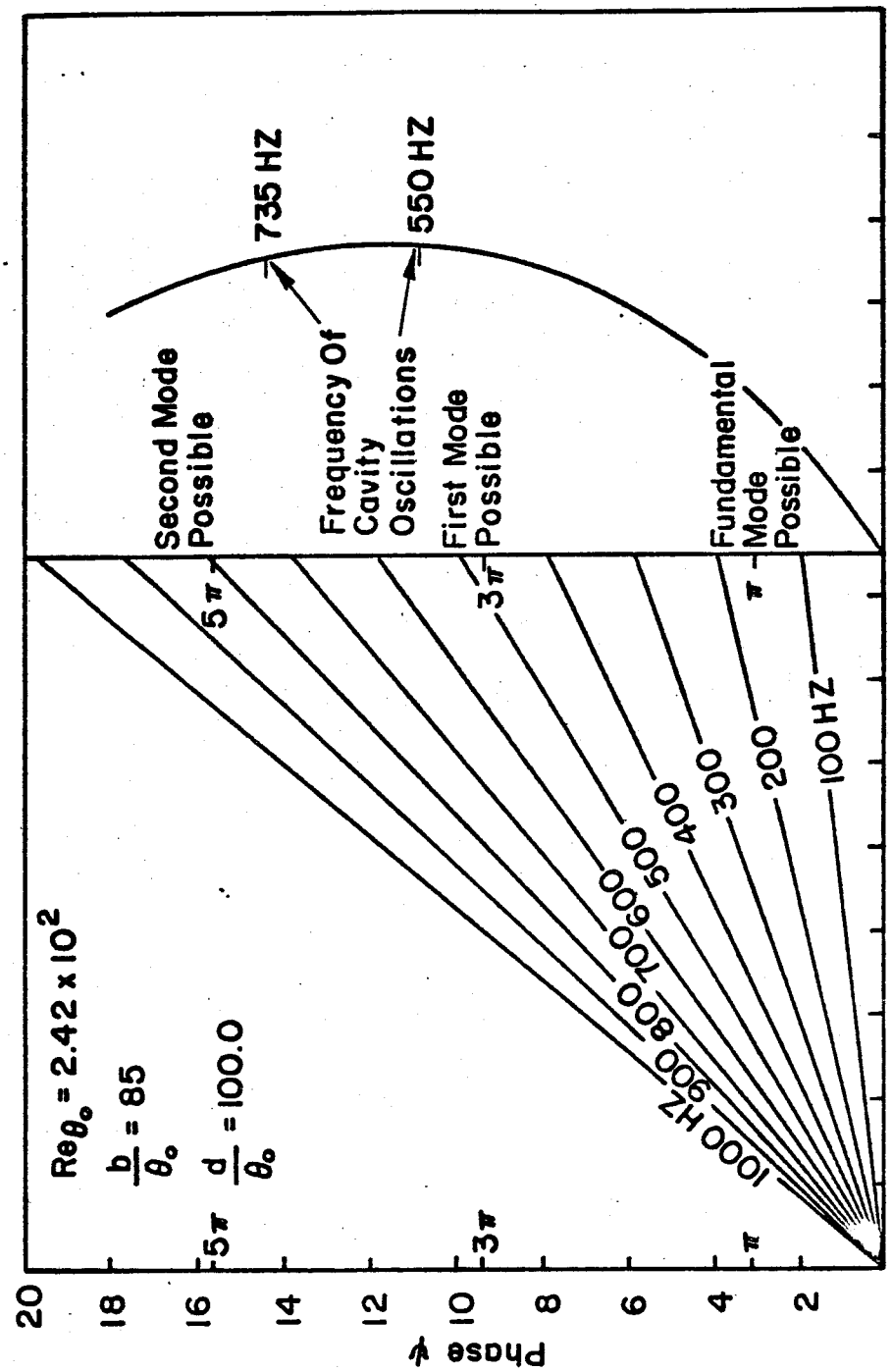

FIG. 31 Comparison of Experimentally Measured Frequency of Cavity Oscillations with Predicted Frequencies of Temporally Growing Disturbances with Cavity Flow Switching Between the First and Second Mode of Cavity Oscillation

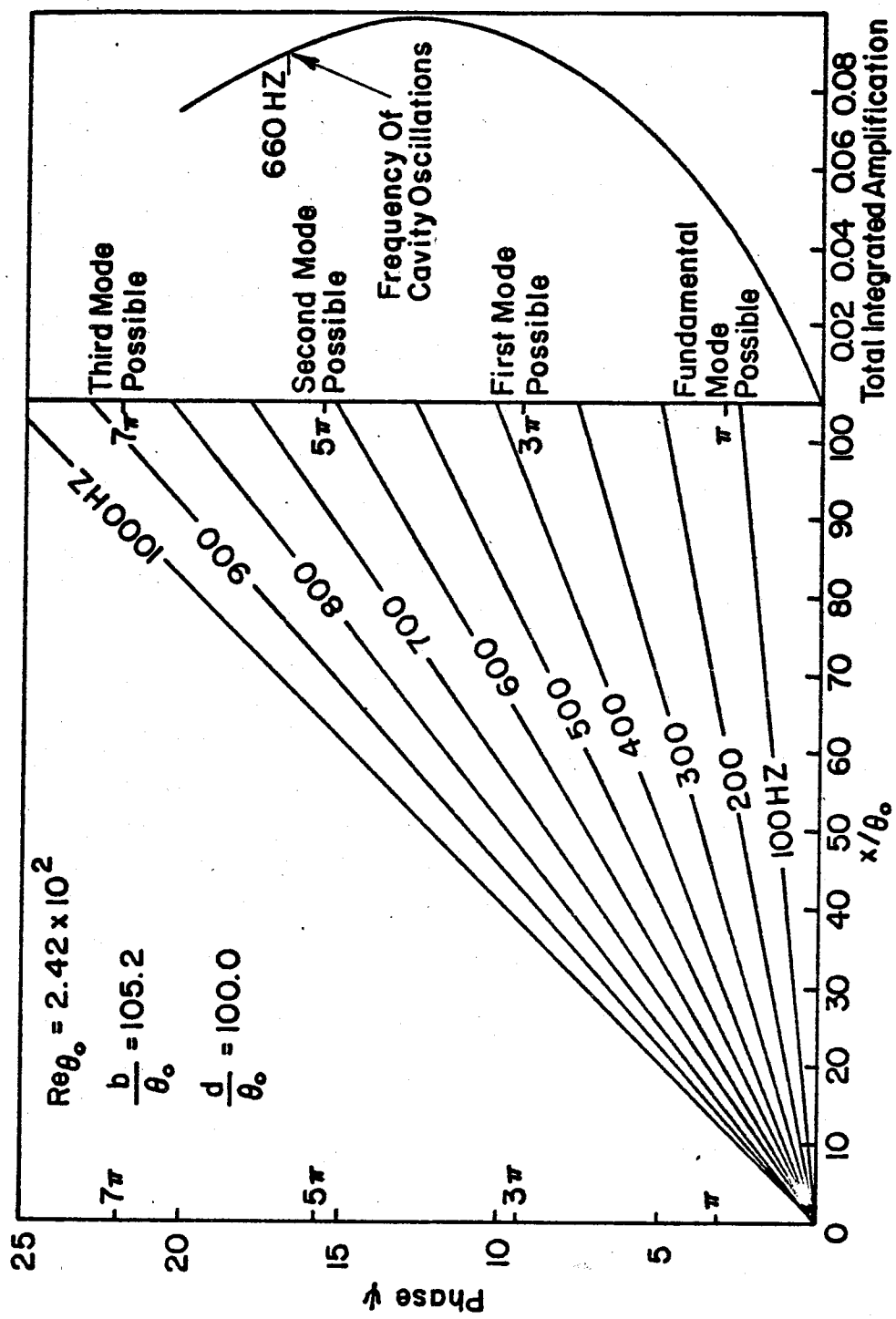

FIG. 32 Comparison of Experimentally Measured Frequency of Cavity Oscillations with Predicted Frequencies of Temporally Growing Disturbances in the Second Mode of Cavity Oscillation

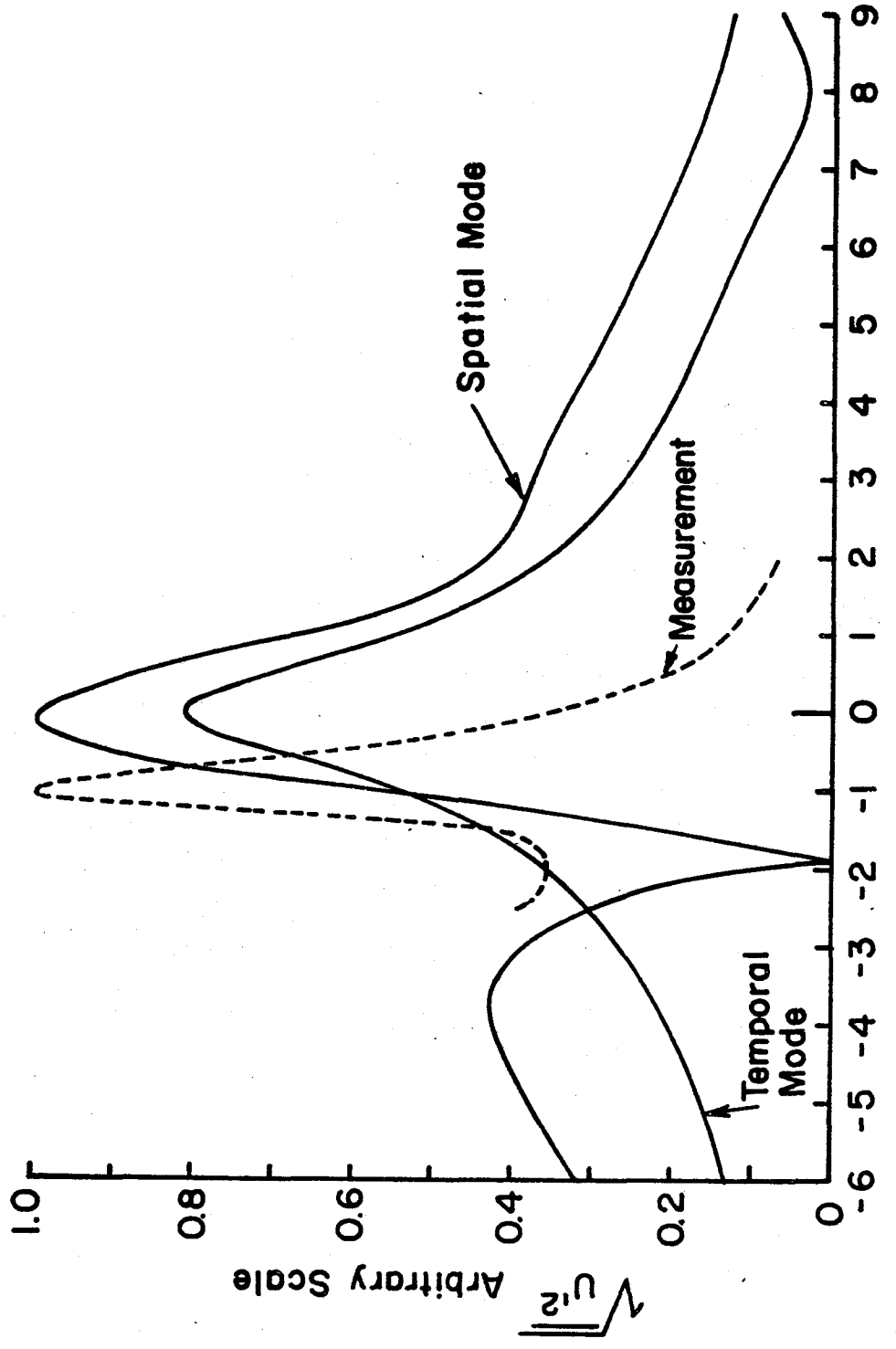

FIG. 33 Measured and Theoretical Amplitude Distribution at Non-dimensional Frequency $\frac{f\theta}{U_e} = 0.01648$

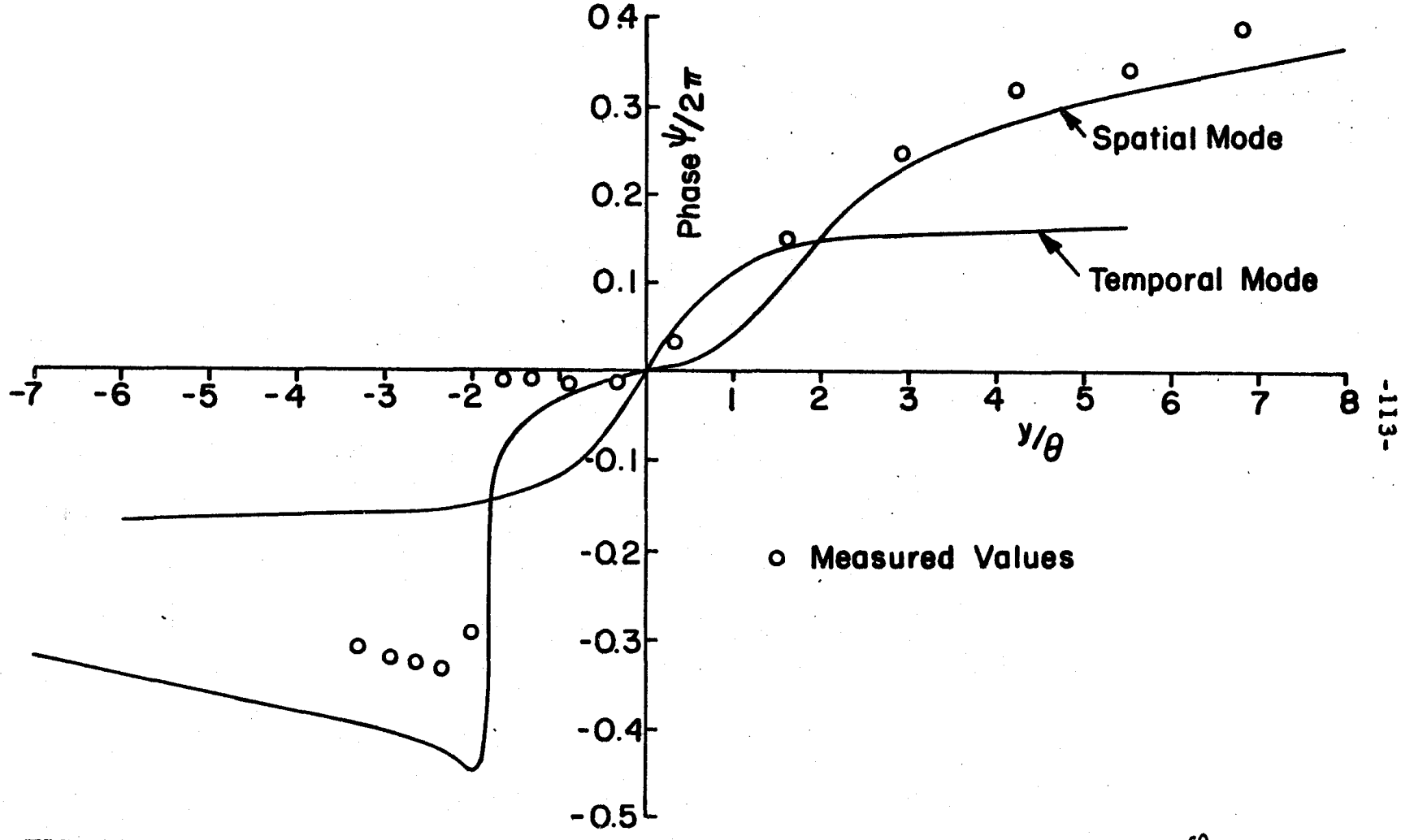

FIG. 34 Measured and Theoretical Phase Distribution at Non-dimensional Frequency $\frac{f\theta}{U_e} = 0.01648$

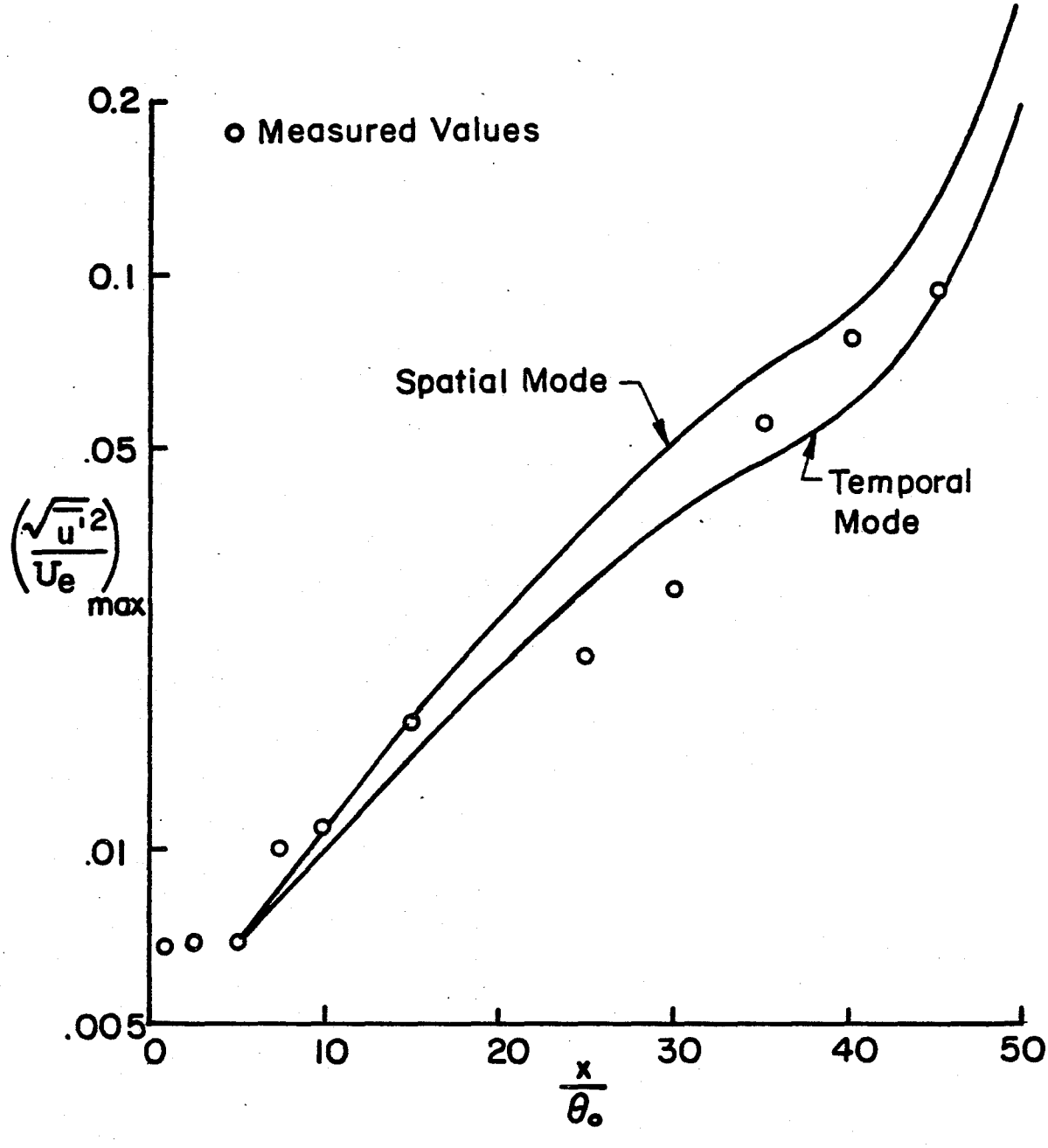

FIG. 35 Theoretical and Measured Growth of Disturbances in the First Mode of Cavity Oscillation at $Re_{\theta_o} = 2.42 \times 10^2$, $\frac{b}{\theta_o} = 60$, $\frac{d}{\theta_o} = 100$, and $\frac{fb}{U_e} = 0.67$